ISBN 978-82-326-6555-6 (printed ver.)
ISBN 978-82-326-5274-7 (electronic ver.)
ISSN 1503-8181 (printed ver.)
ISSN 2703-8084 (electronic ver.)

NTNU
Norwegian University of
Science and Technology

Doctoral theses at NTNU, 2023:43

Cristina Zotică

Optimal Operation and Control of Thermal Energy Systems

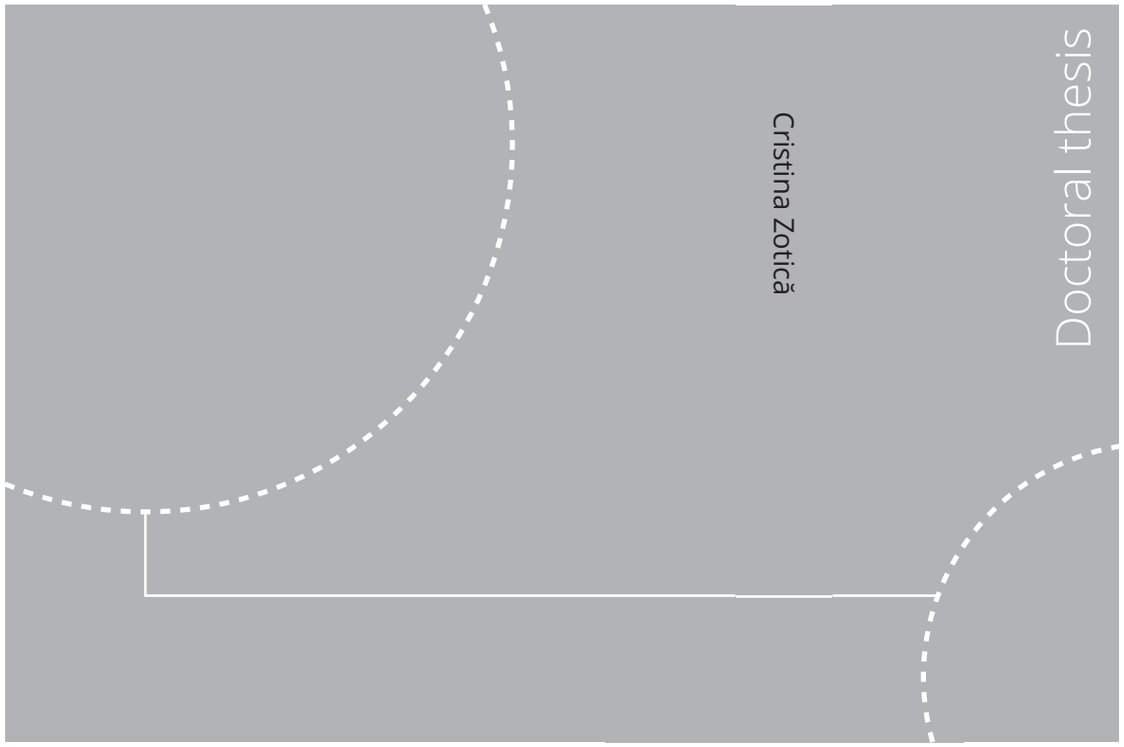

Doctoral theses at NTNU, 2023:43

NTNU

NTNU
Norwegian University of
Science and Technology
Thesis for the degree of
Philosophiae Doctor
Faculty of Natural Sciences
Department of Chemical Engineering

NTNU
Norwegian University of
Science and Technology

Cristina Zotică

Optimal Operation and Control of Thermal Energy Systems

Thesis for the degree of Philosophiae Doctor

Trondheim, February 2023

Norwegian University of Science and Technology
Faculty of Natural Sciences
Department of Chemical Engineering

NTNU
Norwegian University of
Science and Technology

NTNU
Norwegian University of Science and Technology

Thesis for the degree of Philosophiae Doctor

Faculty of Natural Sciences
Department of Chemical Engineering

ISBN 978-82-326-6555-6 (printed ver.)
ISBN 978-82-326-5274-7 (electronic ver.)
ISSN 1503-8181 (printed ver.)
ISSN 2703-8084 (electronic ver.)

Doctoral theses at NTNU, 2023:43

PRINTED IN NORWAY
NO - 1598

NORDIC SWAN ECOLABEL
Printed matter
2041 0731

Printed by Skipnes Kommunikasjon AS

Acknowledgements

There are many people without whom this thesis would not have happened. First and foremost, I am grateful to my supervisor, Prof. Sigurd Skogestad, without whom I would not have started, nor would I have finished this thesis. Thank you for your constant support and patience, for knowing when to motivate me and when to step back, for your willingness to share your vast knowledge and enthusiasm for process control, for challenging me with new and original ideas, even though at times it was overwhelming.

I am thankful to the process systems engineering group at NTNU for creating a supportive work environment both during my masters and PhD studies. Thank you all for keeping the group close, especially considering the changing nature of the group members, and despite a pandemic. I would like to extend my sincere thanks to Prof. Johannes Jäschke and Prof. Heinz Preisig for your kindness, always being open to discussions and offering a different perspective. Many thanks to my colleagues for our time at the office, our lunch and coffee breaks discussions, and also for our time outside the working hours. Special thanks to my office mates Mandar, Adriana, Julian, David, Zawadi and Haakon. Cheers to Bahareh, Fabienne, Andrea, Timur, Tamal, Dinesh, Eka, Adriaen, Christoph, Allyne, Lucas, Ana, Carol, Jose, Leonardo, Risvan, Sigve, Tobias, Cansu, Niloufar, Saket, Simen, Evren and Peter.

I would like to thank Krister Forsman for our always inspiring and

insightful discussions on industrial control problems. Many thanks to Nick Alsop for your insight on industrial nonlinear control. I would also like to thank to my cosupervisor Lars Nord, and to Jenő Kovács for your insights on power plants.

Many credits go to the master students I supervised and worked with: Eirik, Ida, Erik, Alexander, Simen and Callum. It was a pleasure to work with you and learn together with you.

I am much obliged to the IT department at NTNU for recovering my hard disk files when my PC was damaged.

Thanks to my friend Dan for proofreading parts of this thesis.

I gratefully acknowledge the financial support from NTNU and FME HighEFF financed by the Research Council of Norway.

Lastly, I would like to thank to the PhD evaluation committee, Prof. Tore Hägglund, Dr. Knut Wiig Mathisen and Prof. Heinz Preisig for reading and making suggestions for improving this thesis.

Cristina Zotică
Trondheim, Norway
February 2023

Abstract

The work presented in this thesis is part of FME HighEFF - Centre for an Energy Efficient and Competitive Industry for the Future. This thesis explores broad topics in the area of optimal control and operation of thermal energy systems and it is divided into three parts.

Part I is entitled *Optimal operation and control of heat-to-power cycles: a new perspective from a systematic plantwide control approach.* It aims at giving an understanding of the operation and control problem for steam cycles from a plantwide perspective. The analysis concerns a steam cycle with one pressure level and producing power only. The reason for choosing this process is that it is an extremely important thermal process where well-functioning control structures have been developed over many years, and the aim was to study the present control schemes as see if they could be improved by applying a systematic plantwide control approach. The contribution is twofold, consisting of a steady-state, and a dynamic analysis. The former considers the optimal operation and control problem for a heat-to-power cycle and provides a clear and systematic procedure for identifying the operational objectives, specification or constraints and degrees of freedom from a steady-state point of view. The latter examines the dynamic performance of different control structures that can be used to implement optimal operation.

Part II is entitled *Transformed inputs for linearization, decoupling and feedforward control.* It aims at providing a systematic theory for many

nonlinear model-based calculation blocks used in power plants and the chemical industry. These blocks include but are not limited to cascade control, ratio, decoupling or nonlinear feedforward. It introduces inputs transformation derived from a nonlinear process model with the purpose of transforming a nonlinear system into a linear and decoupled system which also has perfect feedforward disturbance rejection. The main assumptions are that there are as many outputs as inputs, and that disturbances, and in some cases additional states can be measured. The transformed inputs can be derived from both a static and a dynamic model. For dynamic systems, this theory is similar to feedback linearization for systems with relative order 1. For higher order systems, we may introduce additional process measurements to account for unmeasured process dynamics or may introduce a chain of transformations. Three implementations are proposed: model-based, feedback-based, and a combination of the two. The first option inverts the process model and, with perfect measurement and perfect model, gives perfect feedforward action, linearization and decoupling both dynamically and at steady-state. Because it requires an inversion, it cannot handle process delays and unstable zero-dynamics (equivalent to right-hand plane zero for linear systems). The second option, uses a fast inner controller and does not require inverting the process model. This is important for higher order systems where the input (u) does not appear explicitly in the output (y) model equation but has an effect through some internal states (w). However, the response is not perfect dynamically because of the dynamics introduced by the inner controller. Several simulation examples are presented. These include case with a static model used to derive the input transformation and applied to a dynamic process model. Because of the model difference, the response may not be perfect dynamically, but some disturbance rejection properties are kept. The process-model mismatch and unmeasured dynamics are handled by an outer linear PID controller.

Finally, Part III is entitled *Handling constraints on manipulated variables*

used for inventory control to balance supply and demand. Specifically, it studies implementing optimal operation to cover cases of manipulated variables (MVs) saturation. The proposal is to use classical decentralized control elements such as split range control or controllers with different setpoints in combination with min or max selectors. Two applications are analyzed. The first advocates the use of a bidirectional inventory control structure that is able to maximize production when temporary or permanent bottlenecks occur for multiple units in series by employing the buffer inventories at intermediate storage. This bidirectional inventory control scheme has for each inventory two controllers, one for the inflow and one for the outflow, with high and low inventory setpoints, respectively. The inventory can typically be liquid (level) or gas (pressure). When production cannot be maintained without breaching physical constraints on the inventory, this control structure automatically reconfigures the loops for consistent inventory control, which means that it is radiating around the throughput manipulator to assure local consistency and feasible operation. The second application is a district heating network composed of a waste heat boiler, an electric boiler, a dump, a hot water storage tank, and a set of consumers. Three alternatives for the supervisory control layer are compared: split range control, controllers with different setpoints, and model predictive control. The closed-loop performance in the face of time-varying supply and demand, and using constant electricity prices is evaluated. All alternatives were found to give similar performance. Controllers with different setpoints is the easiest to implement, while model predictive control is the most difficult.

Contents

List of Figures

List of Tables

Nomenclature

Acronyms

CV	Controlled variable
DHN	District heating network
DV	Disturbance variable
FC	Flow controller
IC	Inventory controller
LC	Level (holdup) controller
LHP	Left-hand plane
LHS	Left-hand side
MISO	Multiple-input single-output
MPC	Model Predictive Control
MV	Manipulated variable
N/A	Not applicable
OTB	Once through boiler

OTSG	Once through steam generator
PC	Pressure controller
PID	Proportional-integral-derivative controller
RHP	Right-hand plane
RHS	Right-hand side
SISO	Single-input single-output
SRC	Split range controller
TC	Temperature controller
TES	Thermal Energy Storage
TPM	Throughput manipulator
VC	Transformed variable v controller
VPC	Valve position controller
WC	Work (power) controller

Greek letters

α	Slopes in split range block
ϵ	Constant compressibility coefficient in Part III
γ	Steam heat capacity ratio
$\mathcal{T}_A$	Inverse of tuning parameter A
μ	Molar mass [kg/mol]
ω	Grid frequency in Part I [Hz]

ω	Weights in the objective function in Part III
ϕ	Turbine constant mass flow coefficient
ρ	Water density [kg/m^3]
ρ_d	Relative order of a system wrt. to disturbance d
τ	Open loop time constant
τ_C	Closed-loop time constant
τ_I	Integral time
τ_T	Tracking time for back-calculation antiwindup
θ	Effective time delay

Mathematical notations

$f(\cdot)$	General nonlinear dynamic process model
$f(\cdot)_0$	General nonlinear static process model
$g(\cdot)$	General nonlinear function defining the transformed input v
$h(\cdot)$	General nonlinear function defining the transformed output z
J	Objective function or operational cost
max	Maximum
mid	Logic block that selects the middle value of its inputs
min	Minimum

Subscripts

A	Attemperator

NOMENCLATURE

B	Bypass
C	Condenser
D	Drum
E	Economizer
G	Generator
P	Pump
S	Superheater
T	Turbine
V	Steam valve

Superscript

g	Flue gas
p	Process in Part I
ref	Reference thermodynamic state
s	Setpoint in Part II and III
s	Steam (usually dropped)
sp	Setpoint in Part I
vap	Vaporization
w	Water (usually dropped)
0	Inlet condition

Variables

xxx

NOMENCLATURE

$1/R$	Droop proportional gain
$\bar{F}$	Average flowrate [kg/s] or [m^3/s]
ΔP	Pressure drop over the valve assumed constant [Pa] or [bar]
A	Tuning parameter for transformed input derived from dynamic model
A_r	Cross-sectional area [m^2]
B	Tuning parameter for transformed input derived from dynamic model
B_0	Tuning parameter for transformed input derived from static model
c_p	Specific heat capacity [J/kg/°C]
C_v	Valve coefficient
d	Disturbance
D_G	Electrical damping coefficient (machine base)
F	Flowrates [kg/s] or [m^3/s]
$F(u)$	Valve characteristic in Part II
$f(z)$	Valve characteristic, assumed linear, i.e. $f(z) = z$
F_c	Flowrate of cold side stream [kg/s]
F_h	Flowrate of hot side stream [kg/s]
H	High level setpoint in Part II
H	Level in Part II
h	Enthalpy in Part I
h	Level [m]

NOMENCLATURE

$H(T,p)$	Specific enthalpy
k	Steady-state gain
k'	Initial slope
K_c	Proportional gain
K_I	Integral gain
K_v	Control valve coefficient
L	Load
L	Low level setpoint in Part II
M	Holdup (mass)
m	Mass [kg]
m	Mass flow rate in Part I
M_G	Angular momentum of the generator (machine base)
n	System's order in Part III
n	Turbine speed in Part I
p	Network pressure [bar]
p	Pressure [bar]
p_0	Pressure of steam supply [bar]
p_{HC}	High pressure consumer [bar]
p_H	High pressure [bar]
p_{LC}	Low pressure consumer [bar]

NOMENCLATURE

p_L	Low pressure [bar]
Q	Energy or power [W]
q	Hot water flowrate to consumers [m^3/h]
q_D	Hot water flowrate to dump
q_F	Feedwater flowrate [m^3/s]
q_S	Hot water flowrate from variable heat source [m^3/h]
q_{EP}	Hot water flowrate from electric boiler to pipelines [m^3/h]
q_{SP}	Hot water flowrate send directly from source to pipelines [m^3/h]
q_{ST}	Hot water flowrate from source to charge the storage tank [m^3/h]
q_s	Steam flowrate [m^3/s]
q_{TP}	Hot water flowrate from tank to pipelines [m^3/h]
R	Gas constant bar m^3/mol/K
r	Relative order of a system wrt. to the input u
T	Temperature [°C] or [K]
t	Time [s], [min] or [h]
t_b	Buffer time [min] i.e., time until a bottleneck can be contained
T_c	Temperature of cold side stream outlet [°C]
T_H	Temperature of high pressure steam [°C]
T_h	Temperature of hot side stream outlet [°C]
T_h	Temperature of hot water in storage tank [°C]

T_L	Temperature of low pressure steam [°C]
T_S	Temperature of heat source [°C]
T_T	Temperature at turbine outlet for steam network example [°C]
u	Input or manipulated variable
UA	Heat transfer coefficient times heat transfer area [W/K]
v	For split range controller, the internal PI controller output to the split range block
v	Transformed input in Part III
v_0	Transformed input derived form a static model
v_A	Transformed input derived from a dynamic model
V_H	Volume of high pressure header [m^3]
V_h	Hot water volume [m^3]
v_H	Transformed input controlling the high pressure for the steam network example
V_L	Volume of low pressure header [m^3]
v_L	Transformed input controlling the low pressure for the steam network example
$v_{0,w}$	Transformed input derived form a static model using measurement of w
V_{Tank}	Design volume [m^3]
W	Mechanical Power

NOMENCLATURE

w	Algebraic states in Part I
w	Other measured dependent variables (states) in Part II
x	Differential states in Part I
x	Internal variables (states) in Part II
y	Output or controlled variable
z	Transformed output in Part II
z	Valve position
z_{HC}	High pressure consumer valve for steam network example
z_H	High pressure steam supply valve for steam network example
z_{LC}	Low pressure consumers valve for steam network example
z_{TB}	Turbine bypass valve for steam network example

Chapter 1

Introduction

1.1 Motivation

The work presented in this thesis is part of FME HighEFF - Centre for an Energy Efficient and Competitive Industry for the Future (HighEFF, 2022).

Within the scope of HighEFF, the initial motivation of this thesis was to analyze the optimal operation and control problem of heat-to-power cycles. Therefore, the motivation of the first part of the thesis is to systematically identify the control objectives, operational and environmental constraints, and degrees of freedom for a heat-to-power cycle. However, it quickly became apparent that control strategies of industrial power plants has been developed over many years to a stage where they are adopted by many plants and work extremely well and it is not straightforward to make improvements. Many of these control structures make extensive use of nonlinear model-based calculation blocks, function blocks, or ratio stations to provide feedforward action, decoupling or linearization (adaptive gain). These examples are case-specific based, and a systematic theory for developing these calculation blocks is missing in the literature. It is therefore the motivation of the second part of the thesis to give a systematic theory for deriving in a systematic manner these

model-based calculation blocks, which we will call input transformations.

Finally, the third part of the thesis aims at implementing optimal operation for inventory control systems used to balance supply and demand. The motivation is to design a supervisory control layer that can handle active manipulate variables (MVs) or controlled variables (CVs) constraints changes, using classical control elements such as split range control (SRC) or PID-controllers with different setpoints in combination with selectors or other simple logic blocks.

1.2 Scope

This thesis is divided in three parts which aims at answering the following questions:

Part I: Optimal operation and control of heat-to-power cycles: a new perspective from a systematic plantwide control approach. What are the operational objective, degrees of freedom and constraints for steam (heat-to-power) cycles? What are the resulted operational strategies? What control structures can we use to implement these resulting operational strategies?

Part II: Transformed inputs for linearization, decoupling and feedforward control. How to derive input transformations that give feedforward, linearization and decoupling in a systematic manner? How to implement the input transformations? How does it relate to previous methods? How to handle higher order systems? What happens if a dynamic model is not available? What happens if we apply a transformed input derived from a static model to a dynamic process? What are the limitations?

Part III: Handling constraints on MV used for inventory control to balance supply and demand. How to handle MV-saturations for inventory control problems used to balance supply and demand? How to switch automatically between using different MVs to control the same CV? How to give up automatically controlling less important CVs? How to maintain production for tanks in series by employing the intermediate inventory?

1.3 Thermal energy systems

The processes analyzed throughout this thesis fall under the general terminology of *thermal energy systems*.

Let us first define a system. Figure 1.1 shows a schematic representation of a system which is as a special domain separated by a boundary from the environment, and which may be composed of several sub-systems interacting with each other and with the surrounding environment (Preisig, 2020).

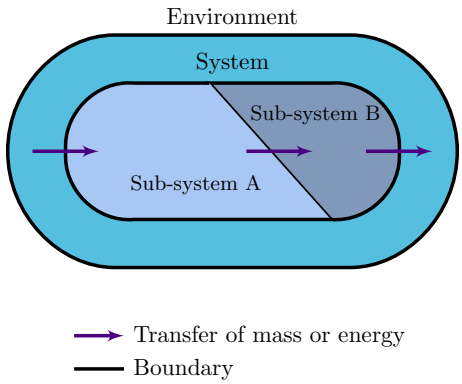

Figure 1.1: Schematic representation of a system and its subsystems separated by a boundary from an environment.

In the context of this work, a thermal energy system refers to transfer

of energy as heat or cooling between between the different subsystems of the system or to the surroundings through boundaries, by convection (i.e., with the fluid) or conduction (i.e., direct contact). Examples include heat exchangers, mixers, tanks used for hot water storage, district heating networks (or more specifically the transport pipelines) or steam networks. It also includes the conversion of heat to mechanical power in a turbine driving an electrical generator to produce electrical power.

1.4 Thesis structure and main contributions

As mentioned before, this thesis is divided into three main parts. Part I presents a new perspective on optimal operation and control of heat-to-power cycles from a systematic plantwide control approach. It consists of a steady-state and a dynamic analysis. The former considers the optimal operation and control problem for a heat-to-power cycle and provide a clear and systematic procedure for identifying the operational objectives, specification or constraints and degrees of freedom from a steady-state point of view. The latter examines the dynamic performance of different control structures that can be used to implement optimal operation. This part is based on (Zotică et al., 2020b).

Part II introduces input transformations for linearization, decoupling and feedforward control. Section 3.1 presents the three-elements drum level control used in power plant as an example supporting the need for a systematic theory for deriving the many nonlinear model-based calculation blocks used in the industry. Section 3.3 gives a brief overview of related methods in the literature. Section 3.4 introduces the theory for deriving transformed inputs from both a static and dynamic model, and Section 3.5 presents how to implement these transformations. Sections 3.7-3.10 present applications and the simulation results of transformed inputs (and outputs) for different thermal energy systems, e.g., mixing processes, heat exchangers and steam

networks. This chapter is adapted from (Skogestad et al., 2023; Zotică et al., 2020a; Zotică and Skogestad, 2021; Zotică et al., 2022).

Part III presents handling constraints on manipulated variables (MVs) used for inventory control to balance supply and demand. Chapter 4 describes a general system for balancing supply and demand by using inventory control. It proposes to handle saturation of the MV used for inventory control by implementing MV-MV switching (split range control or controllers with different setpoints) and potentially CV-CV switching (min or max selectors). Chapter 5, based on (Zotică et al., 2022), advocates the use of bidirectional inventory control to maximize production when temporary or permanent bottlenecks occur for multiple units in series by employing buffer inventories at intermediate storage. Chapter 6, based on (Zotică et al., 2021), compares three alternatives for designing the supervisory control layer of a district heating network with a thermal energy storage tank. The control objective is to minimizes the use of the more expensive electric boiler by using cheaper waste-heat first, and storing excess heat for later use.

Part IV concludes this thesis with the main findings and future research directions.

1.5 Papers not included in this thesis

The following co-authored published papers are related to the topics covered in this thesis. However, these publications are not included in the thesis.

1. Reyes-Lúa A., Zotică C., Das T., Krishnamoorthy D. and Skogestad S. Changing between active constraint regions for optimal operation: classical advanced control versus model predictive control. Computer aided chemical engineering, 43:1015-1020, 2018.

2. Reyes-Lúa A., Zotică C. and Skogestad S. Optimal operation with changing active constraint regions using classical advanced control.

IFAC-PapersOnLine, 51(18):440-445, 2018.

3. Reyes-Lúa A., Zotică C, Forsman K. and Skogestad S. Systematic design of split range controllers. IFAC-PapersOnLine, 52(1):898-903, 2019.

4. Rohde D., Andresen T., Zotică C. and Wilpert P. Energy recovery from furnace off-gas: Analysis of an integrated energy recovery system by means of dynamic simulation. Refrigeration science and technology, 373-380, July 2020.

Part I

Optimal operation and control of heat-to-power cycles: a new perspective from a systematic plantwide control approach

Chapter 2

Optimal operation and control of heat-to-power cycles

This chapter presents using a plantwide control framework to systematically identify the control objectives, operational and environmental constraints, and degrees of freedom for a heat-to-power cycle with a drum, one pressure level and with power as the only valuable product. The result is an unified and systematic perspective on the optimal operation and control problems for heat-to-power cycles.

The chapter is based based on the article "Optimal Operation and Control of heat-to-power Cycles: a New Perspective from a Systematic Plantwide Control Approach" (Zotică et al., 2020b).

2.1 Introduction to heat-to-power cycles

Current industrial control solutions for thermal power plants[1] have evolved over the years based on industrial practices to a stage where it becomes less trivial to understand what are the operational objectives, constraints or degrees of freedom available for optimal operation. Moreover, their transfer to new cases or use by newcomers in the field may not be straightforward.

Often plant operators take established practices for granted, mainly because it has always been done in the same way. On the other hand, optimal operation changes with current operating conditions, i.e. feed composition, product specification, prices or equipment which are subject to change during the operating life of a plant. However, it is difficult to identify the new optimal operation if the control policy is not systematically specified from the beginning.

This effect is particularly marked for steam cycles providing utilities (e.g. steam and power) for downstream units in chemical plants. In these cases, optimal operation of the steam cycles is often overlooked. However, considering the large amount of utilities used in chemical processing, there is much to gain from operating steam cycles at their optimum. For example, we consider the implication of controlling the superheated steam pressure. Often power plants are operated at constant pressure to provide faster changes in produced power. However, operation with floating pressure (i.e. the steam pressure follows the fuel rate) could potentially result in higher efficiency at low load for fossil fuel steam cycles (Silvestri et al., 1972) and especially for combined cycles (i.e. integration of a gas turbine with a steam turbine) (Polsky, 1982), or co-generation plants (i.e. plant providing both heat and power) (Jonshagen and Genrup, 2010).

The contribution of this work is twofold, and consists of a steady-state and a dynamic analysis. The former considers the optimal operation and

[1] Thermal power plants, steam cycles and heat-to-power cycles are used interchangeably.

control problem for a heat-to-power cycle and provides a clear and systematic procedure for identifying the operational objectives, specification or constraints and degrees of freedom from a steady-state point of view. The latter examines the dynamic performance of different control structures that can be used to implement optimal operation.

We accomplish these objectives in the framework of plantwide control, which handles control structure decisions for the entire plant. The goal is to find a control strategy, preferably a simple one, that acts on a short time scale to stabilize the plant (regulatory control), and on a longer time scale to reach optimal economic operation (supervisory control). The advantage of using a systematic plantwide control procedure is that it might reveal new potentially overlooked control policies for existing processes (Downs and Skogestad, 2011).

Plantwide control has been extensively applied to chemical plants, but to a lesser degree for heat-to-power cycles in the open literature. For example, the work by (Niva et al., 2017) presents a plantwide control analysis for the combustion side of oxy-fired circulating fluidized bed boilers. The work by (Prasad et al., 2000) briefly discusses the use of a plantwide control approach to identify the main control objectives, operational constraints, degrees of freedom and controlled variables with the purpose of designing a model predictive control (MPC) strategy for a given thermal plant. The work by (Govatsmark, 2003) applies a plantwide control design procedure to a combined-cycle power plant. However, to the best of the authors knowledge a thorough analysis from a plantwide control perspective for steam cycle is missing, and it is therefore formalized in this work.

2.2 Plantwide control

The typical control hierarchy in a process plant is decentralized and is decomposed on a time scale basis into several simpler layers: scheduling

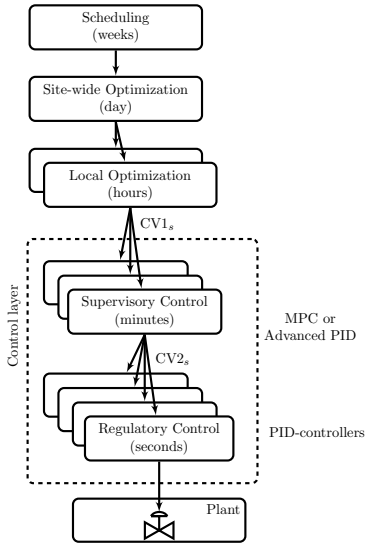

Figure 2.1: Typical control hierarchy in a process plant.

(weeks), site-wide optimization (days), local optimization (hours), supervisory control (minutes) and regulatory control (seconds), as shown in Figure 2.1. Note that some processes can be slower. The top layers are responsible for production planing on a long time scale, while the lower control layer implements the setpoints given by the upper layer for optimal economic operation and stabilizes the plant. Each layer receives process measurements from the layers below, solves an optimization problem by using as degrees of freedom the setpoints to the lower layers (Skogestad, 2004).

To systematically design each layer, we use the plantwide control procedure proposed by (Skogestad, 2004). The procedure consists of a top-down analysis concerning optimal steady-state operation, and a bottom-up analysis targeting the lower control layer structure. The steady-state top-down analysis involves the following steps:

Step 1 Define the optimal economic operation problem: the objective cost

function J and the set of operational constraints.

Step 2 Identify the steady-state degrees of freedom (DOF) (i.e. setpoints for the lower layers). Determine the optimal operation for expected disturbances using a steady-state model.

Step 3 Implement optimal operation. Select the primary controlled variables (CV$\prime$) as the active constraints from *Step 2*, and the self-optimizing variables (for unconstrained degrees of freedom) (i.e. variables that give acceptable loss when kept at constant setpoint).

Step 4 Choose the location of the throughput manipulator (TPM), i.e. decide where to set the production rate. This is both a dynamic issue (with implications on the inventory control structure design), and an economic issue (minimize back-off from active constraints).

The bottom-up design focuses on the control layer, which is divided into the supervisory and the regulatory control layer.

The regulatory control layer typically takes care of control on the fastest time scale. Controlled variables in the regulatory layer (CV$\prime$) include variables that contribute to "stabilization" of the process, for example levels and pressures. In addition, they usually include a subset of the economic controlled variables (CV), typically active constraints, that should be tightly controlled for economic reasons. The regulatory layer is usually not subject to reconfiguration, so one should be careful about what happens if one has MV saturation in this layer (Reyes-Lúa and Skogestad, 2020). Considering the large number of control loops in a typical plant, simple PID-controllers are used for the regulatory layer.

The objectives of the supervisory (advanced) control layer are:

1. Achieve the economic objectives given by the upper optimization layers by controlling the primary CVs at setpoint using as degrees of freedom the setpoints to the regulatory layer or any unused manipulated variables.

2. Monitor the regulatory stabilizing layer to avoid saturation of MVs.

3. Identify active constrains and self-optimizing variables changes based on the current operation region, and switch the control structure.

The steps of the bottom-up design are:

Step 5 Design the structure of regulatory control layer. The main issues are: first, to select what to control on a fast time scale, both for stabilizing control, and to achieve tight control of important active constraints, and second, to chose appropriate MVs and pairings.

Step 6 Design the structure of supervisory control layer. Decide between centralized control (i.e. Model Predictive Control) or decentralized control (i.e. advanced control structures with simple logic block to handle changes in active constraints (Reyes-Lúa et al., 2018).)

Step 7 Design the real-time optimization layer. Its objectives are to identify the active constraints and compute the optimal setpoints for the lower supervisory layer. For many plants, this layer is missing as it requires a full model.

2.3 Plantwide control for a simple heat-to-power cycle

2.3.1 Process Description

We consider the steam side of a heat-to-power cycle as shown in the simplified process flowsheet in Fig. 2.2. Fuel is burned with air in stoichiometric ratio in a combustion chamber resulting in high temperature flue gases. Thermal energy carried by the flue gas superheats the working fluid (water) in a boiler. Then, it is converted to mechanical energy in a turbine, followed by conversion to electrical energy (W) in a generator connected to the grid.

In this paper, we consider only the steam side of the process, that is, the combustion side is excluded.

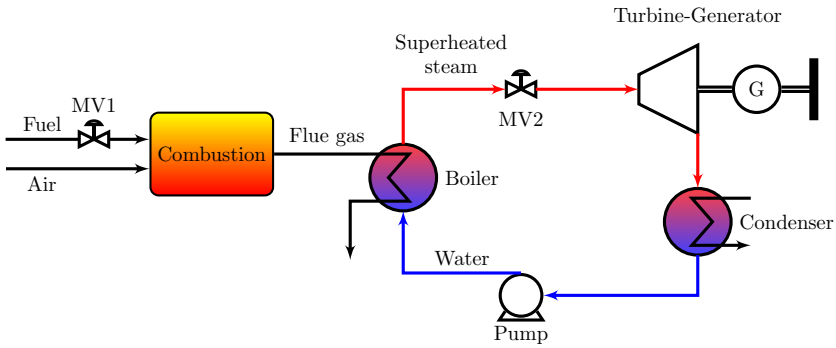

Figure 2.2: Simplified heat-to-power cycle flowsheet. The air feed is set in ratio to the fuel, but the combustion side of the process is not included in this work.

A detailed representation of the boiler-turbine system is shown in Fig. 2.3. The circulating working fluid (water) is heated from liquid (blue) to high-pressure superheated steam (red) by receiving heat resulted from burning fuel (MV1) (black) in a series of three heat exchangers dedicated to well defined regimes, i.e. economizer (heating to saturated liquid), drum (evaporation) and superheater (superheating). The superheated steam is desuperheated by spraying cold feed water in the attemperator, therefore this is a bypass stream of the three heat exchangers. The superheated steam is expanded in a condensing type turbine, which drives a generator supplying electricity to the electric grid. Cooling water (MV4) is used as utility in the condenser. The low pressure water is then boosted by a variable speed pump (MV5) and it is fed to the boiler (i.e. economizer). The cycle process also includes a bypass of the turbine (MV3), and a direct bypass of the economizer cold side (MV6).

We choose this drum configuration over a once-through boiler (with a single heat exchanger instead of three) because it is most common both in

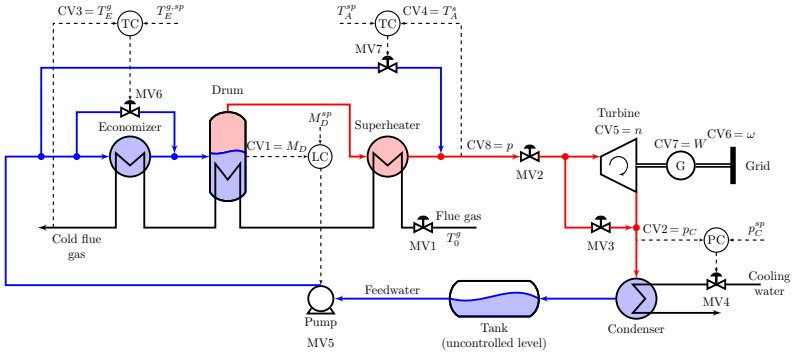

Figure 2.3: Flowsheet of a steam cycle with a drum boiler, one pressure level, and condensing turbine. The system has 7 manipulated variables (MVs). There are shown 8 potential controlled variables (CVs). After closing 4 regulatory loops for temperatures, pressure and level and noting that the bypass MV3 should be kept closed if possible, MV1 (fuel) and MV2 (steam valve) are the two remaining degrees of freedom (See also Table 2.1) and Section 2.3.2.4). Liquid water is in blue, vapor in red.

operating power plants, and in chemical plants with on-site steam generation. The once-through boiler is in theory more efficient because it does not have the requirement of saturation (and thereby a fixed feedwater for a given steam pressure) at a given location inside the heat exchanger sequence. For a once-through boiler, the feedwater (MV5) may be used to control the steam temperature. We choose a single steam pressure level because we want to have a simple base for our analysis on which we can expand. For the same reason, we do not include steam extraction or back-pressure turbines.

2.3.2 Top-down analysis

We proceed to formalize the control problem for steam cycles by applying the top-down analysis to the described process. Therefore we systematically identify the control objectives, operational and environmental constraints, degrees of freedom, main disturbances and the location of the throughput

manipulator.

2.3.2.1 Step 1. Operational objective

The plant has two operational objectives. On a slow time scale (steady-state) it should achieve the economic optimum, while it contributes to the grid stability on a fast time scale. Due to the time scale separation, these objectives are decoupled. However, the grid stability requirement may impose a back-off from the maximum power production. Depending on local conditions, the main operational objectives are:

1. Produce the energy as
   (a) power to the electric grid at the required voltage and frequency (usually large power plants with condensing turbines, i.e. $>$ 100 MW);
   (b) steam at the required flowrate and pressure level (usually for back-pressure turbines in large chemical plants);
   (c) power and steam (combined heat and power cycles);
2. Process a given amount of by-product (e.g. waste gases or biomass residues).

The same economic cost function, i.e. minimize the negative profit, can be defined for all operational objectives, given by Eq.2.1.

$$J = -(p_W W + p_S S - p_F F - p_U U) \qquad [\$/\text{s}] \tag{2.1}$$

Here, W [J/s] is the produced power, S [kg/s] is the produced steam ($= 0$ in this paper), F [J/s] is the fuel (energy source), U [kg/s] is the utility consumption, and p [\$/kg] or [\$/J] is the price of each. There may be additional terms, for example several feed energy sources or several steam

products. We analyze an operating plant and therefore, capital costs, personal, and maintenance costs are not included. The cost J should be minimized subject to satisfying a set of constraints, related to products specifications, safe operation and regulations related to the environment. Typical constraints for the operational objectives listed above for a steam cycle include (Prasad et al., 2000):

- C1 Keep the electrical power (W) at a given value. This is for plants required to participate in grid frequency regulation, i.e.$W \geq 100\,\mathrm{MW}$).
- C2 Produce steam at the required demand (for cycles providing steam as utility for chemical plants, and not included in the described process).
- C3 Stabilize the process (i.e. keep the unstable drum level within limits).
- C4 Keep the temperature of the superheated steam at a given value to maximize turbine work, but within boundaries to prevent large thermal gradients (i.e. $T_A^s = 529°\mathrm{C}$).
- C5 Keep the superheated steam pressure below a maximum value to avoid high thermal and mechanical stress and to extend the operating life (i.e. $p \leq p^{\max} = 220\,\mathrm{bar}$).
- C6 Keep the steam pressure above a minimum value to avoid boiler trip (i.e. $p \geq p^{\min}$).
- C7 Keep the temperature (T_E^g) of the flue gas outlet below environmental limits, and above dew point to prevent corrosion °C ($T_E^g \geq 150\,°\mathrm{C}$). Note that only plants with a higher concentration of pollutants (NOx or SO_2 have constraints on the maximum temperature, due to operation limits on the filters used to reduce emissions.
- C8 Keep MV4 fully open (i.e. MV4=MV4$^{\max}$) to bring the condenser pressure at lower limit to maximize the pressure ratio in the turbine (i.e. $p_C = 0.1\,\mathrm{bar}$).
- C9 Keep the turbine speed at the setpoint ($n = 50\,\mathrm{Hz}$). If connected to the grid, control is only needed at short time scale to avoid wear, because on a long time scale, the turbine speed is given by the grid frequency.

Note that industrial turbines are normally operated at constant speed, which can be the grid frequency or a different frequency (usually higher), depending on their design. In the latter, a gear box is used, but the turbine speed is still kept constant and it is not a degree of freedom available for operation. Variable speed turbines may be used for experimental low load organic Rankine cycles. However, variable speed turbines are out of the scope of this work, and the interested reader is refereed to the work by (Quoilin et al., 2011).

In addition to constraint C7, there are other operational constraints on the combustion side, including requirements for waste incineration, O_2, CO_2 and NO_x percentage in the flue gas or furnace pressure. However, a detailed analysis of the combustion side is outside of the scope of this paper, and we assume that these operational objectives are met on the combustion side of the process. The interested reader is referred to the work by (Niva et al., 2017) for an analysis on the combustion side for an oxy-fired circulating fluidized bed boiler.

2.3.2.2 Step 2 (a). Identify the steady-state degrees of freedom (DOF) (i.e. setpoints for the lower layers)

Table 2.1 shows the degrees of freedom together with comments on their implication to control. The MVs are also shown in Fig.2.3. Note that we have not decided yet on the pairing, and number of the MV and CV are not corresponding in the next sections (i.e. MV1 is not necessarily used to control CV1).

2.3.2.2.1 Steady-state effect of fuel (MV1) and steam valve (MV2)

Fig. 2.4 shows the open loop response for the superheated steam pressure (CV8 = p), and power produced (CV7 = W) to 1% increase in fuel MV2 in blue, and to fully opening the steam valve (MV2 = 1) in green. Let us explain the open loop response from physical considerations. Consider the

Table 2.1: Manipulated variables

Manipulated variable	Comments, analysis
MV1: Fuel	• At steady-state the power produced can only be changed by manipulating (MV1).
MV2: Steam valve	• The turbine valve should optimally be fully open to minimize throttling losses (Shinskey, 1978). • It has mainly a dynamic effect, as the steady-state effect on produced power is insignificant. • It can improve the dynamic response for power. • To contribute to grid frequency stability it may be required at nominal conditions to partly close the steam valve opening (e.g. 90 %). This will provide a back-off for transient operation.
MV3: Turbine bypass	• Normally closed, needed when the energy in the feed is larger than power demand. • Used to avoid too high pressure, i.e. if $p \geq 220$ bar, MV3 opens to reduce the pressure.
MV4: Cooling water	• Open at MV4=$\text{MV4}^{\max}$ to minimize condenser pressure (p_C).
MV5: Feedwater pump	• Use only to control the drum level. • Cannot be used to control the steam pressure, as it has no steady-state effect (see Table 2.3).
MV6: Economizer bypass	• Use only if $T^g < T^{g,\min}$.
MV7: Attemperator	• Use only if $T^s > T^{s,\max}$.

linear valve $m = zK_V\Delta P$ where, m is the mass flow rate, z is the valve opening, K_V is the valve coefficient and ΔP is the pressure drop across the valve. Increasing z causes a fast increase of m, which results in a decrease of the pressure inventory before the valve. The latter results in a smaller ΔP, which results in a decrease of m after its initial increase. To increase m at steady-state, ΔP has to increase, and this can only be achieved by increasing the energy supplied to the system (MV1).

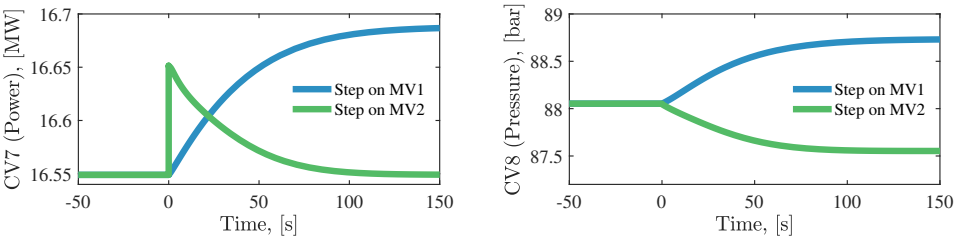

(a) Power **(b)** Pressure

Figure 2.4: Open loop responses for pressure (p) at the valve inlet and power (W) to a step increase of 1% step increase in fuel (MV1) (green), and 0.1 in steam valve opening (MV2) (blue).

2.3.2.3 Step 2 (b). Identify the most important disturbances

The main disturbances for this process are given in Table 2.2.

2.3.2.4 Step 2 (c). Determine the optimal operation (including active constraints) for the expected disturbances using a steady-state model

Active constraints (AC) are variables that should be kept at their limiting value for optimality. To determine which constraints will be active, we can optimize the process at steady-state for the important disturbances. However, engineering insight is often enough to determine which constraints are active, and this is the approach we apply in this work. At the nominal operation

Table 2.2: Main disturbances for steam cycle

Disturbance variable	Comments
DV1: Combustion temperature	Typically for waste heat
DV2: Fuel specific heat	Typically for waste heat
DV3: Grid frequency (Load)	Consumers increasing their demand (load) or producers decreasing their production
DV4: Required power setpoint	Typically for power plants required to participate in secondary or tertiary grid frequency regulation
DV5: Cooling water temperature	

we want to minimize bypass streams, that is the turbine bypass MV3, the economizer bypass MV6 and the attemperator MV7 should be closed to use the boiler efficiently. However, when a CV constraint becomes active, we use the MV to control the respective CV. This implies a CV-MV switch, and it can be handled by single loop PID-controllers without additional logic given that antiwindup is implemented (Reyes-Lúa and Skogestad, 2020).

The active constraints are:

(AC1) MV3=0 (MV constraint);

(AC2) MV4=MV4$^{\max}$ (MV constraint) or CV2 = $p_C = p_C^{\min}$ (CV constraint) to maximize pressure ratio across the turbine and maximize work (W);

(AC3) MV6=0 (MV constraint) or CV3 = $T_E = T_E^{g,\min}$ (CV constraint) to maximize boiler heat transfer area usage;

(AC4) MV7=0 (MV constraint) or CV4 = $T_A^s = T_A^{s,\max}$ (CV constraint) to minimize desuperheating and maximize superheated steam temperature;

(AC5) $n = \omega$, (i.e. the turbine speed is equal to the grid frequency).

We use the term *or* for AC2, AC3 and AC4 because maximizing cooling (MV4=MV4$^{\max}$) results in $p_C = p_C^{\min}$, closing the economizer bypass stream (MV6=0) gives minimum temperature $T_E = T_E^{g,\min}$, and closing the attemperation stream (MV7=0) gives maximum $T_A^s = T_A^{s,\max}$. When $p_C < p_C^{\min}$, we give-up MV4=MV4$^{\max}$ and use MV4 to increase p_C. When $T_E < T_E^{s,\min}$ we give-up MV6=0 and open MV6 to increase T_E^g. When $T_A^g > T_A^{s,\max}$ we give-up MV7=0, and open MV7 to decrease T_A^g. As mentioned, this CV-MV switch is handled by PID-controllers without additional logic block.

2.3.2.5 Step 3. Economic controlled variable (CV) selection

The objective is to select controlled variables such that we keep optimal (or near optimal) operation when disturbances occur. The first controlled variables candidates are the active constraints from Section 2.3.2.4, as well as variables that need to be controlled to stabilize the process. Table 2.3 shows the possible controlled variables including the active constraints (a subset of the operational constraints from *Step 1* in Section 2.3.2.1).

2.3.2.6 Step 4. Location of throughput manipulator

The location of the throughput manipulator (TPM) is important from a dynamic point of view as it determines the structure of the inventory (pressure) control system and also affects the dynamic performance for cases when the TPM is used for control. In general, the TPM can be located at the feed, inside the process or at the product. For a power plant, the "product" is the turbine power output (W), which ideally is given by Eq. 2.2.

$$W = \int_{p_T}^{p_C} \dot{V} dp \tag{2.2}$$

where $\dot{V}$ [m^3/s] is the volumetric flow, p_T and p_C [Pa] are the turbine inlet and outlet pressures. The volumetric flow is affected mainly by the turbine

Table 2.3: Candidates controlled variables

Controlled variable	Comments, analysis
CV1: Drum level (M_D)	• Levels are unstable inventories and they need to be controlled • No steady-state effect
CV2: Condenser pressure (p_C)	• See Section 2.3.2.4
CV3: Cold flue gas temperature (T_E^g)	• See Section 2.3.2.4
CV4: Superheated steam temperature (T_A^s)	• See Section 2.3.2.4
CV5: Turbine speed	• Active constraint for all operation regions.
CV6: Grid freqeuncy	• Imposed by grid stability
CV7: Power produced	• Only for plants required to participate in grid frequency regulation
CV8: Steam pressure	• Given by the fuel (MV1) according to the boiler energy balance • Should not be at fixed setpoint to utilize the fuel and boiler efficiently

speed, which is assumed to be fixed in this work (equal to the grid frequency). Note that the inlet pressure p_T is affected by the steam valve MV2. In summary, for our plant, there are two possibilities for the TPM location:

- TPM at the feed, that is, the fuel (MV1) is the TPM
- TPM inside the plant, that is, the steam valve (MV2) is the TPM.

In many cases, the fuel rate is given (typically for base load boilers) or the fuel rate is limiting the power output. In such cases, we clearly want to have the TPM located at the feed (MV1) in order to maximize power production. This case is considered briefly in the discussion section, but otherwise the main focus of this paper is when the power demand is given. To track variations in the power demand, it would be best from a dynamic point of view to locate the TPM at the steam valve (MV2) at the inlet to the power-producing turbine. Nevertheless, most control structures use the fuel (MV1) as the TPM also in this case, and there are several main reasons for this. First, it may happen that one would like to operate with a fixed fuel under some conditions. Second, as seen from Fig. 2.4, the steady-state effect of the steam valve (MV2) on the power (W) is very small when we have a constant fuel rate (MV1) and in addition we may want to operate with a fully open steam valve to minimize throttling losses. Third, the pressure drop over MV2 is more a dynamic performance matter. The higher the pressure drop, the higher the energy and mass stored in the boiler, and therefore the system has better capability to change the load at the required rate (e.g. %/min).

2.3.3 Bottom-up design

We continue with the bottom-up design for the described process.

2.3.3.1 Step 5. Structure of the regulatory layer

Liquid levels generally need to be controlled to maintain stability (see Section 2.2). The power cycle in Fig. 2.3 contains two liquid levels, but since this is a closed system only one of them should be controlled, usually the smallest holdup. Thus, we decide to control the boiler drum level (CV1 = M_D) and leave the feedwater tank level uncontrolled. The steady-state value of M_D does not matter, except that it contributes to energy storage, which has dynamic implications. Next, the steam pressure (CV8 = p) is often controlled because it may be drifting, and control of it may contribute to more stable and predictable operation. However, as we will see, control of steam pressure requires closing the steam valve (MV2) which gives losses and is not optimal from an economic point of view. We will therefore not include control of CV8 in the regulatory layer, but will leave for the supervisory control layer (step 6 in Section 2.4). Condenser pressure (CV2 = p_C) is usually also controlled, both because this contributes to stability and because it is optimal to keep it above its lower constraint to avoid too much liquid at the outlet of turbine. Two other constraints that are controlled in the regulatory layer are superheated steam temperature (CV4 = T_A) and cold flue gas temperature (CV3 = T_E). CV4 must be below a maximum for material reasons in the turbine and CV3 should be above a minimum, for example, to avoid corrosion caused by condensation. In the regulatory layer, we usually use single-loop PID control, so for each CV we need to identify an appropriate input (MV). We can make a decision based on mathematical tools such as the relative gain array (RGA). Alternatively, as in this work, we can use guidelines such as the pair close rule (i.e. small effective time delay from the MV to CV), or, input saturation rule (i.e. pair an important CV (which cannot be given-up) with an MV that is unlikely to saturate (Reyes-Lúa et al., 2018)).

We have 7 manipulated variables, but for economic reasons the turbine bypass (MV3) should always be closed. The steam valve (MV2) and fuel (MV1) will be used for control of power production and pressure in the

supervisory layer. Thus, to control CV1, CV2, CV3 and CV4 we have as manipulated variables MV4, MV5, MV6 and MV7. We follow the pair-close rule, and suggest the following pairings for the regulatory layer:

- Use the cooling water (MV4) to control the condenser pressure (CV2);
- Use the feedwater pump (MV5) to control the drum level (CV1) (only DOF left to control the level)
- Use the economizer bypass (MV6) to control the flue gas temperature (CV3)
- Use the attemperator (MV7) to control the superheated steam temperature (CV4) (only DOF available)
- Assume turbine speed is equal to the grid frequency

Note that MV4, MV6 and MV7 are likely to saturate at maximum cooling, zero bypass and zero bypass, respectively. Fortunately, this is not a problem, because when we reach one of these constraints, it is optimal to give up control of the corresponding CV. This happens because the corresponding CV will move away from its constraints of minimum pressure (CV2), minimum flue gas temperature (CV3) and maximum steam temperature (CV4), respectively. Thus, no further attention from the supervisory control layer is required when these saturations happen.

2.4 Step 6. Control structures for supervisory control

From an optimal operation point of view, we want on a slow time scale to maximize boiler efficiency (i.e. keep bypass streams closed and let the pressure float) and minimize throttling losses (i.e. keep all valves close to maximum). On a short time scale we may need participate in grid frequency

control. We can meet both objective due to their time scale separation, and this requires using the steam valve (MV2) dynamically, and drive to its nominal opening (e.g. 90 % (Weissbach et al., 2006)) at steady-state.

We assume that all other loops are closed according to the pairing from section 2.3.2.5, and therefore we analyse only the two remaining degrees of freedom: MV1 (fuel) and MV2 (steam turbine valve). The remaining CVs from Table 2.3 are the power produced (CV7 = W) and the superheated steam pressure (CV8 = p). The main issues that we consider concern:

1. pairing, that is what to do with the remaining degrees of freedom, MV1 and MV2?

2. should the pressure be controlled?

In the following, we show a simplified flowsheet of the steam side, with the two remaining degrees of freedom: MV1 (fuel) and MV2 (steam valve). The boiler illustrated symbolizes the economizer and its bypass, drum, superheater and attemperator.

We analyse the case where we want to keep the power produced at its setpoint, and we start by presenting the common control structures in industrial steam cycles.

2.4.1 Standard industrial control structures for control of power and pressure

The standard industrial control structures are boiler driven, turbine driven, floating pressure and its variation, sliding pressure (Klefenz, 1986; Welfonder, 1999; der Autumation, 2003). The objective of this analysis is to understand their steady-state and dynamics characteristics.

2.4.1.1 Floating pressure operation

In floating pressure operation mode, Figure 2.5, the superheated steam pressure (CV8) is not controlled, and it is given by the fuel (MV1), according to the energy balance. The power produced can be controlled by manipulating the fuel (MV1), the only DOF with a significant steady-state effect. Floating pressure operation is optimal from an energy point of view because it allows for the steam valve (MV2) to be fully open. When we say that steam valve is opened, it may well be partly open because of the back-off required to participate in droop control (see the discussion in Section 2.6.3). However, because of the boiler inertia, this operation mode has a slow time constant for controlling the power produced. When the pressure becomes an active constraint (i.e. $p = p^{\min}$ or $p = p^{\max}$), we give-up controlling the power using MV1 (fuel), and use it to control the pressure instead. This is called CV-CV switching, and we can use a *MID* block (i.e. logic to select the middle output of all three controllers). Note that it is more efficient to use MV1 (fuel) directly to control the pressure once it reaches its maximum limit than using MV3 to bypass the steam turbine. Also note that all control structures imply a MID selector to keep the pressure within bounds, but this is not shown to simplify the illustrations.

2.4.1.2 Boiler driven operation

In boiler driven operation mode, the power produced is kept at setpoint by manipulating the fuel MV1 (the throughput manipulator in this case), while the superheated steam pressure is kept at constant setpoint using the steam valve MV2, as shown in Figure 2.6. For this reason, boiler driven can be considered as an extension of floating pressure. In this case, MV2 can only be used to improve the dynamic response of the cycle, as it has a negligible steady-state effect (see Figure 2.4).

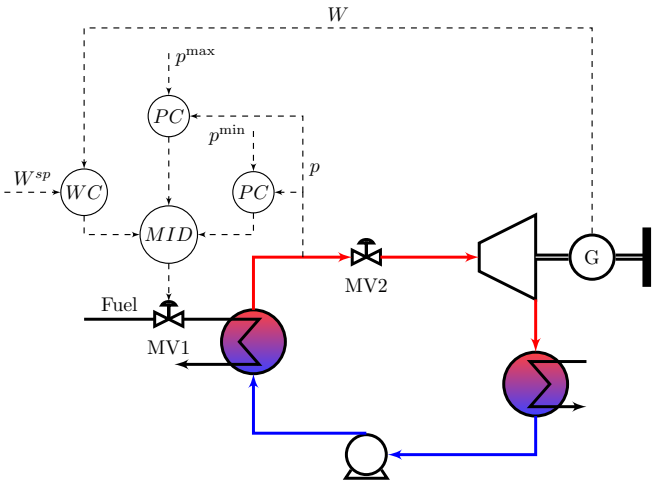

Figure 2.5: Floating pressure operation mode with a MID selector to keep the pressure within bounds ($p^{min} \leq p \leq p^{max}$).

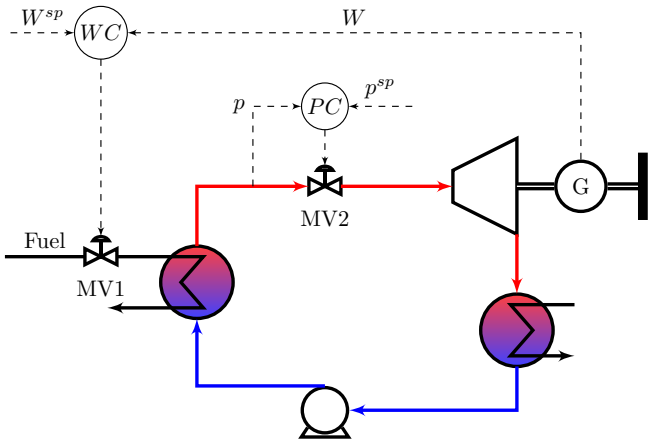

Figure 2.6: Boiler driven operation mode

2.4.1.3 Turbine driven operation

Turbine driven is the reverse pairing of boiler driven, i.e. the power produced is controlled using the steam valve MV2 (the throughput manipulator in this case), and the steam pressure is controlled using the fuel MV1, as shown in Figure 2.7. Its advantage is a faster time response for control of power (CV7 = W).

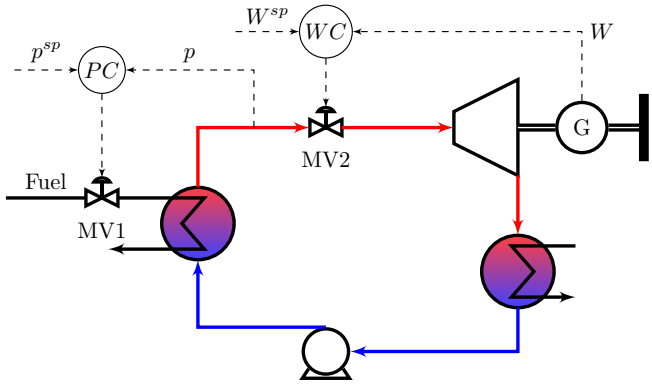

Figure 2.7: Turbine driven operation mode

Both turbine and boiler driven have the advantage of utilizing the system's energy storage because of pressure build-up in the drum and superheater. However, compared to floating pressure, there is some loss of energy efficiency.

2.4.1.4 Sliding pressure operation

In practice, power plants operators prefer to control the pressure. This operation mode is a modification of floating pressure, as shown in Figure 2.8 (Klefenz, 1986). The sliding pressure curve is pre-defined as function of the produced power (as a simple curve), and the steam mass flow is used to as an indirect measure of the power produced in many control loops. Note that disturbances in boiler and combustion may result in changes in steam mass flow (m), and therefore measuring the steam mass flow rate may give a false

indication of the changes in produced power. The pressure setpoint is only changed at steady-state, but not dynamically, during power setpoint changes.

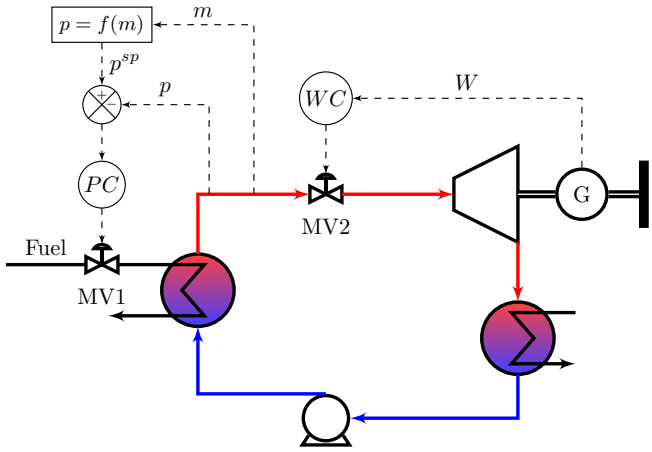

Figure 2.8: Sliding pressure operation (not as optimal at steady state as floating pressure) (Klefenz, 1986).

2.4.1.4.1 Comparison of different pressure operation modes Figure 2.9 illustrates the three pressure operation modes:

- constant (blue line), which is the operation mode for turbine driven and boiler driven. This strategy give fast load changes response.
- sliding (green line), where the pressure is kept constant at high load ($W \geq W^L$) for fast load change response, and it follows the power produced at lower loads ($W \leq W^L$) to increase the boiler efficiency.
- pure floating (mauve line), where the pressure follows the power produced and the throttling losses are minimized.

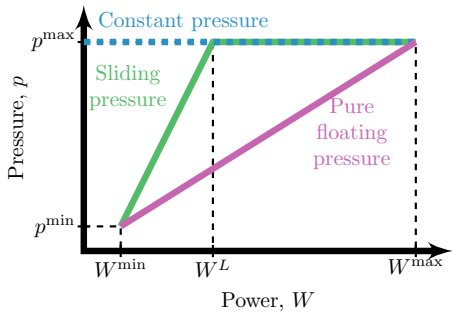

Figure 2.9: The three pressure operation modes discussed in this work

2.4.2 Improved control structures for floating pressure operation

We want to look into dynamic improvements of floating pressure operation. This operation mode is optimal from a steady-state point of view because it is optimal to keep the steam valve (MV2) fully open to minimize throttling losses. However, the dynamic response for controlling produced power (CV7 = W) is rather slow because the throughput manipulator is located at the feed side (MV1). Two alternatives for this are:

1. valve position controller (VPC), Figure 2.10
2. parallel control, Figure 2.11, using two controllers: a PI-controller for MV1 and P-controller for MV2.

2.4.2.1 Valve position control

In VPC there is one fast acting MV1 that controls the CV, and one slow MV2 that acts to bring MV1 to its nominal value (Shinskey, 1988). In our case, the fast MV is MV2 (steam valve), and the slow MV is MV1 (fuel), as shown in Figure 2.10. Valve position control acting on a valve-turbine system is also described in (Farmer and Lipták, 2006).

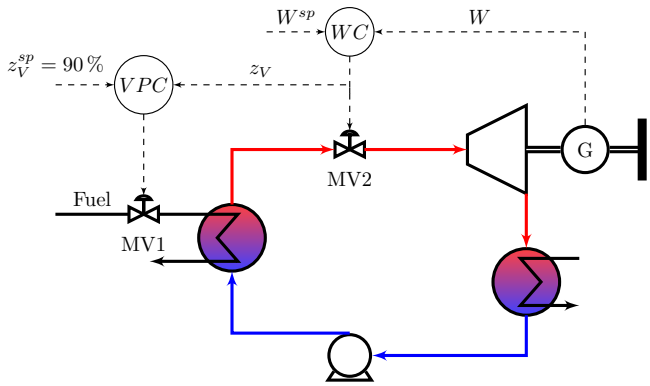

Figure 2.10: Valve position controller (VPC) to improves floating pressure operation

2.4.2.2 Parallel control

Similarly to VPC, this control structure can be used when two MV act on the same CV, but with different time constants (Balchen and Mummé, 1988). Only one of the two controllers can have integral action, otherwise there maybe no unique steady-state solution for the MVs (Åström and Hägglund, 2006). MV1 (fuel) is the only degree of freedom with a significant steady-state effect on the power, and therefore we use a PI-controller for MV1, and P-controller for MV2 (steam valve), as shown in Figure 2.11. Once the error is zero, the P-controller takes MV2 to its nominal values, which is set as the controller bias.

2.5 Simulation study: optimal operation of a simple heat-to-power cycle

We consider a typical steam cycle for simulating the control structures presented in Section 2.4:

- Floating pressure (Figure 2.5)

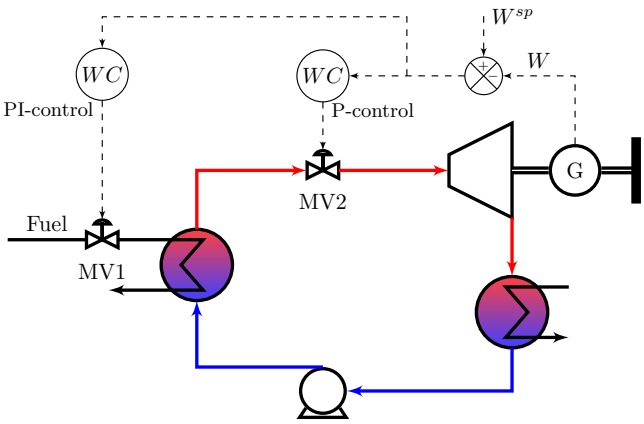

Figure 2.11: Parallel control with one PI-controller and one P-controller to improve floating pressure operation

- Boiler driven (Figure 2.6)
- Turbine driven (Figure 2.7)
- Valve position control (Figure 2.10)
- Parallel control (Figure 2.11).

2.5.1 Model

A heat-to-power cycle can be decomposed into three subsystems (SS), which can be modelled sequentially (Maffezzoni et al., 1983):

- $SS1$: water cycle
- $SS2$: combustion
- $SS3$: generator and connection to the electric grid.

Steam cycles models with different complexity are presented in the open literature, and a good overview of modelling methods and tools is given by (Alobaid et al., 2017).

For control purposes, simpler models are often used, and the work by (Ordys et al., 1994) outlines simple models for each component of a heat-to-power cycle, which can then be used in a modular simulation approach. A detailed dynamic model that has been extensively used for both modelling and controller synthesis is the drum boiler presented in the work by (Åström and Bell, 2000). Object oriented approaches have become an attractive alternative for modelling due to their reusability and versatility. Modelling and regulatory control design of a subcritical steam cycle using an object oriented language and library is described in the work by (Chen et al., 2017).

With respect to steam turbines performance maps, static laws are commonly used because there is no accumulation in the turbine. The most common is Stodola's law of cones (Cooke, 1985), or constant mass flow coefficient (considering choking conditions) (Cordes, 1963). Both of these laws related the current operating conditions (i.e. *off-design* conditions) to the design point. In addition to first principle derived relations, empirical linear relations between the power produced and the steam mass flows, called *Willans lines*, are described and used in the work by (Sun and Smith, 2015).

For our propose, the model has to be simple and robust, yet it also needs to capture the main dynamics of the process. We develop a first principle model for a typical steam cycle to test our analysis. As mentioned in Section 2.3, we consider only the water side subsystem (i.e. SS1). The interface with SS1 is modelled via the hot flue gas inlet temperature, and the interface with SS3 is modelled via the generator frequency.

The model consists of both algebraic mass- and energy balance representing fast time scale processes, as well as dynamic equations representing the longer time scales. Therefore, the model is a system of differential and algebraic equations (DAE).The differential states (x) are the temperatures on the hot side of the heat exchangers (e.g. T_E, T_D and T_S), the superheated steam temperature after the attemperator (T_A), the holdups in the drum (M_D) and superheater (M_S) and the frequency (ω). The algebraic states (w)

are the flue gas temperature on the cold side of the heat exchangers (e.g. T_E^g, T_D^g and T_S^g), turbine inlet pressure (p_T), and the produced power (W). The DAE model has a total of 12 states (7 differential and 5 algebraic). The detailed model equations are given in 2.8.

2.5.2 Nominal operating conditions

We are interested in optimal operation of existing heat-to-power cycles, therefore, the equipment design is given, and we must decide how to use it optimally. We consider reasonable values for the nominal operating conditions for a simple steam cycle with one pressure level (this may be typical for an older operating plant). Similar values are found in Skogestad (2008) and Åström and Bell (1987). Table 2.4 shows the nominal operating conditions. The design parameters are given in Table 2.9, and are computed by solving the model at steady-state for the nominal conditions (Table 2.4).

2.5.3 Controller

Eq. 2.3 shows the time domain expression for the PI-controllers used. Note that we consider the saturation limits for the applied input u^p (i.e. a valve cannot be more than fully open or close, or mass flows cannot be negative.), and therefore antiwindup is implemented. We use the back-calculation antiwindup method, where the controller output tracks the input applied to the process (u^p) with a time constant (τ_T) equal to the integral time (τ_I)(Åström and Hägglund, 2006).

$$u(t) = u^0 + K_C e(t) + \frac{K_C}{\tau_I}\int_0^t e(t)dt + \frac{1}{\tau_T}\int_0^t e^u(t)dt \tag{2.3a}$$

$$e = y^{sp} - y \tag{2.3b}$$

$$e^u = u^p - u \tag{2.3c}$$

$$u^p = \min(u^{\max}, \max(u, u^{\min})) \tag{2.3d}$$

Table 2.4: Nominal operating conditions

Variable	Unit	Value	Unit
Holdup	Economizer	100	kg
	Drum	3000	
	Superheater	100	
	Attemperator	10	
Water temperature	Inlet	45	°C
	Economizer	303	
Steam temperature	Drum	303	°C
	Superheater	595	
	Attemperator	529	
Fuel (combustion temperature)	Economizer	150	°C
	Drum	425	
	Superheater	777	
	Inlet	1000	
Flowrate	Pump	10.6309	kg/s
	Economizer bypass	0	
	Attemperator	0.6309	
	Turbine bypass	0	
	Gas	31.4018	
Power		16.55	MW
Frequency		50	Hz

2.5.3.1 Controller tuning

We find the controllers tuning parameters (proportional gain K_C and integral time τ_I) by identifying a first-order plus time-delay (FOPTD) model ($\frac{k}{\tau s+1}e^{-\theta s}$) or integrating model $\left(g(s) = \frac{k'}{s}\right)$ from a step response in the input u, followed by applying the SIMC tuning rules (Skogestad, 2003) with a chosen closed loop time constant τ_C.

For a first-order model, we use Eq. 2.4.

$$K_C = \frac{1}{k}\frac{\tau}{\tau_C + \theta} \tag{2.4a}$$

$$\tau_I = \min(\tau_0, 4(\tau_C + \theta)) \tag{2.4b}$$

where, k is the steady-state gain from u to y, τ is the open loop time constant, τ_C is the closed loop time constant and θ is the time delay.

For integrating process (i.e. for plants with large time constant such as levels), we use Eq. 2.5.

$$K_C = \frac{1}{k'}\frac{1}{\tau_C + \theta} \tag{2.5a}$$

$$\tau_I = 4(\tau_C + \theta) \tag{2.5b}$$

where, k' is the slope.

2.5.4 Step 5. Regulatory controller design

2.5.4.1 Controller tuning

We begin with tuning the controllers for the regulatory layer (i.e. level controller and active constraints).

An secondary decision in decentralized control, is the order of tuning the PI controllers. This is an important decision in highly coupled processes, and we base our decision based on effective time delays in the process (Skogestad, 2003). In our case, we use a sequential tuning method, that is we first tune the level controller, then close the loop, tune the next controller and repeat the procedure. Table 2.5 gives the tuning parameters for the drum level control (M_D), superheated steam controller (T_A), and flue gas outlet temperature controller (T_E^g). Note that we do not need to tune the condenser pressure controller as we consider it constant, i.e. perfect control. The value for the closed loop time constant τ_C is taken quite large to account for any

unmodelled capacities and holdups, and make the model time scale more realistic.

Table 2.5: Level and temperature controllers tuning

Type	Loop	τ_C [s]	K_C	τ_I [s]
LC	MV5-CV1	10	0.1	40
TC	MV6-CV3	20	0.05	10
TC	MV7-CV4	15	-0.0008	1

2.5.5 Step 6. Supervisory controller design

We proceed with the supervisory control design and we tune the controllers using the fuel MV1 and the steam valve MV2 for the structures presented in Section 2.4. In designing the supervisory control layer, we keep the same tuning for the regulatory layer (Table 2.5), and follow the same tuning procedure. Is important to note that we use the initial response in tuning all controllers for MV2 (steam valve), as we are interested in using it on a fast time scale (see Figure 2.4 and Section 2.3.2.2). For boiler driven, we close first the pressure loop. Then, the open loop response from fuel MV1 to power CV7 has one left-hand-plane zero and one left-hand-plane pole, and we use a pure I-controller tuned based on the initial response.

Table 2.6: Standard industrial controllers tuning

	Floating pressure		Boiler driven		Turbine driven	
MV-CV	MV1-CV7	MV2=0.9	MV1-CV7	MV2-CV8	MV1-CV8	MV2-CV7
τ_C s	30	N/A	30	5	15	5
K_C	0.0028	N/A	0	-1.48	1.1574	0.0004
τ_I	40	N/A	0.1	20	50	1

Table 2.7: Parallel controllers tuning

	VPC		PI and P control	
MV-CV	MV1-MV2	MV2-CV7	MV1(PI)-CV7	MV2(P)-CV7
τ_C s	50	5	30	5
K_C	-2.84	0.0004	0.0041	0.0004
τ_I	115	1	55	N/A

2.5.6 Step 7. Control structure performance

We test the control structures for setpoint changes and disturbance rejection.

2.5.6.1 Setpoint changes

Figure 2.12a shows the response for the power, and Figure 2.12b shows the pressure response, while Figure 2.12c and Figure 2.12d show the input usage for fuel MV1 and steam valve MV2 respectively to a 10% step decrease followed by 10 % step increase in the power setpoint for all five control structures described in Section 2.4.

2.5.6.2 Disturbance rejection

Figure 2.13a shows the response for the power, and Figure 2.12b shows the pressure response, while Figure 2.13a and Figure 2.13d show the input usage for fuel MV1 and steam valve MV2 respectively to a disturbance of 50 °C step increase in the combustion temperature for all five control structures from Section 2.4. This high change in temperature could be for example given by changes in the fuel composition or heat quality.

2.5.6.3 Summary of comparison of the five control structures

Comparing the three common industrial standards (floating pressure, boiler driven, turbine driven) in Figure 2.12, boiler driven structure reacts slower

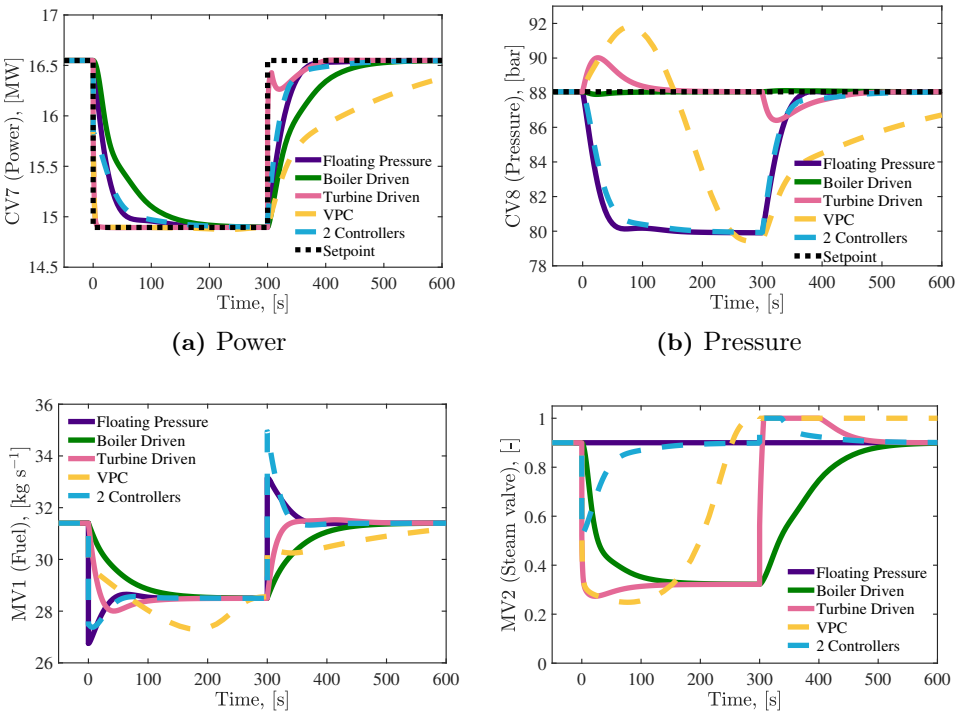

(a) Power **(b)** Pressure

(c) Fuel **(d)** Steam Valve

Figure 2.12: Closed loop responses to 10 % step decrease at time $t = 0$ s followed by 10 % step increase at time $t = 300$ s in the power setpoint. Only turbine driven and boiler driven have pressure control.

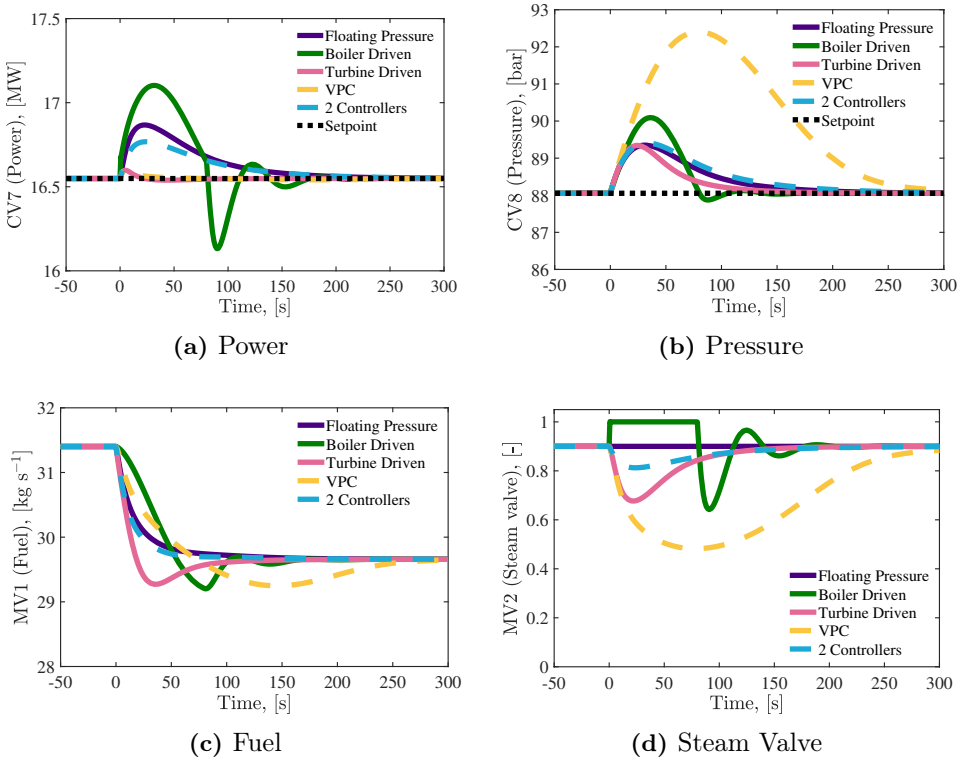

(a) Power **(b)** Pressure

(c) Fuel **(d)** Steam Valve

Figure 2.13: Closed loop responses to a step change of 50 °C in T_0^g at time $t = 0$ s. Only turbine driven and boiler driven have pressure control.

for change in the produced power, but has the advantage that the fuel rate (MV1) changes smoothly, and it does not overshoot as for all other control structures. Turbine driven gives the fastest response to a step change in power (CV7), yet, in comparison to boiler driven, the pressure (CV8) drifts significantly from the setpoint in transient operation. These effects can be explained considering the smaller effective time delay from controlling CV7 or CV8 using the steam valve MV2, contrast to using the fuel MV1. The VPC control structure has as similar response to turbine driven for a power setpoint decrease, while it is the slowest to a setpoint increase because the steam valve MV2 saturates. In addition, by design, the VPC is tuned slow, and tuning it faster would result in an aggressive controller with a high input usage for fuel MV1. In terms of performance the two controllers (parallel control) seems very good and has the benefit of floating pressure at steady state.) Considering throttling losses for the steam valve MV2, both boiler and turbine driven results in higher losses because MV2 needs to close more to keep the setpoint for power (CV7), compared to the other control structures that do not have pressure control. To answer the question if the pressure should be controlled (Section 2.4), we can say that controlling the pressure gives a faster response when steam valve is used to control the power, while letting the pressure float minimizes the throttling losses (also see Section 2.6.1).

The response for a disturbance in the combustion temperature (T_0^g) shows that the boiler driven control structure may not be suited for plants with large variations in this disturbances. An increase in T_0^g increases the enthalpy of the hot flue gases, which results in more heat transferred in the boiler, and an increase in the steam pressure (CV8). To decrease the pressure to its setpoint, the steam valve MV2 has to open (Figure 2.13d), which results in a higher overshoot for the power produced (Figure 2.13a) compared to the other control structures. Moreover, in this particular example, the steam valve (MV2) saturates, and we loose control of the pressure during transient

operation. Note that the pressure response for boiler driven follows the floating pressure initially (Figure 2.13b), but then it decreases faster because the steam valve MV2 is fully open for boiler driven, while for floating pressure is kept at 90 % opening.

2.6 Discussion

2.6.1 Throttling losses

Having the steam valve partly open results in throttling losses. We define throttling as a reduction in pressure without removal of energy in form of heat or work, i.e. isenthalpic process. Throttling is irreversible and it translates into increase of entropy and thereby exergy losses and decrease of available work (Shinskey, 1978).

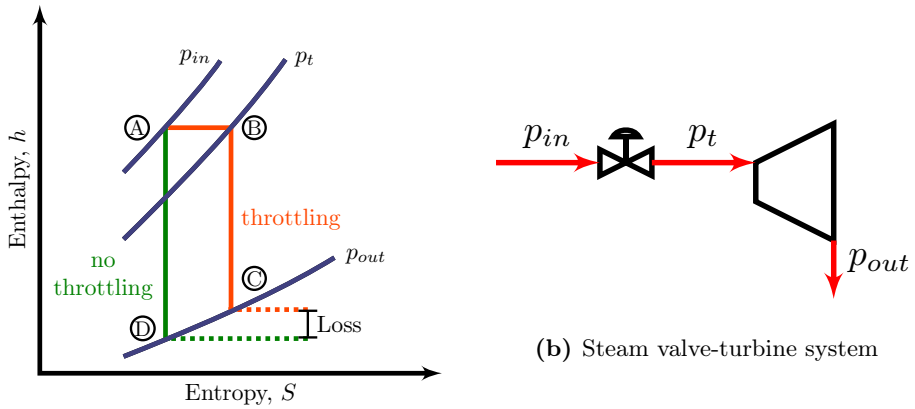

(a) Enthalpy-Entropy diagram

(b) Steam valve-turbine system

Figure 2.14: Enthalpy-Entropy diagram for an expansion process with and without throttling, left, and, a steam valve-turbine system indicating the corresponding pressures, right.

Figure 2.14 shows the enthalpy-entropy diagram for an expansion process with and without throttling, where the purple lines represent the lines of

constant pressure. The green path from A to D represents the isentropic expansion from inlet pressure p_{in} to outlet pressure p_{out} without throttling. The orange path from A to B represents throttling from inlet pressure p_{in} to pressure p_t. The orange path from B to C represents the isentropic expansion from the pressure after throttling p_t to outlet pressure p_{out}.

Considering constant outlet pressure p_{out}, with throttling, steam is expanded at a higher enthalpy, thus resulting in increase of entropy and loss of available work. The loss in available work is graphically represented by the difference in enthalpy between D and C.

Mathematically, the loss of available work is quantified by Eq. 2.6.

$$W_{\text{Loss}} = \dot{V}\Delta p \tag{2.6}$$

where, W_{Loss} = loss in available work, $\dot{V}$ is the volumetric flow (assumed constant), and $\Delta p = p_{in} - p_t$ is the pressure drop across the steam valve.

2.6.2 Floating pressure efficiency

The throttling losses mentioned above are relevant if we could replace the valve by an adjustable small turbine. However, this is not the case here. Instead, we consider keeping the steam valve fully open and let the pressure float, leading to a lower steam drum pressure at low loads. This does not in itself give an increased efficiency in terms of power produced because it does not require more energy to increase the pressure. However, by lowering the pressure and thus the temperature in the drum on the steam side, we get improved temperature driving forces. Thus, with floating pressure operation we are able to extract more energy from the fuel because we get a lower flue gas exit temperature. In some cases, we are not allowed to lower the flue gas exit temperature because of corrosion issues, and then there will be no efficiency benefit of floating pressure operation. In Table 2.8, we analyse the new steady-state operation conditions for a decrease in power by 10 % from

nominal (i.e. at 90 % load), both for floating and constant pressure. We assume that the exit flue gas temperature (CV3=T_E^g) is not controlled, that is, the economizer bypass MV6 is kept closed. We assume that the turbine efficiency is equal in all cases.

Table 2.8: Comparison of the steady-state values for floating and constant pressure operation modes at 90 % load without controlling the cold flue gas temperature.

Pressure	Power (MW)	Fuel (MV1) (kg/s)	Pressure (CV8) (bar)	T_E^g (CV3) (°C)	T_S^s (°C)	Attemperator (MV7) (kg/s)
Floating	14.9	27.79	79.9	128.4	611.4	0.7045
Constant	14.9	27.86	88.05	130.7	616.5	0.74

At 90 % load, the loss in used fuel for constant pressure is only 0.2%, and the additional pump work needed to boost the pressure by 8 bar accounts to 0.05% of the produced power, which adds to only 0.25%. If the temperature of the cold flue gas is controlled at its minimum limit (i.e. CV3= $T_E^g \geq T_E^{g,\min}$), then the loss in efficiency is reduced to 0.05% (i.e. account for the pump), both floating and constant pressure operation modes At 65 % load, the energy efficiency loss for constant pressure operation increases to 1 % (without flue gas temperature control). Therefore, the energy efficiency increases at low loads in floating pressure operation, though the increase is not significant. These numbers depend naturally on the process design, especially how the heat exchange area is distributed between the economizer, drum and superheater.

2.6.3 Steam turbine control

For a stand-alone turbine, or when a gear box is used to connect the turbine and the generator, the turbine rotational speed may be used as a degree of freedom, but we are here considering a turbine connected to the grid without a gearbox. More precisely, the turbine is connected to an electric

generator through a shaft and the electric generator is connected to the grid. In principle, no control of the turbine is needed, because inertia and self-regulation will imply that all these frequencies (turbine speed ω_T, generator speed and grid frequency ω) are the same at steady state. However, in practice, speed (frequency) control is needed for two reasons:

1. Local level (speed control of turbine). To protect the turbine/ generator system from damage caused by fast changes in the turbine speed, we must keep the turbine frequency close to the grid frequency on a fast time scale. This is done by installing a steam valve upstream the turbine (MV2) which controls CV5 $= \omega_t \breve{} \omega$.

2. Grid level (droop control of grid frequency). The grid frequency ω should be kept close to its desired setpoint ω^{sp} (e.g., at 50 Hz in Europe and 60 Hz in the US). The value of ω is directly proportional to the amount of kinetic energy (inertia) stored in all the rotating equipment in the grid. Any imbalance between power production and power demand will therefore change ω. There is a certain self-regulation in the power demand, but this is not enough. Thus, to maintain a desired grid frequency ω^{sp} in spite of variations in the power demand, some of the main power producers must participate in controlling ω. That is, we need to control CV6 $= \omega - \omega^{sp}$. The manipulated variables for this is the power production for each unit i (W_i), which at steady state requires manipulating the fuel rates (MV1$_i$). This control task is divided into primary (droop), secondary and tertiary grid frequency control.

The local level turbine speed control (CV5) is always present (Kurth and Welfonder, 2006), (der Autumation, 2003). As mentioned, the inherent self-regulation will keep CV5=0 at steady-state. Thus, integral action is not needed for control of CV5, so in practice a proportional controller (droop) is used. We will not discuss the control of CV5 in this paper, because it is

generally considered a part of the equipment protection, and is not available for control engineers. Furthermore, because the self-regulation of CV5 is fast anyway, the design of this controller will not affect the rest of the control system.

Next consider grid frequency control. Not all power producers participate in grid frequency control, but the ones that do usually get a higher power price. Let the power production (actually, the setpoint for power production) from each producer be written as $W_i^{sp} = W_{i,0}^{sp} + \Delta W_i^{sp}$ where ΔW_i^{sp} comes from the primary frequency control (proportional droop) and W_{i0}^{sp} from the secondary frequency control. Figure 2.15 shows the primary and secondary control loops for plant i in an isolated area with N power plants participating in grid regulation. Note that the inner turbine control loop are not explicitly shown, but this is inside the *Power plant i* block.

Let us first consider the primary droop control which takes place on a fast time scale.

Ideally, we want to avoid centralized coordination of the participating power producers at the fast time scale. The solution is then that each producer has local control of the grid frequency, CV6. However, these local controllers cannot have integral action, because otherwise there is no unique steady state, and one may even get into cases where the controllers fight each other, possibly resulting in one power plant closing down and another reaching full capacity (Cohn, 1984), (Åström and Hägglund, 2006).

To solve this issue, we use proportional control of CV6$= \omega - \omega^{sp}$. This gives a unique steady state, where the power change from each producer i is uniquely given by the change in grid frequency, $\Delta W_i^{sp} = -1/R_i(\omega^{sp} - \omega)$. Here $1/R_i$ is the proportional controller gain, typically between 3 and 10 %/%, where R_i is the steady-state process gain from power to frequency. The MV available for achieving the desired change in power production (ΔW_i) is as mentioned the fuel (MV1), but to speed up the dynamic response one frequently makes use of the steam valve (MV2). The required response

time is usually specified in the contract for each producer. Note that the steady-state effect of MV2 on the power production is negligible (Figure 2.4).

Next consider the secondary frequency control which involves a centralized controller with integral action. Integral action is needed because the proportional action in droop control results in a steady-state offset in frequency. This controller changes the bias $W_{i,0}^{sp}$ in the power setpoint for each producer (adjusted with a gain α_i) on a slow time scale. Finally, for larger changes in power demand on a longer time scale, it may be necessary to start up or close down power production (tertiary frequency control).

When a plant participates in droop control, the fuel (MV1) has to be lower that its maximum, which gives a loss in power production. Furthermore, for fast response to changes in power demands, the steam valve (MV2) has to be partly closed (e.g. 90 % opening) at nominal operation, which gives a loss in efficiency. These issues explain why producers who participate in droop control get a higher electricity price.

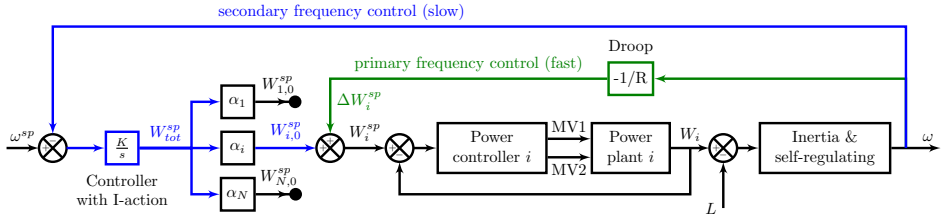

Figure 2.15: Primary (green) and secondary (blue) frequency control for power plant i in an area with N power plants participating in grid frequency control (adapted from (Wood et al., 2014).)

2.6.4 Operation with given fuel rate (MV1)

In this case, MV1 must be used to control the TPM. Hence, from a steady-state point of view, we have no degrees of freedom left to control the power produced, and the steam cycle becomes a "swing power producer" (Fig-

ure 2.16). In this case, the power plant clearly cannot participate in grid frequency control. More importantly, there must be some other means (not shown) to make the power output balance the fuel rate by controlling the steam pressure. For example, there could be another steam flow added to the turbine inlet or excess steam could be withdrawn and used for other purposes. In addition, to make sure that the pressure is kept within bounds, it is suggested (Figure 2.16) to give up controlling the fuel rate when a pressure constraint is reached (i.e. $p = p^{\max}$ or $p = p^{\min}$).

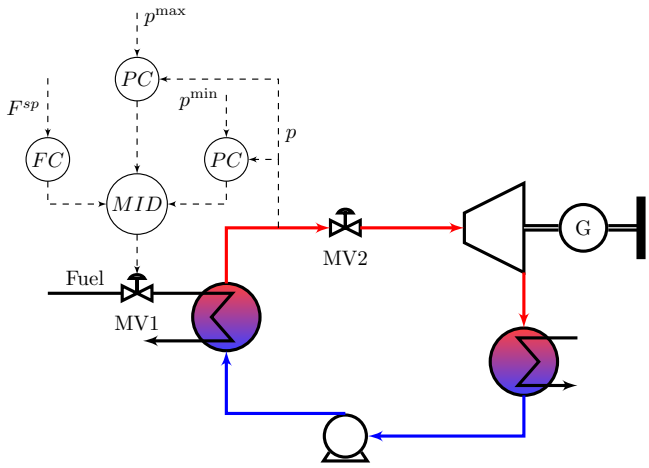

Figure 2.16: Control structure with given fuel rate (MV1) and fully open steam valve (MV2) to maximize power production. The mid-selector gives up controlling the fuel rate when a pressure constraint becomes active. Under normal conditions, pressure is controlled by some other manipulated variable (not shown), for example, by producing steam.

2.6.5 Influence of level control time constant

Similarly to floating pressure, the drum level can be let to float between it's minimum and maximum limits, to utilize the stored energy in the hot water. This can be achieved with a slow level control, in which case, the

drum level would be allowed to decrease to a lower level and the steam flow would be longer sustained when it is required to produce more power, while feedwater is slowly pumped into the system. Note that with tight (fast) level control, cold feedwater is pumped rapidly in the system which decreases the drum temperature faster in transient operation. However, for the studied simulation case, a slow level control showed limited improvement of the dynamic performance. Figure 2.17 shows the power response for setpoint changes (10% decrease at time $t = 0$s and 10% increase at time $t = 300$s) for floating pressure (Figure 2.17a), boiler driven (Figure 2.17b), VPC (Figure 2.17c) and two controllers (Figure 2.17d). Turbine driven has an insignificant change. Note that the larger the closed loop time constant (τ_C), the slower the drum level control is.

2.6.6 Effect of modelling simplifications

The steam cycle model used in this work makes use of several simplification with the purpose of developing a process model becomes easier to develop, use and simulate. The complete set of simplification assumptions are detailed in Appendix 2.8, while their practical implications are discussed next.

The main real effects not included are unmodelled dynamics and effective delays, and more rigorous (non-ideal) thermodynamics for the water-steam side.

The combustion dynamics are not included, as we assume we can directly manipulated the hot flue gas (MV1) resulted from the combustion process. Depending on the type of fuel used, this may or may not good simplification. For example, if the fuel is a gas, the combustion process happens at a much faster scale than the steam cycle dynamics. On the other hand, these dynamics may be in the order of minutes for other types of (solid) fuels such as biomass, coal or waste.

The wall capacities are not included, meaning that the thermal inertia of the steam cycle is smaller than in reality. In addition, each of the three heat

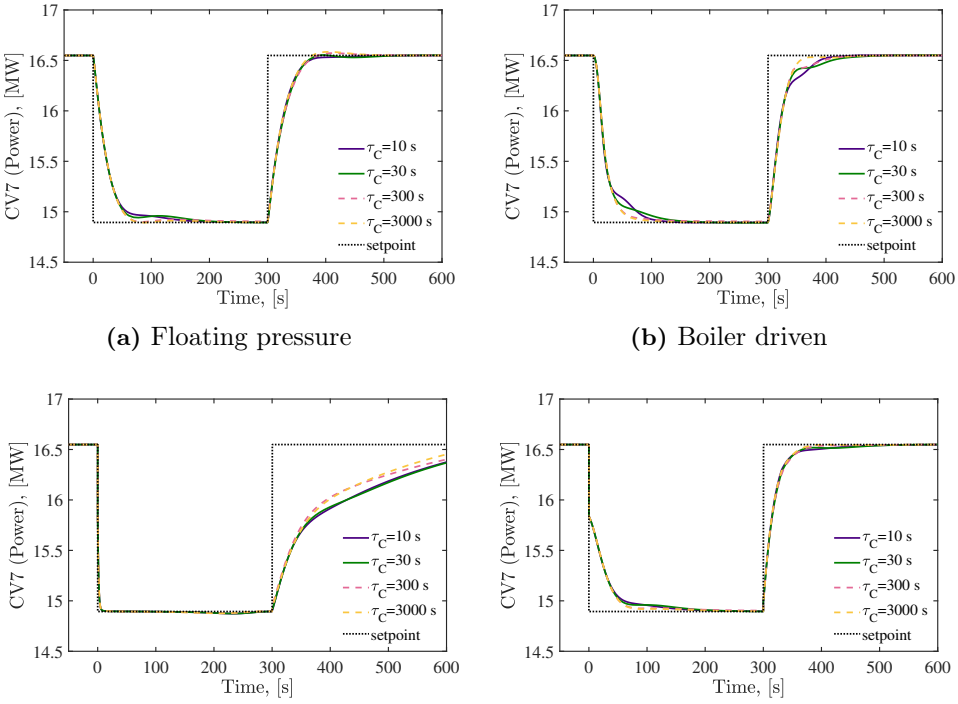

(a) Floating pressure **(b)** Boiler driven

(c) VPC **(d)** 2 Controllers

Figure 2.17: Influence of the tuning of the drum level controller on the power response to setpoint changes.

exchangers are modelled as one cell instead of a distributed cell model. The steam turbine is modelled as one expansion stage. In reality, these effects would contribute to higher effective delays. Overall the dynamic response of the modelled cycle is probably faster than reality.

The steam thermodynamics are assumed to be ideal, that is the water-steam enthalpy is assumed to be a linear function of temperature only. More rigorously, at high pressure and temperature, the steam enthalpy is a highly nonlinear function of both temperature and pressure. One effect of this assumption is higher turbine inlet temperature when using ideal thermodynamics, cause by neglecting the temperature drop over the isenthalpic steam valve throttling.

Nonetheless, these simple models are suitable for the purpose of studying and understanding the dynamic response of the different control structures.

2.6.7 Implications of process simplification

In a real industrial implementation, a steam cycle is more complex, and many more process configurations exists than the simple process analyzed in this work. For example, it may have different pressure levels, a deaeraor for reducing the feedwater oxygen content or steam extraction to provide heat utility.

A steam cycle operating at low, intermediate and high pressure levels, will have for each level the corresponding constraints, MVs and CVs as for only one pressure level.

Extracting steam for process heating at different pressure levels, will act as a disturbance for the existing control loops. With respect to operating combined heat and power cycles, the optimal steam level that maximize efficiency (or minimizes cost) should be identified.

A deaerator is installed downstream of the condenser and receiving steam extracted from the turbine to deadsorb oxygen from feedwater and prevent boiler corrosion. For consistent inventory control in the steam cycle, this

level will be left uncontrolled.

The exceptions are the very few offshore installations where simpler steam cycles, with one pressure level and once-through boiler are preferred due to smaller footprint and simpler operation. As mentioned for once-through boilers there is no drum level to control, and the feedwater flow is used to control the superheated steam temperature.

2.7 Conclusions and final remarks

In this work, we used the systematic framework of plantwide control to analyse the control and optimal operation of a simple steam cycle with one pressure level, drum and condensing turbine.

After controlling the unstable inventory (drum level CV1), and the active constraints: condenser pressure CV2, superheated steam temperature CV4, cold flue has temperature CV3, we have two degrees of freedom left: the fuel MV1 and the steam valve MV2. MV2 only has a dynamic effect on the power produced, as shown in the response to setpoint changes in Figure 2.12 and in the disturbance rejection response in Figure 2.13.

At low loads, letting the pressure float is slightly more efficient. By keeping the pressure constant the dynamic performance is improved, especially for the turbine driven operation (Figures 2.12 and 2.13).

Of interest for future work is a more comprehensive analysis of the control implications of variable heat sources with varying inlet temperature. The extend to which the existing the storage capacity of the process (e.g., drum and pipeline capacity) can be utilized as a short-time buffer between supply and demand, should also be further investigated.

Table 2.9: Design parameters

Parameter	Value	Unit
UA_E	95.12	kW/°C
UA_D	46.4	kW/°C
UA_S	19.94	kW/°C
$C_{v,D}$	10	kg/°C
K_v	2.32	kg/bar
ϕ_D	3.625	kg/s$\sqrt{\text{K}}$/bar
M_0	7.56	pu MW pu /rad/s
D_0	2	pu MW pu /rad/s

2.8 Appendix

2.8.1 Design parameters

where pu represents *per-unit*, and it is used in electrical system to normalize a given parameter wrt. a selected base value (i.e., ratio to a base value).

2.8.2 Model thermodynamics

Assumptions

(A1) Constant specific heat for each fluid (water, steam and flue gas);

(A2) The reference temperature is $T^{ref} = 0$ °C;

(A3) The boiling reference temperature is $T^{refB} = 576$ °C (drum nominal temperature);

(A4) Ideal gas behaviour for steam;

(A5) Saturated steam pressure follows Antoine equation (Eq. 2.8b).

Considering a constant c_p, the specific enthalpy for the gas, water and steam has a linear dependency on the temperature, as shown in Eq. 2.7.

$$\Delta H^g = c_p^g(T_j^g - T^{ref}) \quad \forall j \in (i, S, D, E) \tag{2.7a}$$

$$\Delta H^w = c_p^w(T_j - T^{ref}) \quad \forall j \in (P, E) \tag{2.7b}$$

$$\Delta H^s = c_p^w(T^b - T^{ref}) + c_p^s(T_j - T^b) + \Delta H^v(T^b) \quad \forall j \in (D, S, A, T) \tag{2.7c}$$

Table 2.10 shows the specific heat for each component.

Table 2.10: Specific heat

Component	c_p	Unit
water	4.18	kJ/kg/°C
steam	3	kJ/kg/°C
hot flue gas	1.25	kJ/kg/°C

The saturation pressure in the drum is computed using Antoine relation (Eq. 2.8b) as a function of the temperature.

$$p_D = 10^{\alpha} \tag{2.8a}$$

$$\alpha = A - \frac{B}{T_D + C} \tag{2.8b}$$

where T is in K and p_D is in bar, and the constants are $A = 5.11564\, B = 1687.537\, C = 42.98$ (Reid et al., 1987).

2.8.3 Economizer and bypass model

Assumptions

(A6) Constant inlet temperature (due to tight condenser pressure control,see below);

(A7) Constant water holdup (→ neglect the mass balance);

(A8) Static mixing for the bypass and economizer outlet streams (i.e. fast heat and mass dynamics and negligible holdup)(→ static mass and energy balances);

We write a dynamic energy balance in temperature form for the steam side, and an algebraic energy balance for the gas side.

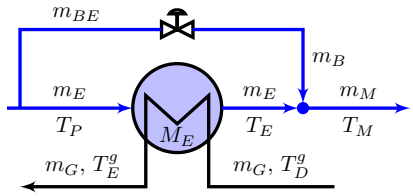

Figure 2.18: Economizer

$$\frac{dT_E}{dt} = \frac{1}{M_E}\left(m_E(T_P - T_E) + \frac{Q_E}{c_p^w}\right) \tag{2.9a}$$

$$0 = m^g c_p^g (T_D^g - T_E^g) - Q_E \tag{2.9b}$$

$$Q_E = U A_E \left(\frac{T_D^g + T_E^g}{2} - \frac{T_D + T_E}{2}\right) \tag{2.9c}$$

$$T_M = \frac{m_E T_E + m_{BE} T_P}{m_M} \tag{2.9d}$$

2.8.4 Mass flowrates model

The flowrate for the pump, economizer bypass and attemperator are directly given by (PI)-controllers (we assume fast inner cascade controllers on the valve position), according to the general Eq. 2.10. Antiwindup with a

tracking time constant equal to the integral time ($\tau_T = \tau_I$) is used.

$$m_i = m_i^0 + K_{C,i} e_i + \frac{K_{C,i}}{\tau_I} \int_0^t e_i(t)dt + \frac{1}{\tau_{T,i}} \int_0^t e_{m,i}(t)dt \tag{2.10a}$$

$$e_i = y_i^{sp} - y_i \tag{2.10b}$$

$$e_{m,i} = m_{i,p} - m_i \tag{2.10c}$$

$$m_{i,p} = \max(m_i, 0) \tag{2.10d}$$

$i \in (P, AE, BE)$ and $y \in (M_D, T^g, T_S)$

The remaining flowrates are computed from steady-state mass balances, according to Eq. 2.11.

$$m_E = m_P - m_{AE} - m_{BE} \tag{2.11a}$$

$$m_D = C_{V,D}(p_D - p_S) \tag{2.11b}$$

$$m_S = m_V - m_{AE} \tag{2.11c}$$

$$m_V = z_V K_C (p_S - p_T) \tag{2.11d}$$

2.8.5 Drum model

Assumptions

(A9) Perfect mixing;

(A10) Equal temperature in liquid and vapour phases;

(A11) Negligible vapour holdup (compared to the liquid holdup);

(A12) Saturated steam;

(A13) Outlet flow is given by a linear valve (fully open) equation as a function of the pressure drop;

(A14) Fixed vaporization in the drum, i.e. the drum inlet is saturated liquid water, and the outlet is saturated vapour. This means that the vaporization is know *a-priori*. Note that fixing the vaporization point may not be optimal for operation, as the heat transfer area is not optimally utilized. However, a variable phase transition point raises additional modelling challenges, which we want to avoid;

For the drum, we write a dynamic mass (Eq.2.12a) and energy balance on temperature form on the steam side (Eq.2.12b), and algebraic energy balance on the gas side(Eq.2.12c).

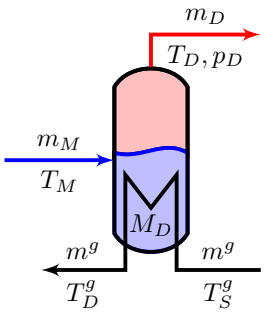

Figure 2.19: Drum

$$\frac{dM_D}{dt} = m_M - m_D \tag{2.12a}$$

$$\frac{dT_D}{dt} = \frac{1}{M_D c_p^w}(m_M(H_M - c_p^s T_D) + \ldots \tag{2.12b}$$

$$- m_D(H_D - c_p^s T_D) + Q_D)$$

$$0 = m^g c_p^g (T_D^g - T_S^g) - Q_D \tag{2.12c}$$

$$Q_D = U A_D \left(\frac{T_S^g + T_D^g}{2} - \frac{T_M + T_D}{2} \right) \tag{2.12d}$$

2.8.6 Superheater and attemperator models

Assumptions

(A15) The steam holdup accounts for the entire steam holdup in the cycle ($\rightarrow$ need to consider a dynamic mass balance);

(A16) Static mixing in the attemperator (i.e. fast heat and mass dynamics and negligible holdup) ($\rightarrow$ static mass and energy balance);

We write a dynamic mass (Eq.2.13a) and energy balance on temperature form on the steam side (Eq.2.13b), and algebraic energy balance on the gas side(Eq.2.13c).

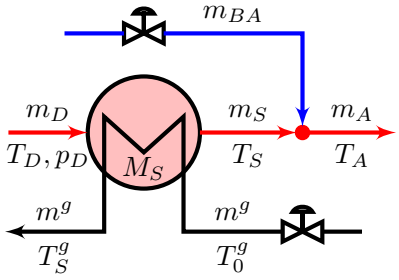

Figure 2.20: Superheater and attemperator

$$\frac{dM_S}{dt} = m_D - m_S \tag{2.13a}$$

$$\frac{dT_S}{dt} = \frac{1}{M_S c_p^s}(m_D(H_D - c_p^s T_S) + \ldots \tag{2.13b}$$

$$- m_S(H_S - c_p^s T_S) + Q_S)$$

$$0 = m^g c_p^g (T_0^g - T_S^g) - Q_S \tag{2.13c}$$

$$Q_S = U A_S \left(\frac{T_0^g + T_S^g}{2} - \frac{T_S + T_D}{2} \right) \tag{2.13d}$$

$$0 = m_s H_s + m_A H_P - m_A H_A \tag{2.13e}$$

2.8.7 Steam valve, turbine and generator models

Assumptions. Steam turbine valve

(A17) Linear valve equation and pressure drop;

(A18) Isenthalpic;

(A19) Negligible holdup;

Assumptions. Turbine

(A20) Turbine map: constant mass flow coefficient ($\phi = \frac{m\sqrt{T}}{p}$);

(A21) Isentropic expanssion with 100% efficiency;

(A22) Speed is given by generator frequency;

(A23) Neglijable holdup;

Assumptions. Generator

(A24) Another power plant is responsible for keeping the frequency at the nominal value, therefore we can only use a P-controller for frequency control;

2.8.8 Condenser models

Assumptions

(A25) Tight pressure control, i.e. constant condenser pressure ($\rightarrow$ is not modelled and the cycle is open);

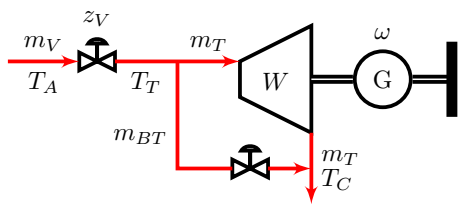

Figure 2.21: Steam turbine

$$m_T = m_V - m_{BT} \tag{2.14a}$$

$$m_{BT} = 0 \tag{2.14b}$$

$$0 = \frac{m_T\sqrt{T_A}}{p_T} - \phi_d \tag{2.14c}$$

$$T_C = T_T \left(\frac{p_C}{p_T}\right)^{(R\backslash c_p^s)} \tag{2.14d}$$

$$0 = W + m_T c_p^s (T_T - T_C) \tag{2.14e}$$

$$\frac{d\omega}{dt} = \frac{1}{M_g}\left(P - L - D_g(\omega - \omega_0)\right) \tag{2.14f}$$

2.8.9 General for heat exchangers models

Assumptions

(A26) Constant and negligible holdup for the hot side;

(A27) Constant UA (heat transfer coefficient U $(W/(m^2K)$ times heat surface area A (m^2);

(A28) Temperature difference (ΔT) is the difference between the algebraic mean on each side.

(A29) Neglected wall capacity

Part II

Transformed inputs for linearization, decoupling and feedforward control

Chapter 3

Transformed inputs for linearization, decoupling and feedforward control

The goal of the previous chapter was to have a better understanding of the operation and control problem of steam cycles. However, it quickly became apparent that control of industrial power plants has been developed over many years to a stage where they are adopted by many plants and work extremely well and it is not straightforward to make improvements.

Many of these control structures make extensive use of nonlinear model-based calculation blocks, function blocks, or ratio stations to provide feed-forward action, decoupling or linearization (adaptive gain). Examples from steam cycles include superheated steam enthalpy control for disturbance rejection (Shinskey and Louis, 1968), two-elements and three-elements drum level control (Lindsley, 2000) or use of simplified reference dynamic models for decoupling and linearization for coordinated load control (Welfonder, 1999). Examples related to chemical processes are available in Shinskey (1981), ch.8. These include air-to-feed ratio control for a Claus sulphur process,

manipulating the ratio reflux-to-distillate for pressure control to provide decoupling. In the latter, changes in the distillate flow used to control the top composition, is reflected immediately in the reflux flow without needing to wait for a change in the column pressure, thus reducing interactions and improving the composition response. An example for stabilizing a distillation column with two reboilers and controlling the two reboiler levels and column temperature by means of "reversing" the static process model (given by mass and energy balances) is also provided. These examples are case specific based, and a systematic theory for developing these calculation blocks is missing. It is therefore one of the the goal of this work to give some theoretical background for these nonlinear model calculation blocks studied in the context of nonlinear input and output transformations. The question we want to answer is

> *How do we derive good transformed inputs in a systematic manner?*

This part is based on the papers:

1. "Transformed manipulated variables for linearization, decoupling and perfect disturbance rejection " (Zotică et al., 2020a)

2. "Input transformation for linearization, decoupling and disturbance rejection with application to steam networks " (Zotică and Skogestad, 2021)

3. "Control of steam bottoming cycles using nonlinear input and output transformations for feedforward disturbance rejection " (Zotică et al., 2022)

4. "Transformed inputs for linearization, decoupling and feedforward control" (Skogestad et al., 2023).

3.1 Motivating example: three elements drum level control

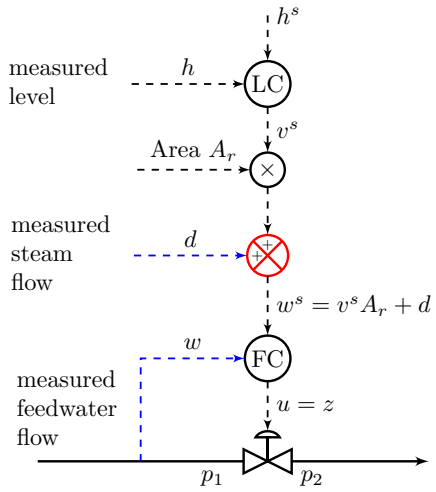

Figure 3.1: Cascade implementation of the three elements drum level control. Adapted from (Lindsley (2000), ch.6). The variables' names and colors reflect the block diagram for transformed inputs in Figure 3.2

This section briefly explains the three elements drum level control solution, and motivates the introduction of transformed inputs theory later in this chapter.

The three elements control was introduced to speed-up the response to a disturbance in the steam demand compared to the conventional feedback solution where the drum level is controlled by manipulating the feedwater flowrate (also see the process flowsheet in Figure 2.3). The name is derived from the three measurements used: drum level, the steam flowrate and the feedwater flowrate. It is widely applied (ABB, 2022; Lindsley, 2000), and many implementations are available. One of them, a cascade based implementation, is shown in Figure 3.1. As we will see later, this is equivalent

to the feedback-based implementation of transformed inputs (see Figure 3.4c).

The control objective is to provide fast feedforward disturbance rejection for changes in the steam demand. It uses the drum steady-state mass balance to set the feedwater flowrate equal to the steam demand. The response is improved compared to feedback only because it accounts for process delays, nonlinearities in the valve characteristics and inaccurate drum level measurement caused by the shrink and swell effect.

The shrink and swell effect may happen when steam demand increases reducing the drum vapour mass and thus decreasing pressure. As a result, the saturation temperature also decreases and, with the same heat input, the evaporation rate increases producing more bubbles entrapped in the liquid causing an "artificial" increase of the liquid level (swelling), although the mass is decreasing. There is some self-regulating effect and eventually with the same heat input, the steam outflow decreases when the pressure decreases.

3.1.1 Deriving the model-based flowsheet in Figure 3.1.

This example is given in the framework of the input transformation theory later introduced in Section 3.4. However, it should be easy to follow without knowing the theory.

Assume for simplicity a drum with constant cross-sectional area (A_r [m^2]) and the mass balance

$$\frac{dh}{dt} = \frac{1}{A_r}(q_F - q_S) \tag{3.1}$$

where the feedwater flow q_F [m^3/s] may be expressed by the valve equation

$$q = C_v f(z)\sqrt{|\Delta P|} \tag{3.2}$$

where C_v is valve coefficient, $f(z)$ is the valve characteristic and $\Delta P = p_1 - p_2$ is the pressure drop over the valve with the opening z.

Defining the right-hand side of the mass balance equation as a transformed

input v,

$$v = \frac{1}{A_r}(q_F - q_S) \tag{3.3}$$

which replaces the feedwater flow q_F to control the level h.

This is selected such that when substituted into the model gives the transformed system

$$\frac{dh}{dt} = v \tag{3.4}$$

which is independent of disturbance q_S.

To implement the transformed input v, we need to generate the feedwater flowrate by solving ("reversing") Eq. 3.3 for q_F knowing the controller output v and the measurement q_S (the red circle in Figure 3.1).

$$q_F = vA_r + q_S \tag{3.5}$$

Finally, to implement q_F an inner flow-controller is used which manipulates the valve position z. This is cascade control which linearizes the nonlinear valve characteristic $f(z)$ in Eq. 3.2.

3.2 Introduction to transformed inputs

Figure 3.2 shows the block diagram for transformed inputs for achieving linearization, decoupling and feedforward disturbance rejection. In Figure 3.2, u is the original (physical) input while v is the transformed input which depends on u and other variables. The main idea is that the controller C (or in some cases the operator) sets the value of the transformed input v rather than the physical input u.

Shinskey (1981) (on page 119) writes in relation to selecting input and output variables for control:

> "There is no need to be limited to single measurable or manipulable variables. If a more meaningful variable happens to

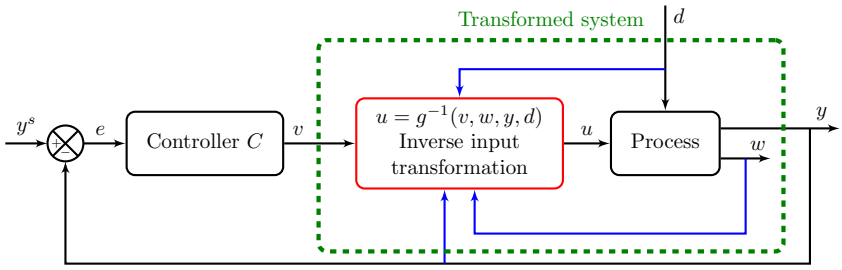

Figure 3.2: Use of transformed inputs v. For example, the transformed input could be the ratio $v = g(u, d) = \frac{u}{d}$, and the "inverse input transformation" block that inverts this relationship would then be $u = g^{-1}(v, d) = vd$.

> be a mathematical combination of two or more measurable or manipulable variables, there is no reason why it cannot be used."

We formalize the above statement and define the objective of introducing the transformed input v as: *The transformed input v replaces the physical input u as the manipulated variable for control of the output y, with the aim of simplifying the control task by including elements such as decoupling, linearization and feedforward action.*

Generally, the transformed input v is defined as a nonlinear static function g of the physical input u and other variables:

$$v = g(u, w, y, d) \tag{3.6}$$

where the specific function g is a design choice, and the other variables are:

$v =$ transformed inputs

$u =$ physical inputs

$d =$ measured disturbances

$y =$ controlled outputs (measured)

$w =$ other measured dependent variables (states).

Note that in this work, we do not include dynamic elements in the definition of the transformed input v, although this is frequently done in industrial practice.

In Eq. 3.6 we assume that we can measure disturbances d and some of the internal variables (states) w. This is often not the case for real applications, and there are two alternatives to deal with this. First, we can simplify the expression for the ideal transformed variable by keeping only parts of the benefits, for example decoupling, and leave the disturbance rejection to the outer feedback controller C. Second, we can use an observer to estimate d or w, though this is outside the scope of this work. To implement the transformed inputs we need to find the physical input u by solving a set of nonlinear algebraic equations that give u as a function of v, y, w, d.

Examples of transformed inputs from the process industry

$$v = u + d \tag{3.7a}$$

$$v = \frac{u}{d} \tag{3.7b}$$

$$v = u_1 - u_2 \tag{3.7c}$$

$$v = \frac{u_1}{u_2} \tag{3.7d}$$

$$v = w \tag{3.7e}$$

Such transformed inputs are often introduced using a physical understanding of the process. The transformed input $v = u + d$ in Eq. 3.7a provides feedforward action from a measured disturbance d, for example, in water make-up systems where u and d represent two feedrates and we want to control the combined flowrate $u + d$. The ratio $v = \frac{u}{d}$ in Eq. 3.7b gives feedforward action and linearization, for example when u and d are two feedrates and we want to control the quality (e.g., composition or temperature) of the

combined feed. The transformed variables with two inputs such as the difference $v = u_1 - u_2$ in Eq. 3.7c or the ratio $v = \frac{u_1}{u_2}$ in Eq. 3.7d may provide decoupling.

Starting from a static or dynamic process model, we derive ideal transformed inputs which achieve linearization, decoupling and perfect disturbance rejection.

To implement transformed inputs, we need to generate the physical input u from a given value of $v = g(u, w, y, d)$. Shinskey (1981) calls this "reversing the process model". There are two main ways of generating this inverse:

A. *Model-based inverse*

B. *Feedback-based inverse* using a cascade implementation with an inner controller for v or w.

3.3 Literature review

The following paragraph give a short overview of a few selected methods relevant to this work. The focus is on methods that are general rather than case specific applications.

Shinskey (1981) presents several examples from his industrial process control experience where nonlinear model-based calculation blocks are used to provide feedforward action, decoupling or linearization for a nonlinear system. These calculation blocks can often be traced back to a steady-state nonlinear process models. However, there is no academic literature that offers a systematic derivation of these calculation blocks based on static process models.

On the other hand, there is a large body of academic literature that uses a thorough mathematical treatment to transform a dynamic nonlinear model into a dynamic linear system. These methods may also be extended to provide disturbance rejection (sometimes called disturbance decoupling) or input-

output decoupling for special classes of systems (Isidori, 1995; Khalil, 2015; Nijmeijer and Schaft, 2016). A comprehensive review of specific nonlinear control methods for process control applications is presented in (Bequette, 1991).

Perhaps the better known and studied in nonlinear control course of these methods is feedback linearization (Isidori, 1995; Khalil, 2015). In its pure form, feedback linearization uses change of coordinates and a full static state feedback law to render the entire input-state map linear. This requires that a full state measurement is available (or estimated) and that the zero-dynamics are stable (i.e., equivalent to LHP-zero for linear systems, so RHP-zeros are not allowed). Feedback linearization uses elements of differential geometry and applies for systems with relative order r greater or equal to 1. The relative order represents the number of times the output needs to be differentiated wrt. time such that the input appears explicitly. For linear systems, the relative order represents the difference between poles and zeros. A similar relative order (ρ_d) can be defined for disturbances. Then, perfect disturbance rejection can be achieved only if $\rho_d \leq r$ (Isidori, 1995; Henson and Seborg, 1997). Note that this is a physical limitation of the system and not of the method itself, as a higher relative order from disturbances implies a smaller effective delay from disturbance d to output y than from the input u to output y.

For systems that either cannot be fully linearized or it is desired to preserve some of their nonlinear dynamics, only the input-output map may be linearized. The remaining dynamics of the system are included in the *zero*-dynamics of the system (Isidori and Ruberti, 1984; Henson and Seborg, 1997). Systems that cannot be linearized include cases where the full state measurement is not available, or the relative order of the systems is lower than the system's order (n).

For higher order systems, the transformed system becomes a chain (series) of linear differential equations. Most examples in the literature transform

the nonlinear system into an integrator system, which brings additional control limitations and a state-feedback controller is needed to stabilize the system. However, there is no requirement of transforming the systems into an integrator and, for process control applications, we generally want to avoid transforming the nonlinear system into an integrating system unless it was originally already integrating. For example, in (Nijmeijer and Schaft, 2016) (ch.5 and 6) a nonlinear system affine in the input of the type

$$\frac{dx}{dt} = f(x) + g(x)u \tag{3.8}$$

is transformed into a linear first-order system of the type

$$\frac{dx}{dt} = Ay + Bv \tag{3.9}$$

.

Similarly, for input-output linearization, Isidori and Ruberti (1984); Bastin and Dochain (1990) proposes obtaining a first order model linear input-output of the form $\frac{dy}{dt} = Ay + Bv$. This is also the methods used in this work for transformed input derived from a dynamic model.

In some cases, the state feedback law may not be possible to implement, for example because the model equation becomes singular for some operating points. To resolve this issues, a dynamic state feedback can be implemented (Lee et al., 2016). Essentially, this is a pure integral controller which solves numerically without the need to invert the transformation to generate the physical input, similar to the feedback-based implementation described later in Section 3.5.

Another method that provides nonlinear feedforward and linearization is *reference system synthesis* (Bartusiak et al., 1989). The focus is not on linearizing the original system, but rather on providing disturbance rejection and offset-free control. A nonlinear feedforward and feedback control law is

derived based on a nonlinear model such that the closed-loop behaviour of the system follows a desired trajectory given by a set of integral-differential equations, which may be linear or nonlinear. For systems with relative order $r = 1$ it is equivalent to the differential geometric approaches of input-output linearization.

Full mathematical treatment of feedback linearization with necessary and sufficient conditions is presented in several nonlinear control books, e.g., Isidori (1995); Khalil (2015); Nijmeijer and Schaft (2016). This literature provides a mathematical basis for issues related to the invertibility and stability of the transformations proposed in this work. However, the mathematical treatment is at a quite low level, such that these results may find their way into industrial practice.

3.4 Derivation of ideal transformed inputs

This section explains how to systematically derive transformed inputs and outputs starting from either a steady-state or dynamic model.

Consider a $n \times n$ system with n inputs u and n outputs y. The goal is to use the steady-state or dynamic model equations to define n transformed inputs v which ideally give linearization, decoupling and disturbance rejection.

Section 3.4.1 presents the derivation from a steady-state process model, while Section 3.4.2 shows the derivation for transformed inputs from a dynamic model. Section 3.4.3 discusses how in some cases, the model and thus the expression for transformed inputs may be simplified by introducing additional measured state variables (e.g., flowrates). Section 3.4.4 shows how in other cases, the model becomes simpler by introducing a transformed output (e.g., enthalpy). As shown in the example in Section 3.7, we may also use a combination of steady-state and dynamic models.

3.4.1 Obtaining ideal transformed system from a steady-state process model

There are many examples from the process industry for specific application that use steady-state process models to derive nonlinear feedforward or decoupling blocks (e.g.,Shinskey (1981)) that on a closer inspection are similar to the static input transformation derived below. While this derivation may seem trivial, its purpose is to provide a formal theory that can be used to move from case specific applications to a systematic approach. This section discusses the *ideal* transformation with no model error and perfect measurement of d.

We start from a steady-state process model with $n + n_x$ independent equations given in its general form by Eq. 3.10.

$$0 = f_x(u, x, y, d) \tag{3.10}$$

where x are internal variables (states) and n_x is the number of additional equations necessary to have determined system.

Assuming that we can separate the variables x and y, we can use the n_x extra equations to eliminate the internal variables x to obtain a model (at least formally) as given in Eq. 3.11.

$$0 = f(u, y, d) \tag{3.11}$$

Assuming that all model equations in Eq. 3.11 independent, we can separate y on the LHS and all the other variables on the RHS to obtain a steady-state nonlinear model in the form of Eq. 3.12.

$$y = f_0(u, d) \tag{3.12}$$

where the subscript 0 in f_0 denotes a steady-state (algebraic) function.

Using the RHS of Eq. 3.12 and by introducing a tuning parameter B_0, we define the *ideal static transformed input* as:

$$v_0 = \underbrace{B_0^{-1} f_0(u, d)}_{g(u,d)} \tag{3.13}$$

where the matrix B_0 is free to choose. The selection of B_0 is discussed in Section 3.4.1.1, for example, we may select to have a steady-state gain of 1.

From Eq. 3.13 we have that $f_0(u, d) = B_0 v_0$ and substituting it into Eq. 3.12 yields the transformed system:

$$y = B_0 v_0 \tag{3.14}$$

The transformed system in Eq. 3.14 is linear and independent of disturbances, and for the multivariable case it is also decoupled if we select B_0 to be a diagonal matrix.

To implement the transformed input v_0, we solve Eq. 3.13 with respect to u given all other variables to obtain the ideal input

$$u = g^{-1}(v_0, d) \tag{3.15}$$

where we assume we can explicitly or numerically find g^{-1}. This implementation is discussed in Section 3.5.

Note that it may not be necessary to explicitly derive the expression for $f_0(u, d)$ in Eq. 3.12. Rather, since the objective is to find the ideal input $u = g^{-1}(v_0, d)$ that gives the transformed system $y = B_0 v_0$ in Eq. 3.14, it may be simpler to keep with the original model equations in Eq. 3.11 or Eq. 3.10, and solve these with respect to u for a given value of $y = B_0 v_0$ to obtain $u = g^{-1}(v_0, d)$. This solution can be done either analytically or numerically, but a numerical solution is usually necessary for complicated models, for example for the heat exchanger discussed in Section 3.8.

3.4.1.1 Choice of the tuning parameter B_0

The choice of B_0 is not critical, as it can be compensated by changing the gain of the outer controller C. It is more intuitive to select

$$B_0 = I_n \tag{3.16}$$

such that the ideal transformed input is simplified to the right-hand side of the model in Eq. 3.12

$$v_0 = f_0(u, d) \tag{3.17}$$

and the transformed system becomes

$$v_0 = f_0(u, d) \tag{3.18}$$

In this case it may be tempting to think of the transformed input v_0 as the setpoint for the output y, but this is misleading because we usually have an outer feedback controller C which has the "true" setpoint y^s as one of its inputs, whereas v_0 is the output from C (see Figure 3.2). Thus, it is better to think of v_0 as the transformed process input, or possibly as a modified setpoint as it is done in (Bastin and Dochain, 1990).

3.4.2 Obtaining ideal transformed input from a dynamic process model

The ideal transformed input (v_A) derived in this section is closely related to the theory of feedback linearization for a system with relative order $r = 1$, that is the input u explicitly appears in the time derivative of the output y.

We start from a nonlinear dynamic model written in the form of Eq. 3.19.

$$\frac{dy}{dt} = f(u, y, d) \tag{3.19}$$

Using the right-hand-side of the model in Eq. 3.19, and by introducing the tuning parameters the matrices A and B, we define the ideal transformed input v_A for as

$$v_A = \underbrace{B^{-1}(f(u,y,d) - Ay)}_{g(u,y,d)} \tag{3.20}$$

where the subscript A in v_A denotes a transformed input derived from a dynamic function f and with a tuning parameter A. The tuning of the matrices A and B is discussed in Section 3.4.2.1.

From Eq. 3.20 we have that $f(u,y,d) = Bv_A + Ay$ which substituted into Eq. 3.19 gives the transformed system from Eq. 3.21.

Then assuming no uncertainty (no model error for $f(u,y,d)$ and perfect measurements of d and y) the transformed system becomes

$$\frac{dy}{dt} = Ay + Bv_A \tag{3.21}$$

The transformed system in Eq. 3.21 is linear and independent of disturbances, and for the multivariable $(n \times n)$ case, it is also decoupled if we select A and B to be diagonal matrices.

Note that we have assumed that we can generate from the transformed input v_A the exact corresponding physical input u using Eq. 3.22.

$$u = g^{-1}(v_A, y, d) \tag{3.22}$$

To guarantee invertibility in Eq. 3.22, it is possible to restrict the class of models to guarantee that we always have a solution, as is done in the literature on feedback linearization. In particular, in this literature it is assumed that the model is linear in the input u, that is, that we can write the right-hand side of Eq. 3.19 as shown in Khalil (2015) (p. 293).

$$f(u,y,d) = f_1(y,d) + f_2(y,d)\ u \tag{3.23}$$

where the functions f_1 and f_2 must satisfy certain smoothness conditions. Interestingly, many process models are linear in the flows, so if we make use of inner flow controllers then many process models satisfy Eq. 3.23. Nevertheless, we do not make this assumption in this paper, so the invertibility may need to be studied separately for each application.

3.4.2.1 Choice of tuning parameter B

To achieve dynamic decoupling in Eq. 3.21 for the multivariable case, we need to select both matrices B and A to be diagonal. Dynamic decoupling is desirable because the optimal outer controller C is then diagonal (single-loop controllers). Otherwise, the choice of B is not critical as it may be compensated by changing the gain in the feedback controller C.

One simple choice is $B = I$, which is often used in feedback linearization. Alternatively, to keep the initial (high-frequency) gain from v_i to y_i equal to that of the original system (from u_i to y_i) we may choose $B = \text{diag}(\tilde{B}) = \text{diag}(\partial f/\partial u)_*$ where the differentiation is performed at the nominal operating point *. However, in most of the examples in this paper we select

$$B = -A \tag{3.24}$$

because this gives $y = v_A$ at steady state (where $\frac{dy}{dt} = f(u, y, d) = 0$). [1] With the choice $B = -A$, the transformed input and corresponding transformed system become

$$v_A = -A^{-1} f(u, y, d) + y \tag{3.25a}$$

$$\frac{dy}{dt} = A(y - v_A) \tag{3.25b}$$

Equivalently, we may introduce the time constant matrix of the transformed

[1] Interestingly, since $y = Iv_A$ at steady state, where I is the identity matrix, the choice $B = -A$ gives decoupling at steady state even if A (and thus B) is not diagonal. However, to also get dynamic decoupling, we must choose A to be diagonal.

system

$$\mathcal{T}_A = -A^{-1} \tag{3.26}$$

and the transformed input and corresponding transformed system may be written as

$$v_A = \mathcal{T}_A f(u, y, d) + y \tag{3.27a}$$

$$\mathcal{T}_A \frac{dy}{dt} + y = v_A \tag{3.27b}$$

3.4.2.2 Choice of tuning parameter A

The choice of the parameter A (or equivalently of $\mathcal{T}_A = -A^{-1}$) is important as it determines the dynamics of the transformed system. However, the importance should not be overemphasized, since we can change the closed-loop dynamics by design of the outer controller C. Note that we must choose $A < 0$ for the transformed system to be stable. We discuss below three choices for the tuning parameter A, which we will then compare in simulations using a mixing example in Section 3.11.2.

1. Keep the original dynamics, $A = \tilde{A}$. In most cases we propose selecting

$$A = \tilde{A} \equiv \left(\frac{\partial f}{\partial y} \right)_* \tag{3.28}$$

where the derivative of f wrt. y is evaluated at the nominal point $*$ of operation. With this choice, the time constant of the transformed system is equal to the time constant of the linearized system. This choice also minimizes the effect of the measurements y on the transformed variables v_A.

Proof: Linearizing the "original" nonlinear model $\frac{dy}{dt} = f(u, y, d)$ yields

$$\frac{dy}{dt} = df = \tilde{A}dy + \tilde{B}du + \tilde{B}_d dd \tag{3.29}$$

where the $\sim$ variables correspond to the linearized dynamics of the original system $\tilde{A} = (\partial f/\partial y)_*$, $\tilde{B} = (\partial f/\partial u)_*$ and $\tilde{B}_d = (\partial f/\partial d)_*$, where the evaluation of the derivatives is performed at the nominal point of operation, denoted by $*$. Thus, if we select the tuning parameter $A = \tilde{A}$ then the transformed system in Eq. 3.21 will locally (close to the nominal operating point $*$) have the same dynamics as the original system in Eq. 3.29.

Furthermore, from Eq. 3.20 the linearized transformed input becomes

$$dv_A = B^{-1}(df - Ady) = B^{-1}(\tilde{B}du + \tilde{B}_d dd) \tag{3.30}$$

and we find that dv_A is independent of dy.

Thus, with the choice for A in (Eq. 3.28), there is no feedback from y on the transformed input v_A at the nominal point $*$. For the multivariable case, to get a decoupled response, we may choose A equal to the diagonal elements of the A-matrix of the original system,

$$A = \text{diag}(\tilde{A}) = \text{diag}\left(\frac{\partial f}{\partial y}\right)_* \tag{3.31}$$

For the multivariable case, this will not exactly keep the original dynamics and there will be some feedback from y to v at the nominal point. However, it provides a good comprise between decoupling and minimizing the feedback from y. In any case, the exact value for A should not be overemphasized, since we can change the closed-loop dynamics by design of the outer controller C.

2. Make the transformed system faster: $|A| > |\tilde{A}|$. To speed up the response from v to y, we may use larger magnitudes for the elements in A than that resulting from Eq. 3.28. However, note that the presence of a time delay in the measurement of y (or other dynamics that result in an effective delay) may give instability if we choose the elements in A too large

in magnitude. Alternatively, note that it is always possible to select $A = \tilde{A}$ as in Eq. 3.28 and instead "speed up" the response with the outer controller C, which can be designed based on the experimental response from v_A to y and for which established robust design methods are available, for example, the SIMC PID-rules (Skogestad, 2003).

3. Make the system integrating: $A = 0$. The choice $A = 0$ is often seen in the examples in feedback linearization literature (Isidori, 1995). This results in an integrating transformed system,

$$\frac{dy}{dt} = Bv \tag{3.32}$$

where usually $B = I_n$.

However, except for cases where the original system is already unstable or close to integrating, the choice $A = 0$ is not recommended, at least not for process control applications. There are two reasons for this. The main reason is that the transformed system will not reach steady state without the outer controller C. In particular, any unmeasured disturbances will cause the output y to integrate and drift away from its desired steady state (also see the simulations in Section 3.11.2). This drifting will only stop when the input u reaches its physical maximum or minimum constraint, when we loose control of y. This is very undesirable, because we may want to be able to operate the transformed system without the outer controller C. The second reason is that we generally want to use integral action in the outer controller C to correct for uncertainty in the model, unmeasured disturbances or delays. With $A = 0$, the integrator in the transformed system poses performance limitations for disturbances at the plant input (e.g., (Skogestad, 2003)). This performance limitation is not considered in the feedback linearization literature because the theory assume state feedback, that is, the outer controller C is a P-controller.

3.4.3 Model and transformed input in terms of measured state variables w

So far we have defined transformed variables for systems with relative order at most $r = 1$ (the steady-state system in Eq. 3.12 and dynamic in Eq. 3.19). Thus, for the scalar case we are restricted to first-order systems. However, if we allow the function f to depend on additional measured states w, then the class of systems is significantly larger.

However, the derived expressions for the ideal transformed inputs (v_0 and v_A) also hold when we include additional measured dependent variables w (states) in the expressions for f_0 and f, that is, if we consider steady-state models in the form

$$y = f_{0,w}(u, w, d) \tag{3.33}$$

and dynamic models in the form

$$\frac{dy}{dt} = f_w(u, w, y, d) \tag{3.34}$$

Thus we treat the additional states w as measured (internal) disturbances. This allows to simplify higher order models, because we no longer require a model for w in Eq. 3.33 or Eq. 3.34.

By including the w variables, the ideal transformed input for the steady-state system in Eq. 3.33 becomes

$$v_0 = \underbrace{B_0^{-1} f_{0,w}(u, w, d)}_{g(u,w,d)} \tag{3.35}$$

and the ideal transformed input for a dynamic model in Eq. 3.34 becomes

$$v_A = \underbrace{B^{-1}(f_w(u, w, y, d) - Ay)}_{g(u,w,y,d)} \tag{3.36}$$

Assuming that we are able to generate the exact inverse g^{-1} and that the resulting transformed system is internally stable (see Section 3.6), the resulting transformed system from the transformed input v to the output y is defined as before, i.e., in Eq. 3.13 for the steady-state case, and in Eq. 3.20 for the dynamic case. That is the system is also decoupled, independent of disturbances. Note that the the transformed system may no longer be steady-state or first-order because it may include "hidden" dynamics through the measured state variables w. These "hidden" dynamics may in some cases result in unstable zeros [2] (inverse response in the scalar linear case) from u to v and in such cases the use of the exact inverse will result in an internally unstable transformed system (also see the simple example in Section 3.6.

Examples of w variables include the temperature in a steam network when the CV is the network pressure (see the example in Section 3.10), or the temperature at the cold outlet of a heat exchanger when the CV is the temperature at the hot outlet (see the example in Section 3.8).

3.4.3.1 Dynamics of transformed system with measured state (w) variables

When we include w-variables in the ideal static transformed inputs v_0, then the dynamics of the transformed system (from v_0 to y) will no longer be the same as of the original system (from u to y). The reason is the feedback from w. An example is given by the variables $v_{0,w}$ for the heat exchanger in Section 3.8 (Figure 3.15) where we find that the the dynamics of the transformed system become slower. Note that for the steady-state case, we have no tuning parameter to change the dynamics of the transformed system.

[2] Unstable zero dynamics go by many names. They are the same as RHP-zeros for linear systems, and linear systems with RHP-zeros and/or time delay are also called non-minimum phase systems. In the linear scalar case, RHP-zeros always give inverse response in the time domain. More generally, for nonlinear systems the unstable zero dynamics from u to v correspond to the unstable dynamics of the inverse map from v to u (Isidori, 1995).

On the other hand, in the dynamic case, that is, with ideal dynamic transformed inputs v_A, we can use the matrix A to freely set the dynamics of the transformed system, also when v_A depends on w. However, note that in such cases the dynamics of the transformed system (from v_A to y) will not be the same as for the original dynamics (from u to y), no matter how we choose A. One reason is that the number of differential equations describing the transformed dynamic system $\frac{dy}{dt} = Ay + Bv$ is generally lower than that of the original dynamic system. The choice $A = \text{diag}(\partial f_w/\partial y)_*$ may be a good starting point as it gives little feedback from y, but this choice will not keep the original dynamics, because u also has an indirect (and possible high-order) effect on y through the variable w.

3.4.4 Transformed outputs

Often, when we develop a process model, we start from a linear model, and we introduce bilinear or nonlinear expressions for variables we cannot measure, thus complicating the model equations. For example we express the mass of a tank as a function of the level or we write the energy balance in form of temperature thus replacing internal energy as a state. The reason to introduce the transformed output z is that the model may be simpler to express in terms of z compared to in terms of the output y. In a way, we want to mimic the linear model we started with. This also simplifies the implementation of the transformed input v because it may be simpler to invert the function g to generate the process input u, as later shown in the steam cycle example in Section 3.9.

The transformed output z can be introduced both for steady-state and dynamic systems and it is generally defined as

$$z = h(y, w, d) \tag{3.37}$$

where y are the outputs that we want to control at a given setpoint y^s and h

is a static function of our choice.

By introducing the transformed output z, the transformed input v becomes a function of z instead of y (and of u, w, d.):

$$v_z = g_z(u, w, z, d) \tag{3.38}$$

where the index z in v_z and g_z denotes the introduction of the transformed output z.

3.4.4.1 Ideal transformed inputs and outputs from steady-state model

Consider a steady-state process where we can write the model in Eq. 3.12 ($y = f_0(u, w, d)$) in its simpler and more general form

$$\underbrace{h(y, w, d)}_{z} = \underbrace{g_z(u, w, d)}_{v_{z0}} \tag{3.39}$$

where h is the function introduced in Eq. 3.37. Note that the outputs y are on the LHS and the inputs u are on the RHS. The key idea now is that the function g_z on the right-hand side is easier to invert.

Similar to the previous section, we want to find a transformed input v and output z that at steady-state give a transformed system $y = v_0$ (Eq. 3.14 with $B_0 = I_n$). It is straightforward to see that this can be achieved by selecting the transformed output as the LHS of Eq. 3.39 which yields the definition of z from Eq.3.37, and the transformed input the RHS of Eq. 3.39

$$v_{z0} = g_z(u, w, d) \tag{3.40}$$

To generate the process input u, we solve Eq. 3.40 for u, given

$$u = g_z^{-1}(v_{z0}, w, d) \tag{3.41}$$

which may be implemented as in Figure 3.7b.

3.4.4.2 Ideal transformed inputs and outputs from dynamic model

The idea is that it is easier to write the dynamic model in terms of the transformed outputs z rather than in terms of the outputs y. Consider a dynamic process where the model Eq. 3.19 can be written in its simpler and more general form

$$\frac{dz}{dt} = f_z(u, w, z, d) \tag{3.42}$$

where $z = h(y, w, d)$ is the transformed output.

From Eq. 3.36 the ideal transformed input is $v_{zA} = B^{-1}(f_z - Az)$, and the transformed system as seen from the controller C becomes

$$\frac{dz}{dt} = Az + Bv_{zA} \tag{3.43}$$

which is decoupled, linear and independent of disturbances. This simplifies the design of the outer controller C. However, note from Figure 3.7a that the disturbances that effect the transformed outputs $z = h(y, d)$ will only be counteracted if the feedback controller C is implemented.

3.4.5 Extension to higher order systems: chain of input transformations

The transformed input derived in Section 3.4 is limited to systems where the relative order from the input u to the output y is 0 for the steady-state model case (v_0) and 1 for the dynamic model case (v_A).

The question we want to answer is how can we extend the theory to higher order systems, that is when the input u does not appear explicitly in the model equation for y, e.g., tanks in series when we want to control the temperature of the last tank by using the inlet flow of the first tank. One option is to introduce additional state measurements w and use the feedback-based

implementation from Figure 3.4b. However, with this approach we will not have perfect control of y because of dynamics introduced by the inner cascade controller in generating the inversion $u = g^{-1}(v, w, y, d)$. Alternatively, if we have a model for w as a function of u, we may introduce a second transformed input $v_2 = g_2(u, w, d)$ resulting in a chain of transformation, see Figure 3.3.

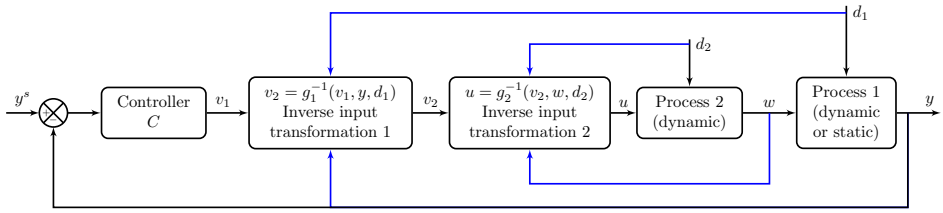

Figure 3.3: Chain of input transformations

Consider a system formed by two processes in series (the relative order from u to y is 2), given by

$$\text{Process 1:} \qquad \frac{dy}{dt} = f_1(w, y, d_1) \tag{3.44a}$$

$$\text{Process 2:} \qquad \frac{dw}{dt} = f_2(u, w, d_2) \tag{3.44b}$$

Note that process 1 (Eq. 3.44a) may be either be steady-state or dynamic, while process 2 (Eq. 3.44b) is dynamic.

Using Eq. 3.20 the transformed inputs for process 1 and process 2 are defined as

$$\text{Input transformation 1:} \qquad v_1 = v_A = \underbrace{B^{-1}\left(f_1(w, y, d_1) - Ay\right)}_{g_1(w,y,d_1)} \tag{3.45a}$$

$$\text{Input transformation 2:} \qquad v_2 = \underbrace{B^{-1}\left(f_2(u, w, y, d_2) - Aw\right)}_{g_2(u,w,y,d_2)} \tag{3.45b}$$

The corresponding inputs are computed as

$$\text{For control of } y: \qquad u = g_2^{-1}(v_2, w, d_2) \tag{3.46a}$$

$$\text{For control of } w: \qquad v_2 = g_1^{-1}(v_1, y, d_1) \tag{3.46b}$$

Note that the transformed system is subject to the same control limitation as the original system. Therefore, we can only have perfect feedforward control for disturbances with the same relative order as the input u. This means that we cannot have perfect disturbances rejection if there is a larger effective delay from u to y than from d to y. For example, consider a continuous process with two mixing tanks in series where the objective is to control the outlet temperature in the second tank ($y = T_2$) using the heat input to the first tank ($u = Q_1$). We have an extra state measurement of the temperature in the first tank ($w = T_1$). In this case the relative order from u to y is 2 and perfect disturbance rejection is not possible for disturbances d_1 directly affecting y (e.g., another inlet stream to tank 2). However, since the relative order from u to w is 1, it is possible, by using a chain of transformations, to get perfect control for disturbances d_2 directly affecting w (e.g., the inlet feed temperature to tank 1).

A more detailed treatment of implementing the chain of transformations together with simulation examples are available in the Master Thesis of Kingstree (2021).

3.5 Implementation of transformed inputs

This section explains how to implement the transformed variables (v and z) introduced in Section 3.4, starting with the the transformed input v.

As mentioned previously in Section 3.4 is is not enough to define and derive the transformed input v, we need also to generate the corresponding physical input u to implement v in the real process, that is we need to solve

$v = g(u, w, y, d)$ for u given all other variables. There are two main options:

A Model-based implementation, which solves numerically or algebraically $u = g^{-1}(v, w, y, d)$ (Figures 3.4a and 3.4a)

B Feedback-based implementation, which uses an inner (P)I-controller to find the u that gives $v = v^s$, where v^s is given by the outer controller C that controls y (Figure 3.4b).

Note that we may also combine A and B (alternative C, Figure 3.4c). We begin with a generalization of these three alternatives, followed by exemplifying them for a level control problem, motivated by the three elements drum level control common in power plants control systems (also see Section 3.1).

3.5.1 Alternative A: Model-based inversion (Figure 3.4a and Figure 3.4a)

The first approach is shown in Figures 3.2 and 3.4a. The idea is to invert the input transformation $v = g(u, w, y, d)$ in Eq. 3.6, by analytically or numerically finding the input u that corresponds to given values of v^s, w, y and d, which gives exactly $v = v^s$ both dynamically and at steady-state. We can formally write the solution as

$$u = g^{-1}(v, w, y, d) \tag{3.47}$$

This gives the exact inverse $g^{-1}(v, w, y, d)$ if the inverse exists, if there is no model uncertainty and if all variables w, y and d are measured perfectly.

3.5.2 Alternative B: Feedback inversion with inner v-controller (cascade control) (Figure 3.4b)

In some cases the analytic inverse function g^{-1} may be difficult to compute. In other cases, the inverse g^{-1} does not exist (even numerically) because g

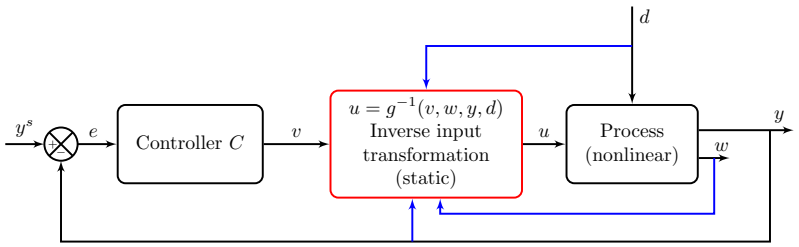

(a) Model-based implementation A of transformed input $v = g(u, w, y, d)$. The physical input $u = g^{-1}(v, w, y, d)$ is generated by a static (algebraic) calculation block which inverts the transformed input model equations. The model-based implementation generates the exact inverse for the case with no model error.

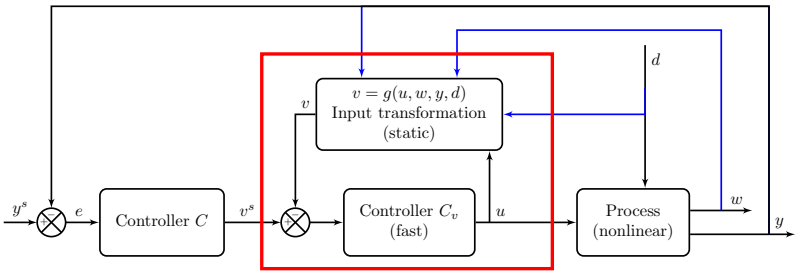

(b) Feedback implementation B of transformed input $v = g(u, w, y, d)$ using cascade control with an inner v-controller. The computed value of v is driven to its setpoint v^s by the inner feedback controller C_v which generates the physical input u. This implementation generates an approximate inverse.

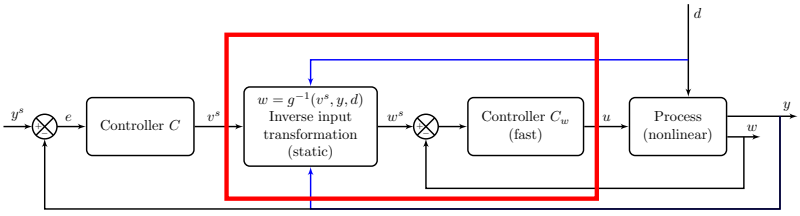

(c) Combined model-based and feedback implementation C of transformed input $v = g(w, y, d)$ using inner w-controller. Commonly, C_w is a flow controller (w = flowrate) and u is the valve position. This implementation generates an approximate inverse.

Figure 3.4: Alternative implementations for inverting the input transformation $v = g(u, w, y, d)$. C, C_v and C_w are usually single-loop PID controllers. The red boxes fulfil the same role.

does not depend explicitly on u (i.e., system with relative order $r > 1$), or it may have a singularity. Finally, when v depends on some state variables w, it may happen that the inverse map g^{-1} gives internal instability (zero dynamics or inverse response). In all these cases, we may instead use the approximate feedback-based approach for generating the physical input u. Note that this approach is equivalent to the dynamic inversion implementation of feedback linearization for avoiding problems with singularities (Lee et al., 2016).

Figure 3.4b shows the second implementation approach. This approach does not imply inverting the transformed input, rather relies on feedback and integral action to generated dynamically the physical input u. The idea is that we compute the transformed input $v = g(u, w, y, d)$ from the physical measurements of u, w, y and d, and the inner controller C_v adjust u dynamically such that $v = v^s$, where v^s is given by the outer controller C controlling y. At steady-state $v = v^s$ and the nonlinearity in the responses from u to v is effectively removed by the action of the feedback (P)I controller C_v.

To tune the inner controller C_v in Figure 3.4b we may use a pure linear I-controller (Eq. 3.48) because the function g is defined as a static function and thus the response from u to v usually has a large direct (static) effect. Note that an I-controller is generally recommended for pure steady-state processes (Skogestad, 2003).

$$u(t) = u(t_0) + K_I \int_{t_0}^{t} (v^s(t) - v(t))dt \tag{3.48}$$

where $u(t_0)$ is the bias and the integral gain K_I is a tuning parameter. The value of $u(t_0)$ does not matter (except initially), because it will be compensated by the integral action. The integral action will make $v = v^s$ at steady state (as time goes to infinity) and a larger value of K_I will make $v(t)$ approach v^s faster.

However, there may be some dynamics from u to v through the w variables.

Thus, more generally, we may tune linear PID-controllers using the SIMC rules (Skogestad, 2003) based on the experimental step response from u to v. For the $n \times n$ multivariable case, we usually design n single-loop linear controllers for C_v, although it is possible to use multivariable control.

3.5.3 Alternative C: Combined feedback- and model-based inversion with inner w-controller (Figure 3.4c)

Figure 3.4c shows the combined implementation (C). This may be applied when v does not depends explicitly on u, and instead we use measurement of w in deriving the transformed input $v = g(w(u), y, d)$ (see Section 3.4.3). This alternative contains an inner C_w-controller that controls w at its setpoint w^s given by inverting the function g in a model-based inversion block ($w^s = g^{-1}(v, y, d)$), which we assume can be inverted. Because of this assumption, the cascade implementation C in Figure 3.4c is less general than the cascade implementation B in Figure 3.4b.

There are a few advantages to the C implementation. First, the model based inversion may contribute to linearization, feedforward and decoupling compared. Second, control of w is usually less interactive than control of v, which is a significant advantage for faster convergence with single-loop control. Finally, the inner controller C_w controls a physical measurement w, whereas v in Figure 3.4b is usually not a physical variable. The inner controller C_w may be tuned in a similar way as C_v, based on an experimental response from u to w.

For examples w may be the flowrate, and C_w is a fast flow controller which allows us to use directly the flow in deriving the transformed input v instead of the true plant input u, the valve position z. Another common example is when w is temperature (T) or power (Q) and u is a valve position (z), and C_w is a temperature or power controller. In both these cases, we may have a model for the relationship from u to w, which we could have inverted and used in a model-based implementation A (Figure 3.4a), but

instead we prefer to use feedback control based on a measurement of w to invert the relationship, either because it is simpler or because it is more accurate. Of course, this assumes that we can use a relatively high gain in the inner controller C_w such that the time constant for the slave loop is much smaller (typically by a factor 10 or more) than the time constant of the outer loop controller C.

3.5.4 Comparison of the three alternative implementations in Figure 3.4

Although the red blocks in the three block diagrams in Figure 3.4 perform the same task of inverting the input transformation and generating the physical input u from a given value of transformed input v and the other measured variables (w, y, and d), there are important differences. First, in the two feedback implementations (B, C), the transformed input v is replaced by its setpoint v^s and the response will not be perfect dynamically. Second, there may be differences in the variables used. For example, and as mentioned, the use of measured w-variables in the two feedback implementations (B, C) may replace some process model equations and disturbance variables (d) in the exact model-based implementation (A).

3.5.5 Implementation of transformed inputs: drum level control example revisited

The objective of this example is to compare the three alternative implementations in Figures 3.4a to 3.4c on a (steam) drum level control problem. Moreover, this example is chosen to show case how the input transformation theory can be applied to derive a well adopted control structure in power plants, i.e., the so-called *3-elements control* (see Section 3.1). Similarly to Section 2.3, we use the inflow to control the level $y = H$. We consider that we have a fixed speed feedwater pump and the physical input u is the valve

position, that is, $u = z$. From a mass balance for a tank with constant cross-sectional area and constant density, the model can be written as

$$\frac{dH}{dt} = \frac{1}{A_r}\left(q_F(u) - q_S\right) \tag{3.49}$$

where H [m] is the level, A_r [m^2] is the tank area, $q_F(u)$ [m^3/s] is the inflow (feedwater) and q_S [m^3/s] is the outflow (steam). The inflow q_F [m^3/s] depends on z by the following valve equation:

$$q_F(u) = F(u)k_V\sqrt{\frac{|p_1 - p_2|}{\rho}} \tag{3.50}$$

where $F(u)$ is the valve characteristic, k_V [m^2] is the valve constant, ρ [kg/m^3] is the liquid density, and $p_1 - p_2$ [N/m^2] (disturbance d) is the pressure drop over the valve.

We assume that the level ($y = H$) measurement is available, but it has a delay and it may be inaccurate because of the shrink and swell effect as explained in Section 3.1. We also have a measurement of the outflow ($w = q_S$) which we may use if desired.

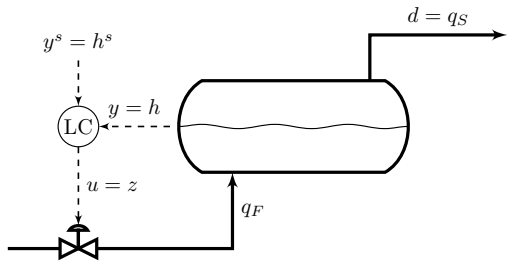

Figure 3.5: Level control with no input transformation.

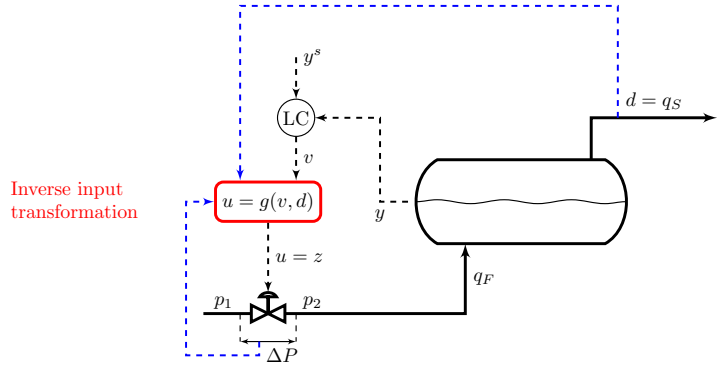

(a) Exact inverse transformation (inverting model).

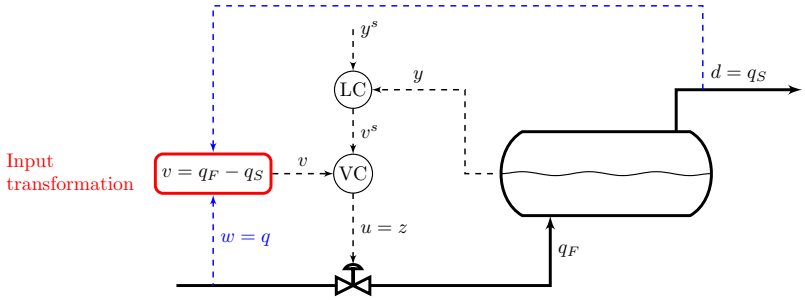

(b) Inner controller for $v = q_F - q_S$.

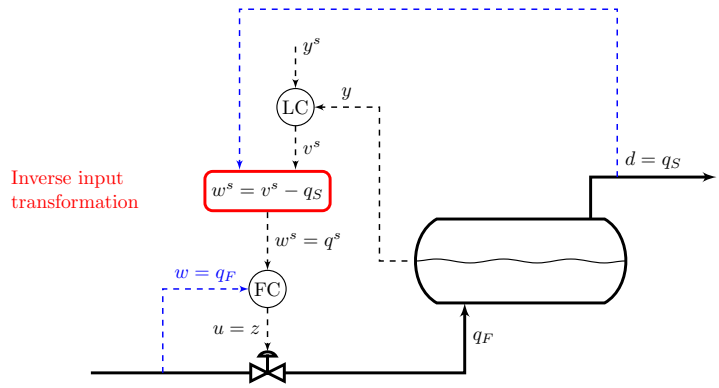

(c) With inner controller for $w = q_F$ (flow controller).

Figure 3.6: Three alternative implementations for level control. The input transformation provides feedforward control from q_S thus linearization of the valve. The transformation also provides disturbance rejection from p_1 and p_2 (by feedforward in *(a)* and through feedback in *(b)* and *(c)*.

3.5.5.1 No input transformation

The simplest solution to implement is conventional feedback, as shown in Figure 3.5. We directly control the level using a controller C, for example a PI-controller, which adjusts the valve position u, that is without making use of the extra measurement $w = q_F$ or of the model Eq. 3.49. While this solution is simple, it may not give a good performance for tight level control when there is delay and inaccuracy in the measurement of $y = H$. Thus, the level may vary if there are disturbances in q_S, p_1 and p_2. Furthermore, the valve characteristic $F(u)$ may be nonlinear which may give a low process gain and thus slow control when $F(u)$ is in a "flat" region, that is, when q_F is insensitive to changes in u. Typically, this will be when the valve approaches fully open or fully closed.

3.5.5.2 With input transformation

We can select the transformed input as the right-hand side of the dynamic model in Eq. 3.49 multiplied with a constant $\frac{1}{B}$ (where B is a parameter that we introduce to generalize the method and that we can choose see Section 3.4.2.1),

$$v = B^{-1} \frac{1}{A_r} \left(q_F(u) - q_S \right) \tag{3.51}$$

Compared to the generic transformed input in Eq. 3.20 derived systematically, we select the tuning parameter $A = 0$, which is typical for integrator systems.

From Eq. 3.51 we have that $\frac{1}{A_r} \left(q_F(u) - q_S \right) = Bv$ which substituted into the dynamic model in Eq. 3.49 yields a transformed system that is an integrator, similar to feedback linearization (Isidori, 1995),

$$\frac{dH}{dt} = Bv \tag{3.52}$$

The system in Eq. 3.52 has two advantages compared to the dynamic

model in Eq. 3.49. First it is independent of disturbance p_1 and p_2. Second, the possible nonlinearities from the valve characteristic $F(u)$ are eliminated, at least from the point of view of outer controller C which manipulates v to control $y = H$.

For simplicity, in the following, we select the parameter $B = \frac{1}{A_r}$ such that the transformed variable becomes

$$v = q_F(u) - q_S \tag{3.53}$$

The transformed input in Eq. 3.53 will give the transformed system in Eq. 3.52 only if we generate and implement the corresponding physical input u from a given value of v and the other measured variables. As described above, there are two main options, model-based and feedback-based using cascade.

3.5.5.2.1 Exact implementation: Inverting the valve model This is the implementation from Figure 3.4a, which adapted to the drum level control problem gives the solution in the flowsheet in Figure 3.6a.

Substituting the valve equation in Eq. 3.50 into Eq. 3.53 yields

$$v = \underbrace{F(u)k_V\sqrt{\frac{|p_1 - p_2|}{\rho}}) - q_S}_{g(u,d)} \tag{3.54}$$

where $d = [q_S,\ p_1,\ p_2]$. Solving Eq. 3.54 with respect to $u = z$ gives

$$u = \underbrace{\frac{F(u)^{-1}(v - qS)}{k_V\sqrt{\frac{p_1 - p_2}{\rho}}}}_{g^{-1}(v,d)} \tag{3.55}$$

where $F(u)^{-1}$ denotes the inverse of the valve characteristic $F(u)$. However, the inverse transformation in Eq. 3.55 requires a good model and it

also requires measurements of the disturbances p_1 and p_2. Therefore, rather than inverting the valve equation, it is more common and easier to measure the inflow $w = q_F$ and use an inner flow controller, discussed next.

3.5.5.2.2 Alternative cascade implementations: Using the flow measurement (cascade control) Introducing the extra measurement w, the transformed input from Eq. 3.53 becomes

$$v = \underbrace{w - q_S}_{g(w,d)} \tag{3.56}$$

Observe that v in Eq. 3.56 does not depend explicitly on u, and we must use one of the two cascade implementations in Figures 3.4b and 3.4c. Adapted to the drum level control problem, this gives the flowsheets in Figures 3.6b and 3.6c. *More importantly, these implementations are similar with the two implementation for* 3-elements control *from Lindsley (2000), p.110 and p.111.*

Note that for the cascade control of v, the controller C_v is actually a flow controller because v is the difference between two flows. For the cascade control of w, C_w is of course a flow controller since $w = q_F$ is a flow. For cascade control of w, we need to invert Eq. 3.56 with respect to $w = q_F$ which gives the "inverse static transformation"

$$w^s = \underbrace{v^s - q_S}_{g_w^{-1}(v,d)} \tag{3.57}$$

The subscripts superscript s on w and v denote that w^s and v^s are the setpoints for w and v, respectively. To achieve the desired disturbance rejection and linearization, we must assume that the inner flow controller (C_v or C_w) can be made fast compared to the expected process dynamics for $y = H$ and compared to the outer controller C. This is most likely possible,

since the valve response from u to $w = q_F$ is usually very fast, that is, the process is essentially static with a time constant (τ) close to zero. From the SIMC PID rules (Skogestad, 2003), a pure I-controller may then be a good choice for this flow controller.

3.5.6 Implementation of transformed outputs

Figure 3.7a shows the general implementation of combined transformed inputs and outputs, whereas Figure 3.7b shows the block diagram for the case when the transformed input is derived from a steady-state model. In Figure 3.7, the outer controller C is controlling the transformed outputs z rather than the (physical) outputs y for which we have a setpoint y^s. However, because both y and y^s are sent through the same static transformation h, we will achieve $y = y^s$ at steady state. Also note from Figure 3.7 that the input transformation g_z needs to be inverted (or approximately inverted using one of the three options in Figure 3.4a), whereas inversion is not necessary for the output transformation h.

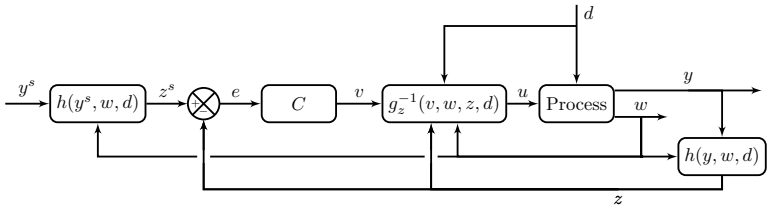

(a) General implementation of transformed output z

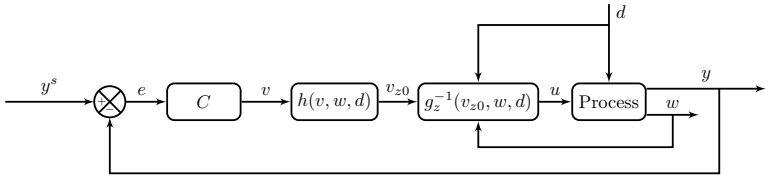

(b) Alternative implementation of transformed output when the ideal transformed input is based on a steady-state model.

Figure 3.7: System with both input and output transformations.

3.6 Stability of the transformed system

It is beyond the scope of this work to give a detailed stability analysis of nonlinear systems, and the reader is referred to the literature on feedback linearization for related mathematical proofs (Isidori, 1995; Khalil, 2015). The main objective of this section is to give the reader some insight into how instability may arise and how to avoid it, particularly for using the state measurement w.

3.6.1 Unstable zero dynamics and internal instability resulting from using the model-based inverse

So far, the w variables have been treated as a measured disturbances. If w is a dynamic state variable, that is, w depends on the input u in a dynamic way, then this will introduce dynamics in the map from u to the transformed input v. If this results in unstable zero dynamics from u to v (which may be v_0 or v_A or any other transformed input), then this will result in internal instability for the transformed system if we implement the model-based inverse $u = g^{-1}(v, w, y, d)$. This follows because the unstable zeros of the original map become unstable poles of the inverse map. A simple example is given in Section 3.6.

The model-based implementations (Alternative A) in Figures 3.4a and 3.2 may yield internal instability in some cases. Fortunately, it is not very likely to happen in practice, because unstable zero dynamics require that the indirect dependency of v on u through w is strong.

The internal instability can in any case be avoided if we use the alternative feedback-based implementation with an inner v-controller in Figure 3.4b, but the inner controller C_v then needs to be tuned sufficiently slow so that the unfavorable zero dynamics do not cause closed-loop instability. Thus, linearization, decoupling and disturbance rejection will not be perfect in this case.

The internal instability resulting from using an exact inverse $u = g^{-1}(vw, y, d)$ (model-based implementation) for systems with unstable zero dynamics from u to v applies to any transformed input $v = g(u, w, y, d)$ that depends on internal state variables w. For the systematically derived transformed inputs v_0 and v_A, we have the additional property that the zero dynamics from u to v are the same as the zero dynamics from u to y. This follows because of the direct relationship between these variables, for example, $y = v_0$ for the static case. The problem with internal stability for the model-based inverse, is then seen to be a special case of the well-known fact that with a causal controller (no prediction allowed) and requiring internal stability, perfect control of the output y cannot be achieved for a system with unstable zero dynamics from u to y, no matter how good the model is or what we measure.

3.6.1.1 Example: Simple linear system with unstable zeros

As an example, we will analyze a simple linear system with unstable zero dynamics. Consider the steady-state system

$$y = u + w + d \tag{3.58}$$

The ideal transformed input is defined as the right-hand-side of Eq. 3.58.

$$v_0 = g(u, w, d) = u + w + d \tag{3.59}$$

For implementation, Eq. 3.59 may be solved with respect to u to get the "inverse input transformation"

$$u = g^{-1}(v, w, d) = v_0 - w - d \tag{3.60}$$

Note that in deriving v_0 or generating u we have treated w as a measured disturbances which we counteract by using the "feedforward" controller in

Eq. 3.60. However, there is a "hidden" problem with potential internal instability caused by the dynamic map from u to w. As an example, assume the response from u to w is first-order with a steady state gain of -2

$$w = \frac{-2u}{4s+1} \quad \text{or} \quad \frac{dw}{dt} = -0.25(2u + w) \tag{3.61}$$

Substituting the $w-$dynamics (Eq. 3.61) into the input transformation (Eq. 3.59) gives (in transfer function form)

$$\begin{aligned} v_0 &= u - \frac{2u}{4s+1} + d \\ &= \frac{4s-1}{4s+1}u + d \end{aligned} \tag{3.62}$$

which has a RHP-zero at $z = 0.25$ from u to v. The reason is the combined effect of a direct static effect from u to v with a gain of 1, and an indirect dynamic effect from u to v (through w) with steady-state gain of -2. Therefore, the indirect effect of u on v through w is larger in magnitude than the direct effect.

This will result in internal instability if we use the exact inverse in Eq. 3.59. To see this, we substitute Eq. 3.61 into Eq. 3.60, to get

$$u = \frac{4s+1}{4s-1}(v_0 - d) \tag{3.63}$$

which as expected is unstable because of the RHP-pole at $p = 0.25$.

Similarly, the response from v to w is also unstable

$$w = \frac{-2}{4s-1}(v_0 - d) \tag{3.64}$$

The two instabilities in Eqs. 3.63 and 3.64 cancel each other in Eq. 3.58 to give

$$y = v_0 \tag{3.65}$$

The system from v_0 to y therefore appears to be stable, but this is not true if we consider the input u, and the "hidden" internally instability will eventually appear also in the output y, either because of model error or because infinite inputs u are not physically realizable. This "hidden" internally instability may be avoided by implementing the feedback-based method in Figure 3.4b which does not require generating an inverse for u.

We compare the model-based inversion (Figure 3.4a) and feedback-based implementations (Figure 3.4b) by simulations. The outer controller is set to $C = 0$. Figure 3.8 shows the response for the transformed system to a setpoint change of $\Delta v^s = 1$ at time $t = 1\,\text{s}$. Similarly, Figure 3.9 shows the simulation responses for a step change in disturbance d of $\Delta d = 1$ at time $t = 1\,\text{s}$. For the cascade implementation, we use an I-controller, with the integral gain $K_I = -1/16$. To find this value, we use the first order Padé approximation, that is $G_v = \frac{4s-1}{4s+1} \approx -\exp(-8s)$. Then we apply the SIMC-rules (Skogestad, 2003) with $\tau_C = 8\,\text{s}$.

As explained and as expected, the exact model-based inversion implementation gives perfect control of y (Figures 3.8a and 3.9a respectively), at the expense of internal instability for w (Figures 3.8b and 3.9b) and u (Figures 3.8c and 3.9c)

In summary, the requirement for using the model-based inverse in Figure 3.4a is that the response from u to v has stable zero dynamics. For the case when the transformed input v is obtained using one of the systematic methods in Section 3.4, this is equivalent to requiring that the transfer function from u to y has stable zero dynamics. In other cases and if one is uncertain, the safest is to use the feedback-based implementation in Figure 3.4b which gives an approximate inverse, but which can always be tuned to be stable.

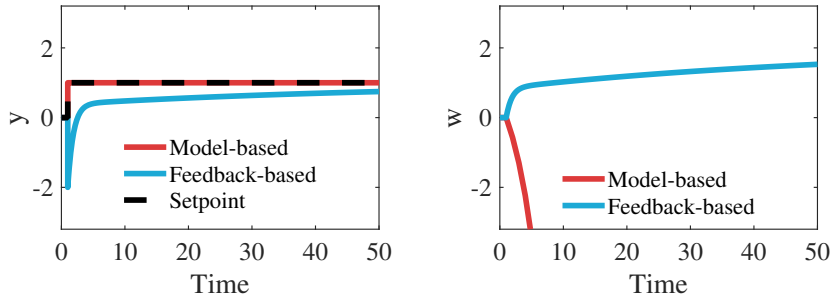

(a) Controlled variable (y)

(b) Measured variable (w)

(c) Physical input (u)

(d) Transformed input (v)

Figure 3.8: Comparison of model-based and cascade implementations for the model in Eqs. 3.58 and 3.61 for a setpoint change of $\Delta v^s = 1$ at time $t = 1\,\mathrm{s}$.

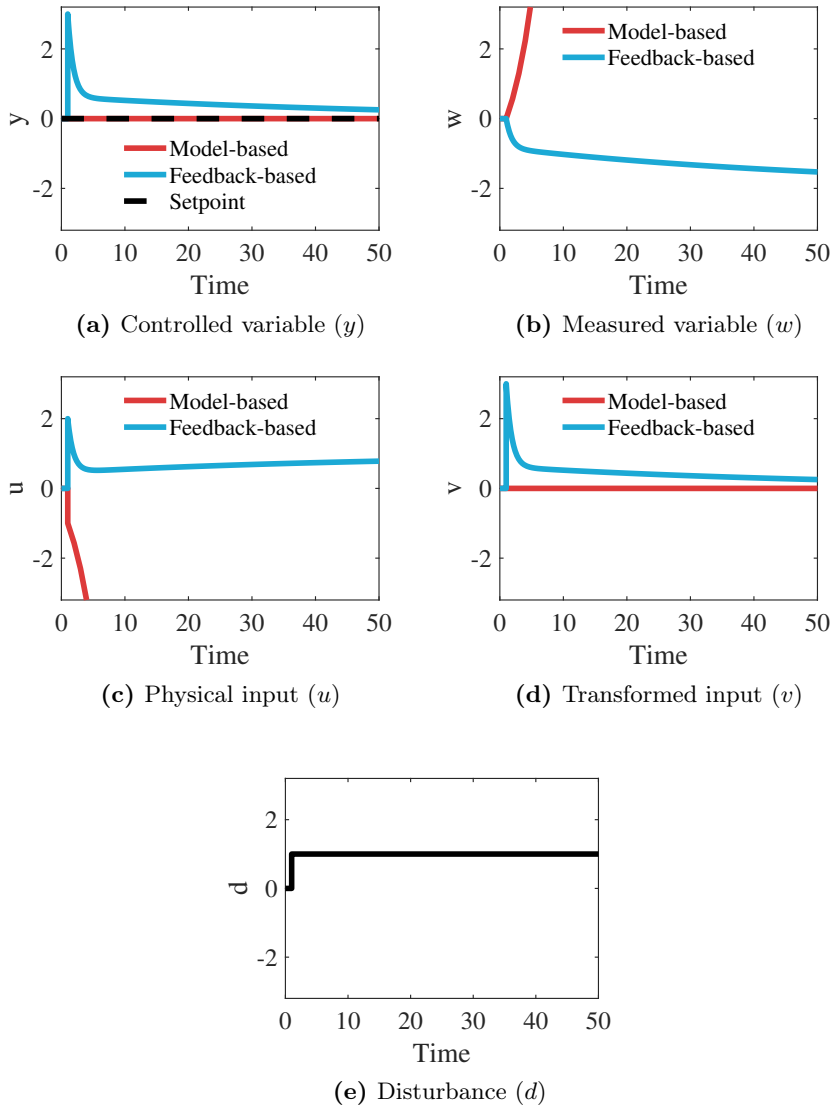

(a) Controlled variable (y)

(b) Measured variable (w)

(c) Physical input (u)

(d) Transformed input (v)

(e) Disturbance (d)

Figure 3.9: Comparison of model-based and feedback-based implementations for the model in Eqs. 3.58 and 3.61 for disturbance rejection. $\Delta d = 1$ at time $t = 1$ s.

3.7 Example 1: mixing process flow and temperature control

Fig. 3.10 shows the mixing process with two inflows and one outflow for which we systematically derive transformed inputs with the purpose of linearization, decoupling and feedforward disturbance rejection. The purpose of this example is to illustrate how we can combine the transformed inputs derived from steady-state and dynamic model equations.

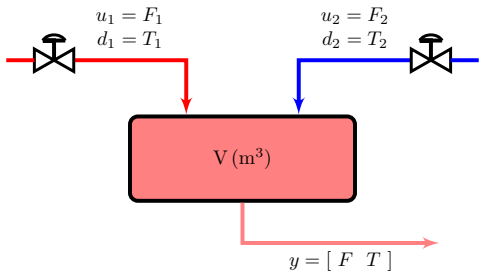

Figure 3.10: Mixing process with two original MVs ($u_1 = F_1$ and $u_2 = F_2$) and two CVs ($y_1 = F$ and $y_2 = T$).

The original inputs of the process are the two inlet flows: $u_1 = F_1$ [kg/s]; $u_2 = F_2$ [kg/s]. The outputs are the outlet flow F and temperature T: $y_1 = F$ [kg/s] $y_2 = T$ [°C]. The main disturbances are the temperatures of the two inlet flows: $d_1 = T_1$ [°C]; $d_2 = T_2$ [°C]. Assuming constant m holdup, and fast mixing (reasonable assumption for a pipe), the mass balance (static) is given by Eq. 3.66.

$$\begin{aligned} F &= F_1 + F_2 \\ y_1 &= \underbrace{u_1 + u_2}_{f_1(u)} \end{aligned} \tag{3.66}$$

Assuming constant and equal heat capacity c_P, and after substituting the mass balance (Eq. 3.66), the dynamic energy balance can be rearranged as given by Eq. 3.67.

$$\begin{aligned}\frac{dT}{dt} &= \frac{F_1}{m}(T_1 - T) + \frac{F_2}{m}(T_2 - T) \\ \frac{dy_2}{dt} &= \underbrace{\frac{u_1}{y_1}(d_1 - y) + \frac{u_2}{y_1}(d_2 - y)}_{f_2(u,y,d)}\end{aligned} \tag{3.67}$$

We see from Eq. 3.66 and Eq. 3.67 that this is a coupled (interactive) process, since both inputs ($u_1 = F_1$ and $u_2 = F_2$) affect both outputs ($y_1 = F$ and $y_2 = T$). This makes single-loop control challenging and control performance may be poor. We therefore want to consider the use of ideal transformed inputs which has the potential of giving a linear and decoupled transformed system, and in addition give perfect feedforward action from the disturbances in $d_1 = T_1$ and $d_2 = T_2$.

3.7.1 Ideal transformed inputs for the mixing process

We can derive two ideal transformed inputs, one from the steady-state mass balance in Eq. 3.66 and one from the dynamic energy balance in Eq. 3.67.

The first transformed input is defined in Eq. 3.68 as the right-hand side of the mass balance ($f_1(u)$ in Eq. 3.66). We chose the tuning parameter $B_0 = I$ (also see the theory in Section 3.4 and the general definition in Eq. 3.14).

$$v_{0,1} = u_1 + u_2 \tag{3.68}$$

The second ideal transformed input is defined in Eq. 3.69 by using the right-hand side of the dynamic energy balance ($f_2(u, y, d)$ in Eq. 3.67) and by introducing the tuning parameter A and $B = -A$ (which gives $y_2 = v_{A,2}$ at steady state) from the theory in Section 3.4.

$$v_{A,2} = y_2 - A^{-1} f_2(u, y, d) \tag{3.69a}$$

$$= \underbrace{y_2 - A^{-1} \frac{1}{m} \left(u_1(d_1 - y_2) + u_2(d_2 \ - y_2)\right)}_{g_2(u,y,d)} \tag{3.69b}$$

3.7.1.1 Implementation of transformed inputs

To implement the transformed inputs $v_{0,1}$ and $v_{A,2}$ in practice, we need to compute the physical inputs u (flowrates u_1 and u_2) from the inverse transformation $u = g^{-1}(v, y, d)$, see Figure 3.4a. From Eq. 3.68) and Eq. 3.69b we solve for u:

$$u_1 = g^{-1}(v, y, d)_1 = \frac{v_{0,1}(y_2 - d_2) - Am(v_{A,2} - y_2)}{d_1 - d_2} \tag{3.70a}$$

$$u_2 = g^{-1}(v, y, d)_2 = \frac{v_{0,1}(d_1 - y_2) + Am(v_{A,2} - y_2)}{d_1 - d_2} \tag{3.70b}$$

Note that the denominator in Eq. 3.70 becomes 0 when $d_1 = d_2$. However, physically, temperature control of the mixing is clearly not possible when both inlet stream have equal temperature, so this is then a control limitation of the system, and not of the transformed inputs method.

3.7.1.2 Transformed system for the mixing process

Introducing the ideal transformed inputs $v = [v_{0,1} \ v_{A,2}]$ into the model equations yields the transformed system in Eq. 3.71

$$y_1 = v_{0,1} \tag{3.71a}$$

$$\frac{dy_2}{dt} = (y_2 - v_{A,2}) \tag{3.71b}$$

which is decoupled, independent of disturbances and linear since the tuning parameter A is a constant.

As discussed in Section 3.4.2.2 and Eq. 3.28, we may eliminate the feedback from the output $y_2 = T$ to the transformed variable v_2 in Eq. 3.69b at the nominal operating point, by choosing A such that we keep the nominal linearized dynamics of the original system, which from Eq. 3.28 gives

$$\begin{aligned} A &= \left(\frac{\partial f_2}{\partial y_2}\right)_* \\ &= -\frac{F^*}{m} \end{aligned} \tag{3.72}$$

where $*$ denotes nominal condition, i.e., $F^* = u_1^* + u_2^* = v_{0,1}^*$ is the nominal total flowrate.

3.7.1.3 Outer controller C

The outer controller C in Figure 3.4a manipulates the transformed input such that the output y is kept at its setpoint. Because the transformed system in Eq. 3.71 is decoupled and we may use single-loop controllers $C = \text{diag}(C_1, C_2)$. Here, C_1 is a flow controller with integral action only[3] that computes $v_{0,1}$, and a temperature controller (PI) that computes $v_{0,2}$.

With perfect model and measurement, the outer controller C is not necessary. The effect of disturbances is eliminated in the input calculation block in Figure 3.4a, while the setpoint y^s can be changed by directly setting $v_{0,1}$ and v_2 equal to the setpoint y_1^s and y_2^s, respectively. However, in practice, there will always be unmeasured disturbances (for example heat losses) and model or measurement uncertainty. In addition, the outer controller C can be used to speed up or slow down the response of from v to y.

[3]From the SIMC tuning rules (Skogestad, 2003), it results that a pure I-controller is used for a static process.

3.7.2 Ideal static transformed input derived from steady-state model

The purpose of this example is to illustrate the effect of using a transformed input derived from a steady-state model applied to a dynamic system. These types of transformations are often applied in industrial process control applications, e.g., see (Shinskey, 1981). Therefore, we use transformed inputs derived from a steady-state model for control of both the total flow and temperature.

We start by deriving the steady-state energy balance. Setting $\frac{dy_2}{dt} = 0$ in the dynamic energy balance in Eq. 3.67, dividing by the mass m (non-negative) and solving for T yields

$$\begin{aligned} T &= \frac{F_1 T_1 + F_2 T_2}{F_1 + F_2} \\ y_2 &= \underbrace{\frac{u_1 d_1 + u_2 d_2}{u_1 + u_2}}_{f_{0,2}}(u, y, d) \end{aligned} \tag{3.73}$$

The transformed input derived from a steady-state model ($v_{0,2}$) for controlling the temperature is simply the right-hand side ($f_{0,2}$) of Eq. 3.73

$$v_{0,2} = \frac{u_1 d_1 + u_2 d_2}{u_1 + u_2} \tag{3.74}$$

The transformed input ($v_{0,1}$) for controlling the total flow (y_1) remains the same as given in Eq. 3.68. To answer what happens when we apply the static transformed input $v_{0,2}$ to the dynamic system in Eq. 3.67, we need to solve wrt. the physical inputs u_1 and u_2 the system formed by Eq. 3.68 and Eq. 3.74 given all other variables. This results in

$$u_1 = g^{-1}(v, y, d)_1 = \frac{v_1(v_2 - d_2)}{d_1 - d_2} \tag{3.75a}$$

$$u_2 = g^{-1}(v, y, d)_{0,2} = \frac{v_1(d_2 - v_2)}{d_1 - d_2} \tag{3.75b}$$

Substituting u_1 and u_2 from Eq. 3.75 into the steady-state mass balance (Eq. 3.66) and the dynamic energy balance in Eq. 3.67, and simplifying the expression gives the transformed system

$$y_1 = v_{0,1} \tag{3.76a}$$

$$\frac{dy_2}{dt} = -\frac{v_{0,1}}{m}(y_2 - v_{0,2}) \tag{3.76b}$$

Note that at the nominal point, the fraction $-\frac{v_{0,1}}{m}$ in Eq. 3.76b is equal to the tuning parameter A from Eq. 3.72. This indicates that the two systems in Eq. 3.76b and Eq. 3.71 will respond similarly if starting from the same steady-state, as later shown in the simulations results in Figure 3.11.

The transformed system in Eq.3.76 is independent of both disturbances d_1 and d_2 both dynamically and at steady-state[4]. However, the transformed system in Eq. 3.76 is not decoupled dynamically because $v_{0,1}$ also affects output y_2. Nevertheless, if the system is initially at steady-state, we have that $y_2 = v_{0,2}$ and the right-hand side of Eq. 3.76b is 0 regardless of change in $v_{0,1}$. Moreover, compared to transformed system derived from a dynamic energy balance (Eq. 3.71) the transformed system derived using a steady-state energy balance (Eq. 3.76) is no longer linear because of the multiplication with the term $v_{0,1}$ which is time-varying.

In conclusion, the advantage of using a transformed input derived from a more complex dynamic model is that the transformed system is linear dynamically. In addition, in some cases, the steady-state process model is simpler to derive (see the heat exchanger example in Section 3.8 and the steam generator example in Section 3.9). Therefore, it not surprising that

[4]Generally, when we apply static transformed inputs v_0 to a dynamic system of the form $\frac{dy}{dt} = f(u, y, d)$, we need to make the assumption that the system is initially at steady state to get perfect dynamic disturbances rejection. However, this assumption is not necessary for this particular case since the disturbances drop out completely in the transformed system.

these static transformations are commonly used.

3.7.3 Dynamic simulations results

We illustrate how the input transformations work in a simulation case study, assuming no model error and perfect measurement of the disturbances. In all simulations, the process is given by the nonlinear model in the steady-state mass balance (Eq. 3.66) and the dynamic energy balance (Eq. 3.67). In addition, all simulations use the implementation with the model-based inverse in Figure 3.4a. That is, the physical input is calculated using the inverse transformation in Eq. 3.70 when we use the ideal transformed inputs $v_{0,1}$ and $v_{A,2}$ based on a dynamic model for temperature (y_2) or Eq. 3.75 when we use the ideal transformed inputs $v_{0,1}$ and $v_{0,2}$ based on a steady-state model for temperature (y_2). The outer controller is not needed in these simulations because we assume perfect model and perfect disturbance measurement. That is we set $C = 0$, and setpoint changes are handled by directly changing v.

Process data Table 3.1 shows the nominal operating conditions for the mixing process. At the nominal operating point the two inputs are equal ($F_1 = F_2$), which makes the process highly coupled and difficult to control using conventional single-loop PID-controllers.

Table 3.1: Nominal operating conditions for Example 5 (mixing process).

Variable	F_1	F_2	F	T_1	T_2	T	m
Value	5	5	10	20	50	35	100
Unit	kg/s	kg/s	kg/s	°C	°C	°C	kg

With no model error and perfect disturbance measurement, the simulations show that both outputs $y_1 = F$ (Figure 3.11a) and $y_2 = T$ (Figure 3.11b) are independent of the two disturbances, and for setpoint changes

they follow the original system dynamics. This holds for both ideal static transformed variables v_0 and the ideal dynamic variables v_A. The inputs u_1 in Figure 3.11c and u_2 in Figure 3.11d change in a step-wise manner because we use a static algebraic block to compute them.

The simulation results are not very exciting or surprising, and simply confirm what is expected from the transformed system models in Eq. 3.71 and Eq. 3.76b. The responses for the ideal static and dynamics transformed inputs are identical, except for the dynamic transients when we have a setpoint change for y_2 (at $t = 100$s). This is because $v_{0,1}$ is at 12 kg/s, rather higher than at it's nominal value of 10 kg/s, which results in a slightly faster response for y_2 for the static case (v_0). We also see that the inputs u_1 and u_2 make a larger initial change at $t = 100$s for the static case.

The benefit of using the dynamic transformed input v_A rather than the static transformed input v_0 is mainly that we get a linear transformed system for designing the outer controller C, but this benefit is not seen in these simulations since we have used $C = 0$.

3.8 Example 2: heat exchanger process outlet temperature control

We continue the analysis of the systems behaviour when we apply a static transformation on a dynamic system. We now consider a heat exchanger, which may benefit from introducing input transformations to reduce nonlinearity and improve the disturbance rejection.

The objective of the heat exchanger in Figure 3.12 is to control the outlet temperature of stream 1 (the process side) by exchanging heat with stream 2 (the utility side). The MV is the utility flowrate, $u = F_c$, where we assumer a fast inner loop flow controller manipulates the true MV which is the valve position z. The MV and CV for this example are the utility flowrate and

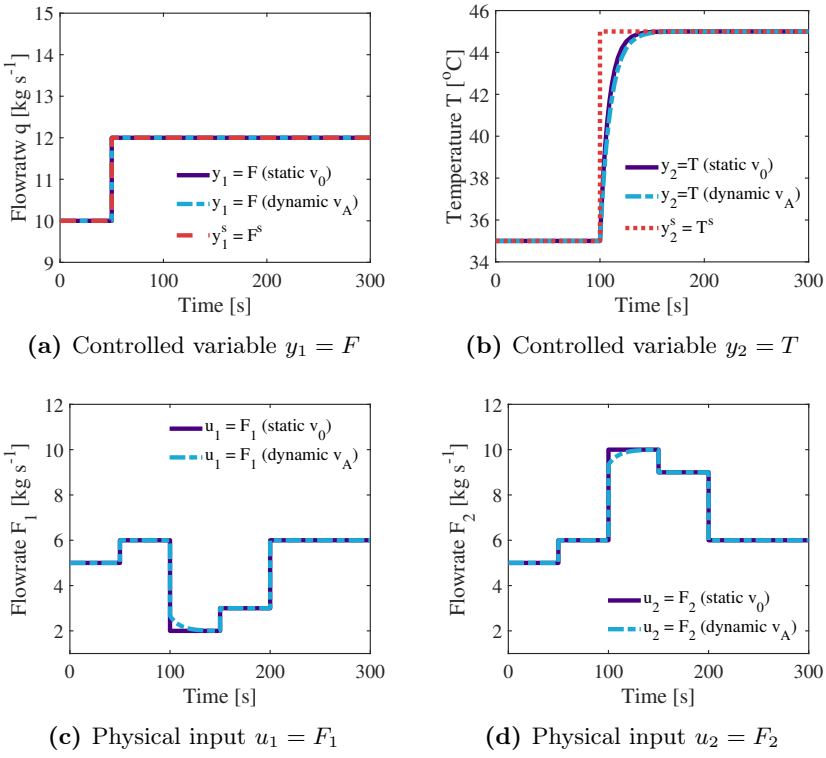

(a) Controlled variable $y_1 = F$ **(b)** Controlled variable $y_2 = T$

(c) Physical input $u_1 = F_1$ **(d)** Physical input $u_2 = F_2$

Figure 3.11: Simulation response for the mixing process in Example 5 using using both ideal static (v_0) and dynamic (v_A) transformed inputs and using the exact implementation of the inverse (Figure 3.4a).
The simulations are for the following four step changes: 1 kg/s increase in setpoint $y_1^s = F^s$ at time $t = 50$ s. 1 °C increase in setpoint $y_2^s = T^s$ at time $t = 10$ s. 2 °C increase in disturbance $d_1 = T_1$ at time $t = 150$ s. 5 °C increase in disturbance $d_2 = T_2$ at time $t = 200$ s. The responses are without the outer controller C, so the setpoint changes are implemented by changing the corresponding v_0 and v_A.

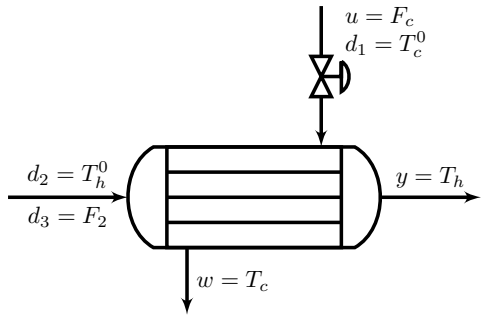

Figure 3.12: Heat exchanger where the objective is to control the outlet temperature T_h of stream 1 (hot process side) by exchanging heat with stream 2 (cold utility side).

process side temperature respectively:

$$u = F_c,\ y = T_h$$

The measured disturbances are the inlet temperatures and the flowrate of stream 1:

$$d = [T_h^0\ T_c^0\ F_h]$$

In the simulations, we will also consider an unmeasured disturbance in the UA-value, for example, caused by fouling or gas bubbles in the streams:

$$d_{\text{unmeasured}} = UA$$

A possible extra measurement (in addition to F_c) which depends on the input u is the utility outlet temperature

$$w = T_c$$

The dynamic and steady-state behaviors of heat exchangers are highly nonlinear. For example, for small values of $u = F_c$ (relative to F_h), the process

gain $k = \frac{dy}{du}$ is large and relatively constant, but for large values of $u = F_c$, the gain k approaches 0 and makes it difficult to control $y = T_h$. This is because we get a pinch for T_h (constant value) with $y = T_h$ approaching the inlet temperature T_c^0.

3.8.1 Dynamic cells heat exchanger model

The process is given by the dynamic lumped model given in Eq. 3.77 (Mathisen, 1994), where the heat exchanger is discretized in space in $N = 100$ cells. The boundary conditions for cell $i = 1$ is $T_h^0 = T_h^0$, and for cell $i = N$ is $T_c^{N+1} = T_c^0$. With infinite cells, the dynamic model has the same steady-state as the steady-state model. Wall capacities are neglected. Phase changes are not considered.

$$\frac{dT_c^i}{dt} = \frac{F_c}{\rho_c V_c^i}(T_c^{i+1} - T_c^i) + \frac{UA(T_h^i - T_c^i)}{N\rho_c V_c^i c_{p_c}} \tag{3.77a}$$

$$\frac{dT_h^i}{dt} = \frac{F_h}{\rho_h V_h^i}(T_h^{i-1} - T_h^i) + \frac{UA(T_h^i - T_c^i)}{N\rho_h V_h^i c_{p_h}} \tag{3.77b}$$

$$\forall i \in 1 \dots N$$

where, $N = 100$ well-mixed cells, c is the cold side, h is the hot side, V is the volume, U is the heat transfer coefficient, A is the heat transfer area, ρ is density and c_p is specific heat.

In total, the model in Eq.3.77 gives 200 differential equations to represent the temperature dynamics, and we cannot use it to derive the input transformation because its relative order is greater than 1. That is, we cannot rewrite it in the form of the general model in Eq. 3.19 ($\frac{dy}{dt} = f(u, y, d)$) which which allows for only one differential equation.

3.8.2 Input transformation

This leads us to consider transformed inputs based on a steady-state model of the heat exchanger. We will consider two transformed inputs, defined formally in Eq. 3.78.

$$v_0 = f_0(u, d) \tag{3.78a}$$

$$v_{0,w} = f_{0,w}(u, w, d) \tag{3.78b}$$

The transformed input v_0 is defined from a detailed steady-state model using as variables the input u and the three disturbances d. The second transformed input $v_{0,w}$ is defined from a simpler steady-state energy balance where we use as additional measured variables the cold side outlet temperature $w = T_c$. This is inspired by an actual industrial implementation.

3.8.3 Ideal transformed input v_0 based on full steady-state model

Assuming ideal countercurrent flow, no phase change and constant heat capacity for each fluid, the steady-state energy balance for the heat exchanger in Figure 3.12 is given by the following three equations for the heat transfer Q from the hot stream to the cold stream:

$$Q = F_h c_{p_h}(T_h^0 - T_h) \tag{3.79a}$$

$$Q = F_c c_{p_c}(T_c - T_c^0) \tag{3.79b}$$

$$Q = UA\frac{\left(T_h^0 - T_c\right) - \left(T_h - T_c^0\right)}{\ln\left(\frac{T_h^0 - T_c}{T_h - T_c^0}\right)} \tag{3.79c}$$

The system in Eq. 3.79 has 3 equations with 3 unknowns (Q, T_h, T_c) and it can be solved analytically to find the following expression for T_h as a function

of the input and disturbances (e.g., Soave and Barolo (2021)),

$$y = T_h = \underbrace{T_h^0 + \epsilon(T_c^0 - T_h^0)}_{f_0(u,d)} \tag{3.80}$$

where

$$\epsilon = \frac{1-E}{C-E}$$
$$C = \frac{F_1 c_{p1}}{F_2 c_{p2}}$$
$$E = \exp\left(UA\left(\frac{1}{F_1 c_{p1}} \ \frac{1}{F_2 c_{p2}}\right)\right)$$

The transformed input v_0 is then defined in Eq. 3.81 as the right-hand side of Eq. 3.80. Note that we choose the tuning parameter $B_0 = 1$.

$$v_0 = f_0(u,d) = T_h^0 + \epsilon(T_c^0 - T_h^0) \tag{3.81}$$

3.8.4 Transformed input $v_{0,w}$ using $w-$ variables

To derive the second transformed input $v_{0,w}$, we ignore the third expression for Q equation Eq. 3.79c because we make use of the measured state $w = T_c$ to replace the model in Eq. 3.79c for Q. Setting Eq. 3.79a equal to Eq. 3.79b and solve for $y_2 = T_c$, yields

$$y = T_h = \underbrace{T_h^0 + \frac{F_c c_{p_c}}{F_h c_{p_h}}(T_c^0 - T_c)}_{f_{0,w}(u,w,d)} \tag{3.82}$$

The ideal transformed input $v_{0,w}$ is defined as the right-hand side of Eq. 3.82

$$v_{0,w} = f_{0,w}(u,w,d) = T_h^0 + \frac{F_c c_{p_c}}{F_h c_{p_h}}(T_c^0 - T_c) \tag{3.83}$$

3.8.5 Comparison between v_0 and $v_{0,w}$

Both transformed inputs based on steady-state expressions for $y = T_h$ and give $y = v^s$ at steady state (also see the open loop responses in Figure 3.14). Hence, they will give linearization and perfect disturbance rejection for the three measured disturbances d at steady-state. However, without the outer controller C, changes in the unmeasured disturbance UA will results in a steady-state offset when implementing the transformed input v_0. We will not have an offset when implementing $v_{0,w}$ because changes in UA are captured in the measurement $w = T_c$ (see Eq. 3.77a). The drawback of using the measurement $w = T_c$ is that we introduce the dynamics from $w = T_c$ into the input transformation, and these propagate when computing the physical input u. Thus, input u is no longer changing in a step-wise manner. Overall, the effect is that the dynamic response for $y = T_h$ is slower compared to using the static v_0. Note that these dynamics correspond to an left-hand plane zero so they are stable.

3.8.6 Implementation

The open-loop responses from v_0 and $v_{0,w}$ to y respectively are generated using the exact model-based inverse (Figure 3.4a) to be able to observe the dynamic response without any influence from the inner cascade controller used in the feedback-based implementation (Figure 3.4b). However, Eq. 3.81 (v_0) does not have an analytical solution and it has to be solved numerically. This proved to be slow and prone to convergence issues with the inbuilt Matlab numerical solvers. Therefore, we avoid implementing a numerical solver by using the pure feedback-based implementation to generate the closed-loop responses for both transformed inputs.

Controller tuning The response from $u = F_2$ to v_0 in Eq. 3.81 is purely static, and therefore, for the inner v_0-controller a pure I-controller is recom-

mended (Skogestad, 2003).

The response from $u = F_2$ to $v_{0,w}$ has an initial overshoot cause by introducing the measurement $w = T_c$ which depends on u (left-hand plane zero). We choose to tune also a pure I-controller based on the initial process gain rather than on the steady-state gain because this give a smaller controller gain which is more robust (Skogestad, 2003).

In summary, we use I-controllers for both v_0 and $v_{0,w}$, tuned based on the initial gain, and with the same closed-loop time constant ($\tau_C = 10\,\mathrm{s}$); see Table 3.4.

3.8.7 Simulations

We consider a cooler with data as given in Table 3.2 (Skogestad, 2008).

Table 3.2: Nominal operating conditions for the heat exchanger from (Skogestad, 2008)

Variable	Value	Unit
F_h	3	kg/s
F_c	5	kg/s
T_h^s	24.2	°C
T_h^0	20	°C
T_c^0	70	°C
U	150	$\mathrm{W/m^2/°C}$
A	90	$\mathrm{m^2}$
$V_h = V_h$	0.45	$\mathrm{m^3}$
c_{p_h}	1200	J/kgK
c_{p_c}	1500	J/kgK
ρ_h	980	$\mathrm{kg/m^3}$
ρ_c	890	$\mathrm{kg/m^3}$

3.8.7.1 Open-loop responses

Figure 3.13 shows the open-loop responses for the two transformed input v_0 and $v_{0,w}$ to a step change in the physical input u of $\Delta u = 0.5\,\mathrm{kg/s}$ (left) and $\Delta u = -0.5\,\mathrm{kg/s}$ (right) at time 100 s. The response for v_0 is purely static, while the response for $v_{0,w}$ is dynamic and shows an overshoot (LHP zero) caused by introducing dynamics from the measurement $w = T_c$ in the transformation.

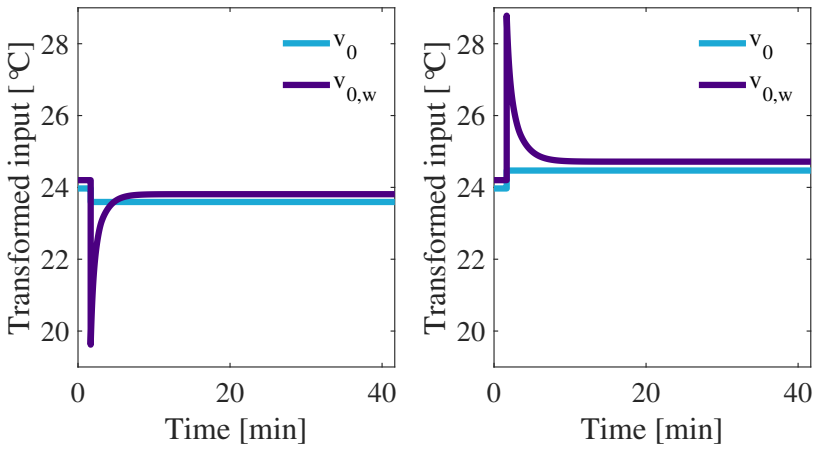

Figure 3.13: Open-loop response for v_0 and $v_{0,w}$ to a step change in the physical input of $\Delta u = 0.5\,\mathrm{kg/s}$ (left) and $\Delta u = -0.5\,\mathrm{kg/s}$ (right) at time 100 s.

Figure 3.14 shows the open-loop response for $y = T_h$ to a step change in the transformed inputs v_0 and $v_{0,w}$ together with the original process dynamics (dashed black line). The size of the step changes are selected such that they correspond to change in the physical input u of $\Delta u = 0.5\,\mathrm{kg/s}$ (left) and $\Delta u = -0.5\,\mathrm{kg/s}$ (right) at time 100 s (same as in Figure 3.13). Implementing v_0 keeps the original process dynamic, while $v_{0,w}$ slows the process.

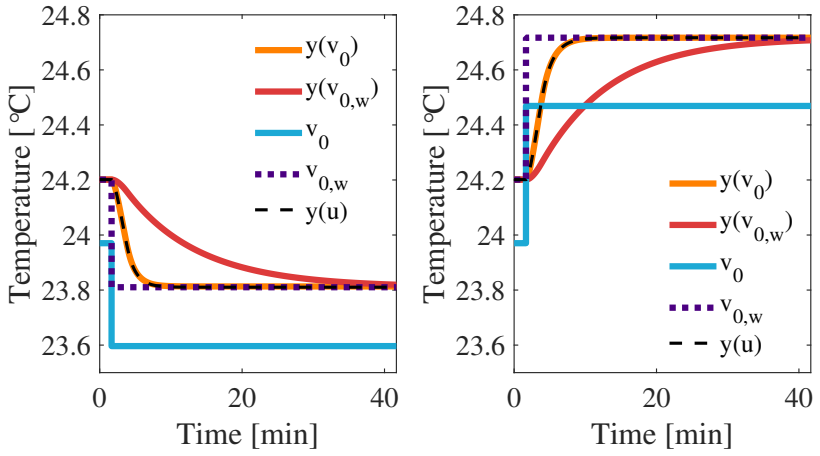

Figure 3.14: Open-loop response for for step changes in the transformed inputs v_0 and $v_{0,w}$ with a magnitude equivalent to a step change in the physical input of $\Delta u = 0.5\,\text{kg/s}$ (left) and $\Delta u = -0.5\,\text{kg/s}$ (right) at time 100] s. Original process dynamics are in black dashed line.

Steady-state gains from u to y and from v to y. Table 3.3 shows the steady-state gains from the physical input u to the output y (k_{uy}) and from the transformed inputs v_0 and $v_{0,w}$ in both for an increase and a decrease in input.

Table 3.3: Steady-state process gains from u to y and from v to y

Process gain	Input increase	Input decrease [s]
k_{uy}	-0.78	-1.03
k_{v_0}	1.04	1.04
$k_{v_{0,w}y}$	1	1

For both transformed systems the steady-state gains in both directions are equal, whereas for the original system they are not. The reason the process gain from $v_{0,w}$ to y is 1, while the process gain from v_0 to y is 1.04 is the feedback from the state measurement $w = T_c$ in generating the physical input u from $v_{0,w}$. In addition the dynamic model used in the simulations is

a cell model which does not give perfect countercurrent flow as is assumed in the model used to derive v_0.

In summary, the process gains in Table 3.3 together with the dynamic response from in Figure 3.14 illustrated that the benefit of using $v_{0,w}$ compared to v_0 is a steady-state gain of 1, while the drawback is slower dynamic response. For the transformed system the steady-state gains in both directions are equal, whereas for the original system they are not. If the models used for the transformation and dynamic simulation were identical, we would have 1. a process gain of 1 (rather than 1.04) and 2. $y = v$ at steady state (so the read and blue lines should start and end at the same value in Fig. 3.14).

3.8.8 Closed-loop responses

Table 3.4 shows the controller tuning for the $v-$controllers. The outer controller is set to $C = 0$.

Table 3.4: Tunings for inner v-controller heat exchanger example

Transformed input	K_I	τ_C [s]
v_0	-0.125	10
$v_{0,w}$	-0.01	10

The simulations in Figure 3.15 compare the two alternative transformed inputs (the setpoints for v_0 or $v_{0,w}$ are given) with the open-loop (OL) response with no input transformation (Coolant flow $u = F_2$ is constant). The setpoint of the transformed input v^s is initially at 24.2 °C and changes to 29.2 °C at time $t = 167$ min. The simulations show responses to step disturbances in F_h, T_c^0 and T_h^0 (all measured) and to a step change in the heat transfer parameter UA (unmeasured).

From the response for the controlled variable ($y = T_h$) in Figure 3.15a, we clearly see that there is a benefit of using transformed inputs. Both transformed inputs give in theory perfect control at steady state ($y = v$)

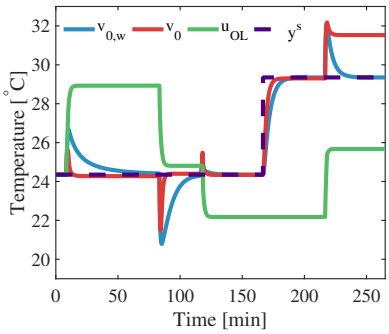

(a) Controlled variable $y = T_h$

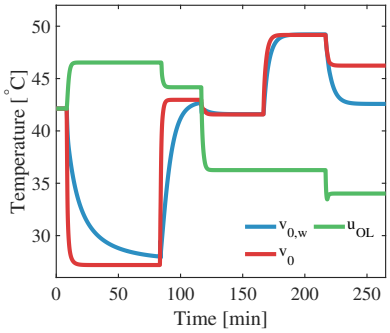

(b) State variable $w = T_c$ (measured variable for $v_{0,w}$)

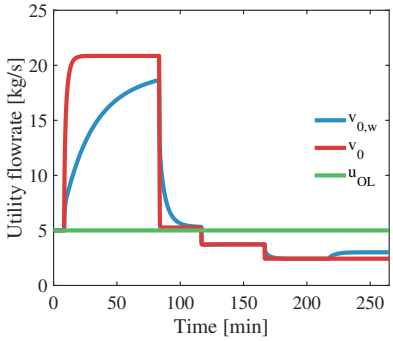

(c) Physical input $u = F_c$

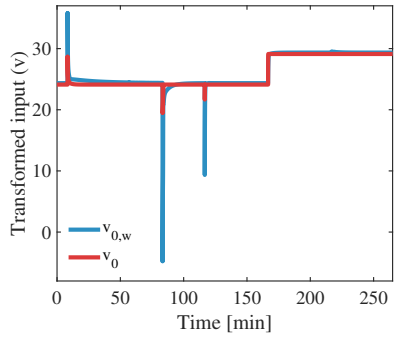

(d) Computed transformed input from Eq. 3.81) and Eq. 3.83) (measurement to v-controller C_v)

Figure 3.15: Dynamic simulation of heat exchanger (Example 6) using the cascade feedback implementation B in Figure 3.4b with a v-controller. Two choices of the transformed input, v_0 and $v_{0,w}$, are compared with the open-loop (OL) case with no transformation.
The simulations are for the following step changes: F_h from 3 to 4 kg/s at $t = 8$ min, T_c^0 from 20 to 25 °C at $t = 80$ min, T_h^0 from 70 to 55 °C at $t = 117$ min, setpoint $v^s = y^s$ from 24.2 to 29.2 °C at $t = 167$ min and U from 150 to 100 W/m^2/°C at $t = 217$ min.

for measured disturbances and this is confirmed by the simulations. Note however, that, there is a small offset for v_0 (but not for $v_{0,w}$) (corresponding to the process gain in Table 3.3), but this is hard to see. For the unmeasured disturbance in UA (towards the end of the simulation in Figure 3.15a), we see as expected that we get an offset for $y = T_h$ when we use v_0 (red curve) as the transformed input, but not when we use $v_{0,w}$ (blue curve) which makes use of the state measurement $w = T_c$.

Dynamically, we find that the responses are best (fastest) when we use v_0 as the transformed input (red curves). As expected, the dynamics are similar to the quite fast dynamics of the uncontrolled heat exchanger (green curves). However, even with v_0, the disturbance rejection is not perfect dynamically because of the process dynamics are quite complex and not described by a first-order model.

On the other hand, when we use $v_{0,w}$ (blue curves), which contains feedback from $w = T_c$, the dynamics for the return to the steady state are much slower. There is not much we can do about this, as there is no tuning parameter for ideal transformed inputs based on a steady-state model. The inner controller can be used to make the inversion faster, but it will not help in this case. Even with a perfect inverse, the dynamics caused by the feedback from $w = T_c$ will be present, as seen in the open-loop response in Figure 3.14. It may be possible to use the outer C controller to speed drive up the response for y, but this could give instability if there is a measurement delays for y.

In summary, for this example, the responses are best (fastest) when we use the transformed input v_0 based on the full steady-state model. The exception is for disturbances in the heat exchanger model parameters, including the UA-value, but these can be taken care of by the outer controller C. On the other hand, the implementation of v_0 based on the full steady-state model is complex, so it is nevertheless likely that the simpler implementation using $v_{0,w}$ may be chosen in practice.

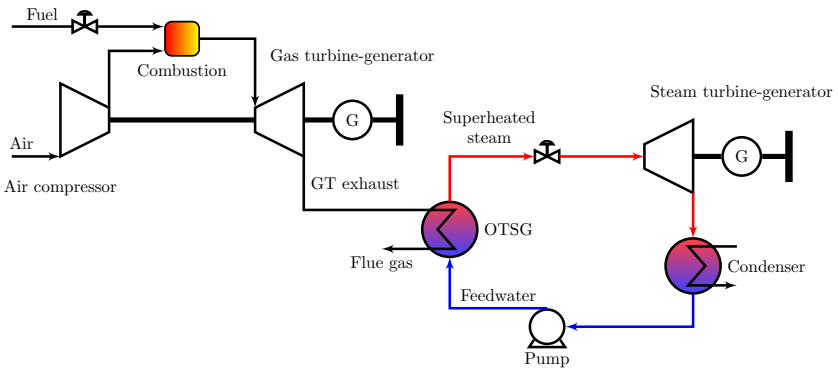

Figure 3.16: Simplified flowsheet of a combined cycle where steam is generated in a once-through steam generator (OTSG). The boundary for this example is shown in black dashed line.

3.9 Example 3: phase change heat exchanger outlet temperature control

This example is based on the work in (Zotică et al., 2022). It presents controlling the superheated steam temperature in a once-through boiler in the framework of the input (and output) transformation theory.

This example has several purposes. First, it further unifies the input transformation theory with the analysis of operation and control of steam cycles in Part 2 of this thesis. Second, it provided a case study for combining inputs and outputs transformations. Third, it extend the heat exchanger example in Section 3.8 to include a phase change process with non-ideal thermodynamics.

Figure 3.16 shows a simplified flowsheet of a combined cycle where heat from the exhaust of a gas turbine is recovered by generating steam in a once-through steam generator (OTSG). The superheated steam is then expanded in a turbine-generator system to produce electrical power, thus increasing the thermal efficiency of the system. The low-pressure steam is condensed

to water and fed back to the boiler by a pump. The dashed black line shows the boundary of this example. The gas-turbine may be operated over a wide range of loads (power setpoint), thus its exhaust gas may have a large variation in mass flowrate and temperature. The steam cycle is fast to respond to these disturbances because of the small OTSG inventory (no drum storage). As already discussed in Section 2.3, the superheated steam temperature should be kept with a small operating region to reduce thermal stresses on the turbine blades. For this reason, feedforward information from the gas turbine exhaust may improve the disturbance rejection response of the steam temperature. Similar examples using a steady-state model-based nonlinear feedforward are present in the literature (e.g., Shinskey and Louis (1968), Montañés et al. (2021)). The difference is that in this example the control

Process model The dynamic behaviour of the OTSG is rigorously modelled in Dymola. The model is developed in the work of Montañés et al. (2021). The detailed geometry of the OTSG is discretized in space in 72 cells and for each cells dynamic mass and energy balances are solved. The model considers ideal behavior for the exhaust gas behaviour, and non-ideal thermodynamic for the water and steam modelled using the IF97 standard (Åberg et al., 2017).

Process variables for control purposes Compared to the drum-based configuration in Part 2 (see the flowsheet in Figure 2.3), there is no drum inventory to be controlled and there is no attemperator (i.e., bypass of the boiler in the water side used to control the steam temperature). Thus for controlling the steam temperature $y = T_s$, we use as physical input the feedwater flowrate $u = F_f$. Note that the actual actuator is the feedwater pump, but we will use a fast cascade flow-controller (pump in reality). The available measured disturbances are the inlet temperature ($d_1 = T_g^0$) and

flowrate of the exhaust gas ($d_2 = F_g$).

Additional available state measurements are the feedwater inlet temperature ($w_1 = T_f$) and pressure ($w_2 = p_f$), the steam pressure ($w_3 = p_s$) and the exhaust gas outlet temperature ($w_4 = T_g$).

3.9.1 Derivation of transformed input output

The OTSG dynamic model has more than 40 000 states, and it cannot be used to derive a transformed input because it is far too complex to be written as a model with relative order 1. Similar to Example 3.8, we use a steady-state energy balance to derive the transformed input v_0. Compared to Eq. 3.79 in the previous example, we can no longer assume constant specific heat c_p for the water side because of the phase change and non-ideal water/steam properties. This leads to using directly the enthalpy of the water (H_l) and steam (H_s) in the steady-state energy balance in Eq. 3.84.

$$Q = F_f \left(H_s(T_s, p_s) - H_f(T_f, p_f)\right) \tag{3.84a}$$

$$Q = F_g c_{p_g} (T_g^0 - T_g) \tag{3.84b}$$

where $H(T, p)$ is the specific enthalpy. The steam flowrate is assumed to be equal to the water flowrate.

Because the model in Eq. 3.84a is simpler to express in term of the specific enthalpy, we will introduce this as the transformed output z

$$z = h(w) = H_s(T_s, p_s) \tag{3.85}$$

While the specific enthalpy cannot be measured directly, it can be estimated, for example by using a look-up table. Note that selecting to control the steam enthalpy is not new, e.g.,Shinskey and Louis (1968).

To derive the input transformation v_0, we set Eq.3.84a equal to Eq. 3.84b

and solve for $H_s(T_s, p_s)$ to get

$$\underbrace{H_s(T_s, p_s)}_{z(w)} = \underbrace{H_f(T_f, p_f) + c_{p_g}(T_g^0 - T_g)\frac{F_g}{F_f}}_{f_{0z}(u,d,w)} \tag{3.86}$$

The ideal transformed input v_0 is then the right-hand side of Eq. 3.86

$$\begin{aligned} v_0 &= f_{0z}(u, d, w) \\ &= H_f(T_f, p_f) + c_{p_g}(T_g^0 - T_g)\frac{F_g}{F_f} \end{aligned} \tag{3.87}$$

The physical input $u = F_f$ is computed as the inverse of Eq. 3.87

$$F_f = \underbrace{\frac{F_g c_{p_g}(T_g^0 - T_g)}{v_0 - H_f}}_{f_{0z}^{-1}(v,w,d)} \tag{3.88}$$

3.9.2 Simulation results

To implement in input and output transformations in the rigorous dynamic model, we use the combined model based inversion (Eq. 3.88) and cascade approach from Figure 3.4c because the model has an inner flow controller for feedwater pump. This inner controller is tuned with the SIMC rules with a closed-loop time constant $\tau_c = 5\,\text{s}$. The outer controller is active and to have a time scale separation between the two, we use a closed-loop time constant 5 times slower of $\tau_c = 60\,\text{s}$.

Table 3.5 summarizes the nominal operating conditions for the OTSG from (Zotică et al., 2022).

Figure 3.17 shows the disturbance rejection response for the physical input ($u = F_f$) (left) and the superheated steam temperature ($y = T_s$) (right). The disturbances in $d_1 = T_g^0$ and $d_2 = F_g$ are simultaneously caused by setpoint changes in the combined cycle power. Initially, the cycle produces 92 MW,

Table 3.5: Nominal operating conditions for the OTSG

Variable	Symbol	Value	Unit
Superheated steam pressure	p_s	23	bar
Superheated steam temperature	T_s	354	°C
Exhaust gas inlet temperature	T_g^0	443	°C
Exhaust gas outlet temperature	T_g	169	°C
Feedwater inlet temperature	T_f	27	°C
Feedwater inlet pressure	p_f	0.034	bar
Feedwater mass flowrate	F_f	21.9	kg/s
Exhaust gas mass flowrate	F_g	225.5	kg/s

and at time 30 min, this is reduced to 46 MW with an increment of 2 MW each 1000 s (16.67 min). At time 400 min the power setpoint is increased back to 92 MW with the same increment. As expected, the response for $y = T_s$ in Figure 3.17 is not perfect because of the difference the model used in the simulation and in deriving the input transformation. However, the temperature is kept within 10 °C variation over a wide-range of operating points of the gas-turbine.

It may seem that the system in Figure 3.17 is oscillating. To illustrate better the responses, Figure 3.18 shows a close-up of Figure 3.17. The two overshoots are cause by the the feedback and feedforward acting simultaneously and compensating for each other. This happens only when the outer controller C is active and there is a mismatch between the plant model and the model used to derive the transformed input for the feedforward action.

3.10 Example 4: steam network pressure control

Pressure-flow networks are inherently multivariable, coupled and nonlinear systems that are not straightforward handled by conventional PID controllers. In this work we analyze the control problem for a steam distribution network in the framework of of the theory for inputs transformation from Section 3.4.

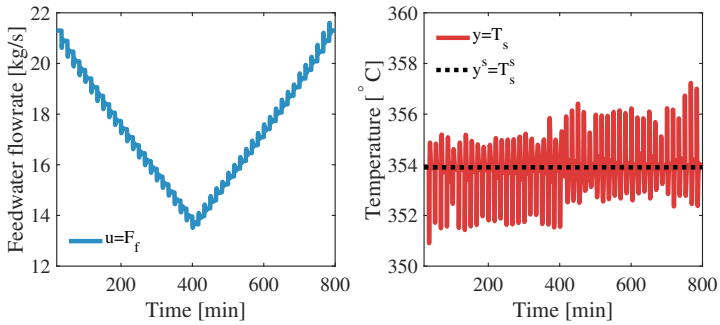

Figure 3.17: Simulation responses for the physical input ($u = F_f$) (left) and the superheated steam temperature () (right) to step changes in the combined cycle power setpoint from 92 MW to 46 MW with an increment of 2 MW each 1000 s (16.67 min) from time 30 min until 400 min followed by an increase back to 92 MW with the same increment. These step changes introduce simultaneous disturbances in the exhaust gas inlet temperature and flowrate (d_1 and d_2).

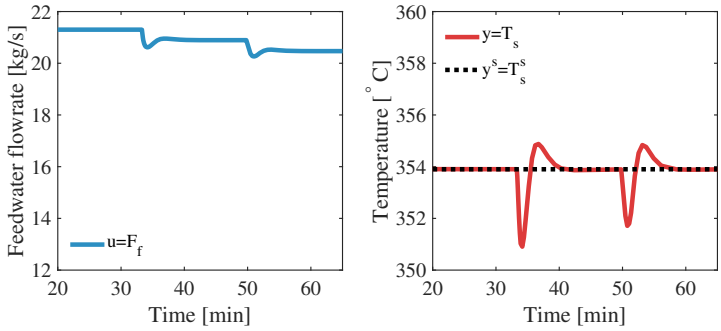

Figure 3.18: Close-up of the responses in Figure 3.17.

Steam networks are used to produce and transfer steam as utility for downstream processes such as distillation column, paper machines, reactors etc. Pressure-flow networks are inherently highly coupled system where a large and fast disturbance such as a shut-downs or start-ups becomes a large disturbance both on the generation and the demand side. In addition, the dynamics of steam generators are much slower compared to the dynamics of the steam network. Therefore, to be able to respond fast to load changes, control of the network pressure is commonly implemented in industry (Majanne, 2005). There is however a self-regulating effect: a decrease in the network pressure increases the pressure drop on the supply side (i.e the steam flow increases), but decreases the pressure drop on the demand side (i.e. the steam flow decreases) until a new equilibrium is reached. However, the pressure might not satisfy the requirements for the pressure levels which may cause process shut-downs, and control of steam header pressure is needed.

Both decentralized and centralized control methods for steam networks are presented in the literature. The work by Bertrand and McAvoy (1986) presents a solution based on PI-controllers that has good performance for disturbance rejection. The work by Kristoffersen et al. (2014) implements model predictive control (MPC) combined with real time optimization approach to increase the energy efficiency. The work by (Majanne, 2005) compares the performance of PI-controllers and MPC, and the MPC outperforms due to its ability of handling coupled systems.

Figure 3.19 shows the steam network we analyze within the transformed inputs method. It is composed of a high-pressure header (i.e. pipelines that physically connect the steam generators and consumers), a turbine and a low-pressure header. High-pressure steam is produced at a pressure p_0 by burning fuel in a boiler. Note that we do not include the boiler in our analysis. The high-pressure steam is supplied as utility to one high pressure consumer with receiving pressure p_{HC}. The remaining steam is expanded to lower pressure steam, either through a fixed-speed back pressure turbine connected

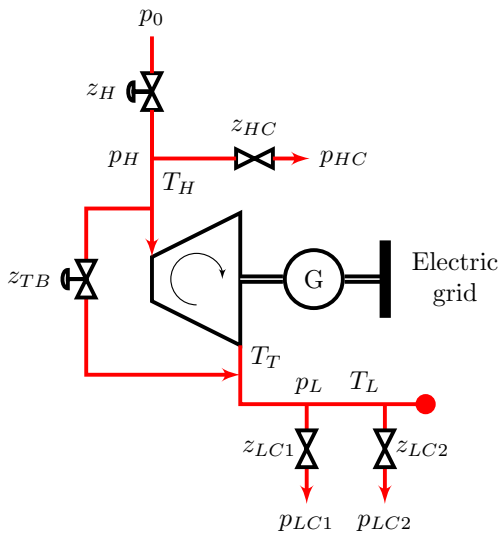

Figure 3.19: Process flowsheet of the steam network with two pressure headers (high and low) considered in this work.

to the electric grid to produce electricity or through a valve that bypasses the turbine (z_{TB}). Note that the fixed-speed turbine is not a degree of freedom available for operation. The low-pressure steam is supplied as utility to two consumers, with receiving pressures p_{LC1} and p_{LC2} respectively.

The manipulated variables are $u = [z_H \ z_{TB}]$ (the supply of high pressure steam and the turbine bypass). The controlled variables are $y = [p_H \ p_L]$ (pressure in the high and low pressure headers). The main disturbances are $d = [p_0 \ z_{HC} \ z_{LC1} \ z_{LC2} \ p_{HC} \ p_{LC1} \ p_{LC2}]$ (the high pressure steam supply, and the consumers demand given by changes at the consumers pressure or of the valve positions (z_{HC}, z_{LC1} and z_{LC2}). The additional states are: $w = [T_T \ T_L]$ (the temperature at the turbine outlet and in the lower pressure header.)

3.10.1 Nominal operating conditions for the steam network

Table 3.6 shows the nominal operating conditions, typical for a steam network found in a chemical plant. Here, V is the volume of the two headers.

Table 3.6: Nominal operating conditions

Variable	p_0	p_H	p_{HC}	p_L	p_{LC1}	p_{LC2}	z	T_H	T_L	V_H	V_L
Value	42	40	38	7	6	5	0.5	380	200	1	5
Unit	bar	bar	bar	bar	bar	bar	-	°C	°C	m^3	m^3

3.10.2 Model

We assume ideal gas, constant specific heat capacity, no pressure losses and perfect mixing in both pressure headers. Assuming isothermal conditions in the high pressure header (T_H constant), the dynamic mass balance in pressure form becomes Eq. 3.89.

$$\frac{dp_H}{dt} = \frac{RT_H}{V_H}(q_H - q_{HC} - q_{TB} - q_T) \stackrel{\text{def}}{=} f_H \tag{3.89}$$

where q_j is the molar flow though a valve.

The low pressure header is not isothermal because work is extracted in the turbine, and therefore the mass and energy balance become coupled. The energy balance in temperature form is given in Eq.3.90.

$$\frac{dT_L}{dt} = \frac{RT_L}{V_L p_L}\left(q_{TB}(T_H - T_L) + q_T(T_T - T_L)\right) \tag{3.90}$$

The mass balance in pressure form is given in Eq. 3.91.

$$\frac{dp_L}{dt} = \frac{R}{V_L}(q_{TB}T_H + q_T T_T - q_{LC1}T_L - q_{LC2}T_L) \stackrel{\text{def}}{=} f_L \tag{3.91}$$

We assume isentropic expansion in the turbine and that there are no con-

straints for the power supplied to the electric grid. Therefore the temperature at the turbine outlet (T_T) is computed from Eq.3.92.

$$T_T = T_H \left(\frac{p_L}{p_H} \right)^{\frac{\gamma-1}{\gamma}} \tag{3.92}$$

where γ is the steam heat ratio capacity.

To model the molar flows through valves, we use a valve equation with a linear valve characteristic (Eq.3.93).

$$q_i = C_{v,i} z_i \sqrt{|p_{in}^2 - p_{out}^2|}, \quad \forall i \in (H, HC, TB, LC) \tag{3.93}$$

where $C_{v,i}$ is the valve coefficient, z_i is the valve opening, p_{in} and p_{out} are the pressures before and after the valve respectively.

To model the molar flow through the turbine, we assume a constant mass flow coefficient (ϕ), equivalent to a chocked turbine (Eq. 3.94).

$$q_T = \phi \frac{p_H}{\sqrt{T_H}} \tag{3.94}$$

3.10.3 Derivation of transformed inputs

The transformed input $v = [v_H \; v_L]$ is defined by applying Eq. 3.20 resulting in Eq. 3.95. We assume that the measurements for T_H, T_L and T_T are available. We consider the tuning parameter $B = I$.

$$v_i = f_i - A_i p_i, \quad \forall i = (H, L) \tag{3.95}$$

where $A_i = \frac{\partial f_j}{\partial p_i}, \forall i = (H, L)$, evaluated at the nominal conditions from Table 3.6.

The transformed system in Eq.3.96 is linear, decoupled and has perfect

disturbance rejection.

$$\frac{dp_i}{dt} = v_i - A_i y_i, \quad \forall i = (H, L) \tag{3.96}$$

3.10.4 Input calculation

We find the unknown variable $u = [z_H \; z_{TB}]$ by solving the system of linear equations (Eq. 3.97) resulted from rewriting Eq. 3.95.

$$\begin{bmatrix} z_H \\ z_{TB} \end{bmatrix} = \begin{bmatrix} \alpha & -\beta \\ 0 & \beta \end{bmatrix}^{-1} \begin{bmatrix} \frac{V_H}{RT_H}(v_H + A_H p_H) + q_{HC} + q_T \\ \frac{V_L}{R}(v_L + A_L p_L) - q_T T_T + (q_{LC1} + q_{LC2}) T_L \end{bmatrix} \tag{3.97}$$

with $\alpha = C_{vH}\sqrt{|p_0^2 - p_H^2|}$, $\beta = C_{vTB} T_H \sqrt{|p_H^2 - p_L^2|}$, the flows q calculated from Eq. 3.93.

Note that from Eq. 3.90, T_L depends on u, therefore it is not a true disturbance. However, the use of a measured T_L in the input transformation is not a problem in this case because the dynamics from the inputs u to the outputs y have a stable inverse (have no RHP-zeros), hence the inverse generated by the input transformation will be stable.

3.10.5 Simulation results

Figure 3.20 shows the responses for disturbance rejection and setpoint changes for $y = [p_H \, p_L]$ (Figures 3.20a) and 3.20b), $w = [T_H \, T_L]$ (Figure 3.20d), $u = [z_h \, z_{TB}]$ (Figure 3.20c) and $v = [v_H \, v_L]$ (Figures 3.20e and 3.20f) to $p_0 = 42$ bar at time $t = 10\,s$, $p_{HC} = 39$ bar at time $t = 20\,s$, $p_{LC1} = 5.5$ bar at time $t = 30\,s$, $p_{LC2} = 1$ bar at time $t = 40\,s$, $p_H^s = 39$ bar at time $t = 50\,s$ and $p_L^s = 6$ bar at time $t = 60\,s$. We tune the PI-controllers with $\tau_C = -\frac{1}{2A}$, which are only used for setpoint changes. The results in Figure 3.20 show a decoupled process with perfect disturbance rejection.

In summary, steam networks are interactive systems, where the main task of the control system is to reject disturbances either on the steam generation

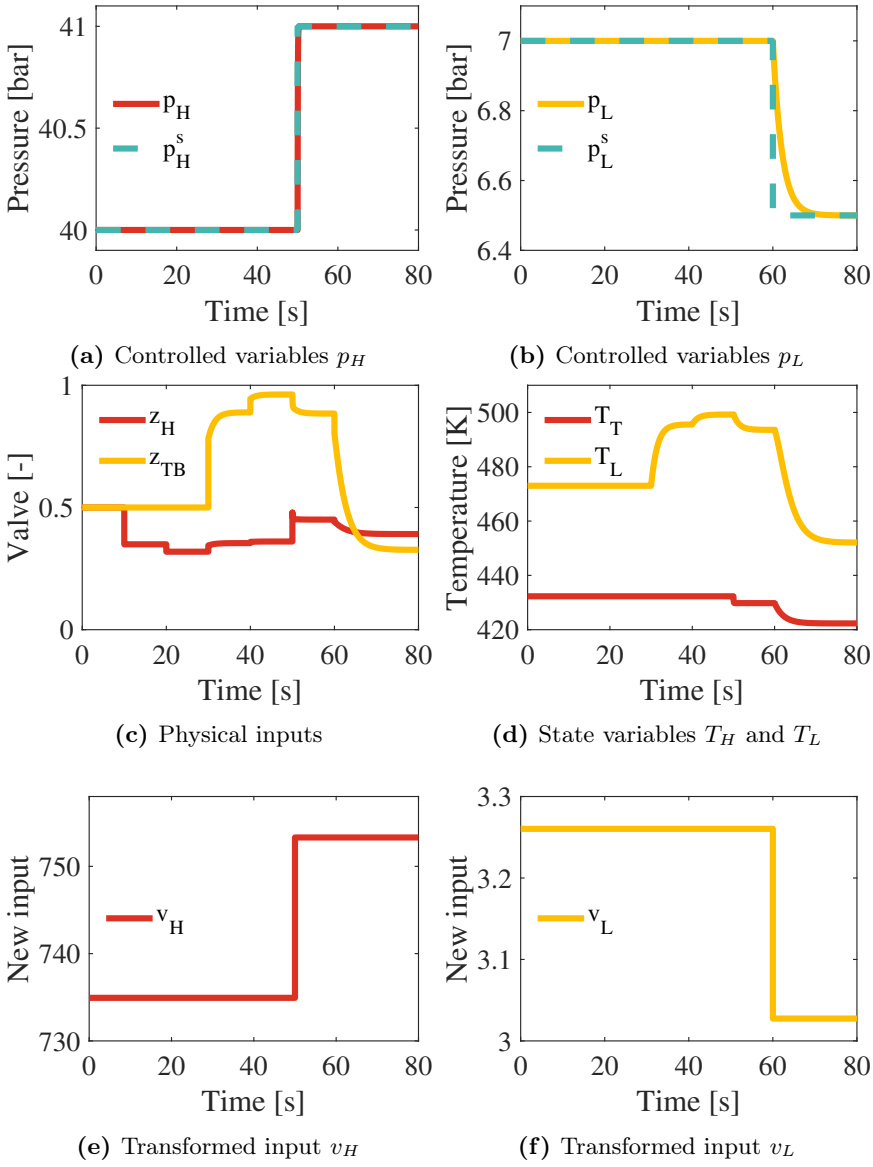

(a) Controlled variables p_H **(b)** Controlled variables p_L

(c) Physical inputs **(d)** State variables T_H and T_L

(e) Transformed input v_H **(f)** Transformed input v_L

Figure 3.20: Simulation results for disturbance rejection and setpoint changes.

or demand side. We design the control structure by using a method for input transformation that gives decoupling and perfect disturbance rejection both dynamically and at steady-state (Eq. 3.96), which makes it a good fit for the control structure of a steam network, as seen in Figure 3.20.

3.11 Discussion

This section continues the mixing example introduced in Section 3.7 and it presents how to handle input saturation and the effect of selecting the parameter A when there are unmeasured disturbances.

3.11.1 Example 5 (example 3 continued): accounting for input saturation

In most of the previous examples we have considered the flows as the manipulated variables. In reality, the inputs are valves or pumps that have limited operating range (actuation). Therefore, we show by simulation how the input transformation implementation behaves in presence of (physical) input constraints for the mixing example introduced in Section 3.7. The ideal input transformations were derived in Eq. 3.68 and Eq. 3.69, respectively. We compare two implementation, the model-based inversion (Figure 3.4a) and feedback-based (Figure 3.4b). For the feedback-based implementation, we need to decide on the pairing $u - v$. For the mixing example there are two possible choices: $u_1 - v_1; u_2 - v_2$ and $u_1 - v_2; u_2 - v_1$, and we them consider both for simulation purposes. For both loops, we use an I-controller tuned on the initial response that also has antiwind-up (back-calculation method) that tracks the real plant input a time constant $\tau_T = 1$ s. In addition, v is calculated using the real plant input.

Figure 3.21 shows the simulation results to a setpoint change at $t = 100$ s of $\Delta q_1^s = 5$ kg/s, a disturbance step change at $t = 200$ s of $\Delta T_1 = 5$ °C and finally a disturbance step change at $t = 300$ s of $\Delta T_2 = 20$ °C. Note that for

simplicity, we set the constraints directly on the flows $q^{\max} = 10\,\mathrm{kg/s}$. The simulation results in Figure 3.21 show that with model-based inversion we loose control of all CVs, while with the feedback-based (cascade) implementation we retain control of the CVs controlled by the transformed input which does not saturates. The difference between the two implementations is that the feedback-based uses the real plant input to calculate the transformed input v. Thus, it has knowledge about the input constraints.

In summary, we may handle input saturation using the feedback-based implementation. For multivariable systems, we select the pairing $u - v$ according to the input saturation rule (Reyes-Lúa and Skogestad, 2020), i.e. pair the input that is most likely to saturate with the CV that we can give up controlling.

3.11.2 Example 6 (example 3 continued): choice of the tuning parameter A and effect of unmeasured disturbances

We analyse by simulation the effect of tuning parameter $A = -\frac{1}{\tau}$ when there are errors in the disturbance measurements. We consider four cases:

1. $A = \mathrm{diag}\left(\frac{\partial y}{\partial f}\right)_*$, i.e. keeping the original system dynamics
2. $A = 2\mathrm{diag}\left(\frac{\partial y}{\partial f}\right)_*$, i.e. making the system faster
3. $A = 0.5\mathrm{diag}\left(\frac{\partial y}{\partial f}\right)_*$, i.e. making the system slower
4. $A = 0$, i.e. equivalent to feedback linearization.

where $*$ denotes nominal operating conditions.

The ideal input transformations were derived in Eq. 3.68 and Eq. 3.69, respectively.

Figure 3.22 compares the simulation responses for four choices of the tuning parameter A to a step disturbance $\Delta d_1 = \Delta T_1^0 = -2$ °C at time 100 s considering 5 °C disturbance measurement error for $d_1 = T_1^0$. The

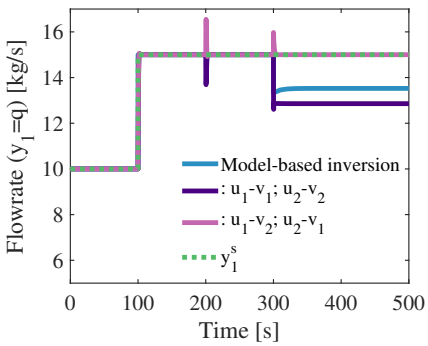

(a) Controlled variable $y_1 = q$

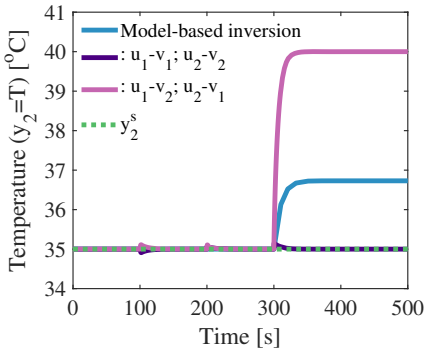

(b) Controlled variable $y_2 = T$

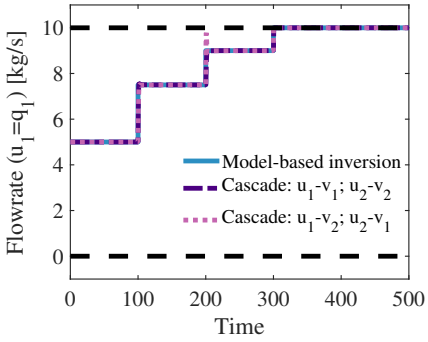

(c) Input $u_1 = q_1$

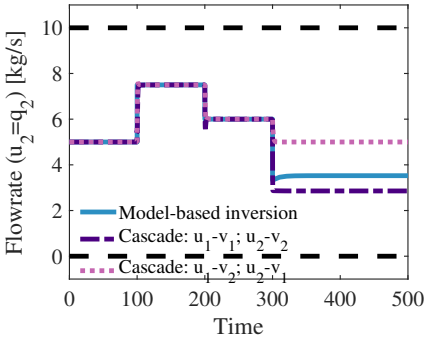

(d) Input $u_2 = q_2$

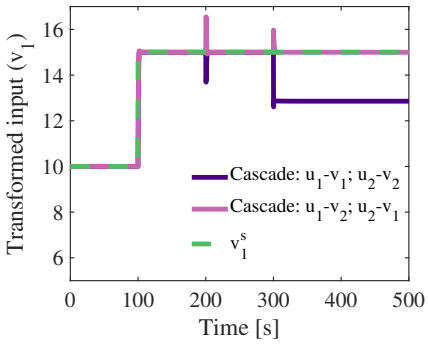

(e) Feedback: transformed input v_1

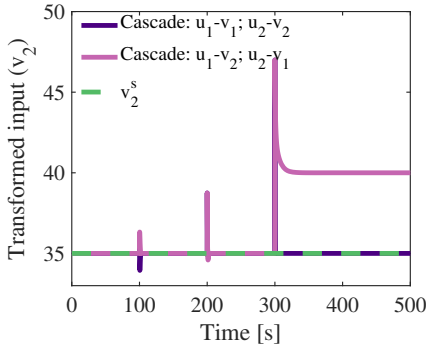

(f) Feedback: transformed input v_2

Figure 3.21: Simulation results for the mixing example with input saturation for the model-based implementation, and feedback-based implementation with the two possible pairing ($u_1 - v_1; u_2 - v_2$ and $u_1 - v_2; u_2 - v_1$)

disturbance error implies that the calculation block in Figure 3.4a uses the nominal value for $d_1 = T_1^0$.

The choice of tuning parameter A only affects the dynamics for y_2 (Figure 3.22b). In Figure 3.22a, y_1 is perfectly controlled because the model assumes steady-state mass balance and we use a static input transformation to define v_{10} (Eq. 3.68). Selecting $A = \frac{\partial y_2}{\partial f_2}$ (blue line) means that for small changes, there is no feedback from y in the transformation and the system behaves as in "open loop". Increasing (in absolute value) A (indigo line) makes the system faster, and the steady-state offset is reduced because now there is some feedback from y to v. On the other hand, decreasing (in absolute value) A (pink line) slows down the system and the offset is increased. Finally, selecting $A = 0$ (i.e. as in feedback linearization) makes the system unstable as both input saturate (green line). This simulation example demonstrates the danger of selecting $A = 0$ when there are measurement errors.

3.12 Summary and conclusion

In this work we introduce transformed inputs $v = g(u, w, y, d)$ to provide a systematic approach to derive model-based nonlinear calculation blocks and cascade control schemes which are frequently used in industrial practices for linearization, decoupling or feedforward disturbance rejection.

The transformed input v replaces the physical input u for controlling the output y. The main assumptions are that we can measure the disturbances and in some cases additional state variables w, and that we have equal number of input and outputs. Measurement of the w variables may be used to replace the model equations describing its dynamics, thus simplifying the model for y.

To derive these transformations, we start from either a steady-state model ($y = f_0(u, d)$) or a dynamic model ($\frac{dy}{dt} = f(u, y, w, d)$). For the steady-state case, the ideal transformed input is then simply the right-hand side of the

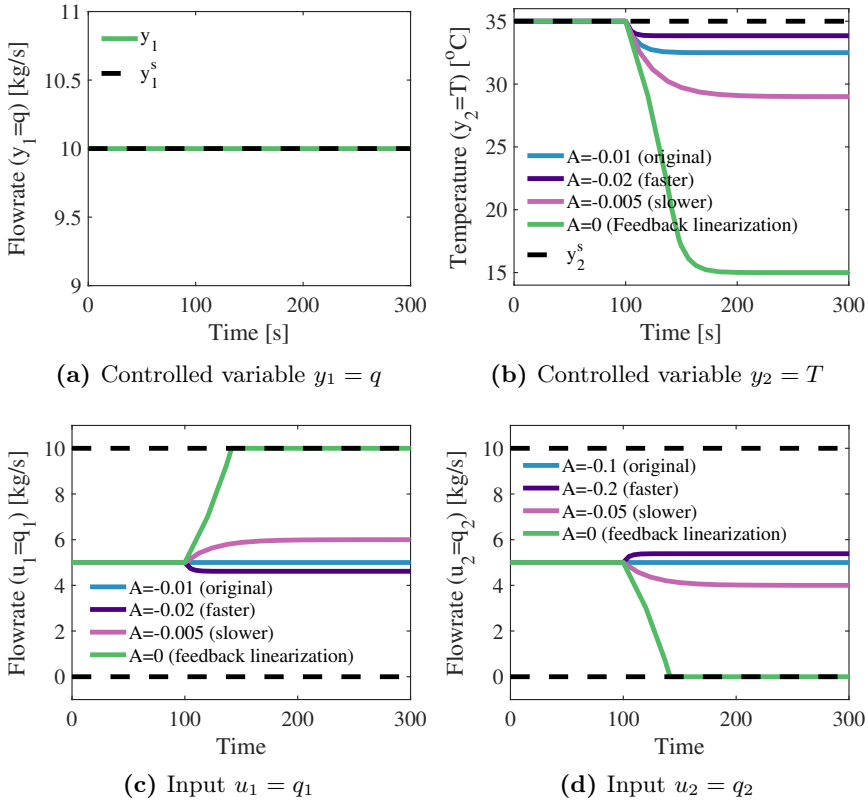

(a) Controlled variable $y_1 = q$ **(b)** Controlled variable $y_2 = T$

(c) Input $u_1 = q_1$ **(d)** Input $u_2 = q_2$

Figure 3.22: Comparison of simulation responses to a step disturbance $\Delta d_1 = \Delta T_1^0 = -5$ °C at time 100 s for four choices of the tuning parameter A considering 5 °C measurement error for $d_1 = T_1^0$. The system becomes unstable for $A = 0$. The outer controller is not included.

model, $v_0 = f_0$, which substituted in the model gives $y = v_0$ which is linear, decoupled and has no effect from the disturbances.

For the dynamic case, we also use the right-hand side of the model equation, but we introduce two tuning parameters A and B to define the transformed input v_A in Eq. 3.20 (see Sections 3.4.2.2-3.4.2.1 for how to select A and B). The idea is to obtain a first-order transformed system on the form $\frac{dy}{dt} = Ay + Bv_A$ which is also linear, decoupled and with no effect from disturbances.

Note that we may also apply input transformations derived from a steady-state model to a dynamic process model, see the heat exchanger example in Section 3.8. In this case, the response will not be perfect dynamically, but it will retain some of the feedforward disturbance rejection effect.

The main advantage of v_A over v is that we may select A to change the dynamics of the transformed system compared to the original system. This is relevant when we introduce measured states w in v_0, the resulting feedback gives changes in the dynamics. For the heat exchanger in Section 3.8, the response of the transformed system became worse (slower), but there may exist cases where the dynamics in w make the response faster than the original system.

In some cases, the implementation of transformed input may be simplified by introducing transformed outputs $z = h(y, w, d)$ because the model is easier to express in terms of z than y. This was used in the heat exchanger example in Section 3.9.

To implement v, we need to solve the input transformation equation ($v = g(u, y, w, d)$ wrt. to the physical input u, given all other variables. In some cases, we may use the exact model-based inverse in Figure 3.4a. In other cases, for example when there is no analytical solution, or for systems with relative order greater than 1, we may use feedback control as a "trick" to solve the equations by using the cascade implementation in Figure 3.4b with an inner v-controller. The cascade implementation is be more robust

than the model-based inversion when we make use of the w measurement because of the potential problem with internal instability of the hidden w dynamics. Internal instability may occur if the indirect (dynamic) effect of u on v through w is large compared to the direct (static) effect of u on v.

The outer controller C is needed to correct for errors in the model and measurements and to reject unmeasured or unmodelled disturbances thus to achieve offset-free control at steady state. For multivariable systems, single-loop PID-controllers are usually sufficient because the response from v to y is linear and decoupled, at least in the ideal case.

Finally, for higher order systems, it possible to introduce chain of transformations, similar to the feedback linearization techniques. However, for more general cases, including cases with more complex dynamics or constraints, there are other control approaches that may be more suitable. One approach is nonlinear model predictive control which allows for more general dynamic models and allows for taking into account much more general control objectives, including constraints and the trade-off between input usage and output performance. The main advantage with the use of transformed inputs is the simplicity, ease of understanding and that they can be implemented into the basic control layer.

Part III

Handling constraints on manipulated variables used for inventory control to balance supply and demand

Chapter 4

General system for balancing supply and demand

This chapter is based on the papers "Supervisory control design for balancing supply and demand in a district heating system with thermal energy storage" (Zotică et al., 2021) and "Bidirectional inventory control with optimal use of intermediate storage" (Zotică et al., 2022).

4.1 Introduction

Consider a general system for balancing supply and demand in Figure 4.1. This is an inventory (m) control problem with two main MVs: adjustable supply (MV_s) and flexible demand (MV_d), and two DVs: given time-variable supply (d_1) and given time-variable demand (d_2) and the mass balance in Eq.4.1. Each MV in Figure 4.1 may consist of different sources for the supply side (e.g., u_1 and u_2) or different sinks for the demand side (e.g., u_3, u_4 and u_5). Thus we make use of input transformations in defining each MV as a sum of its corresponding physical inputs (flows u).

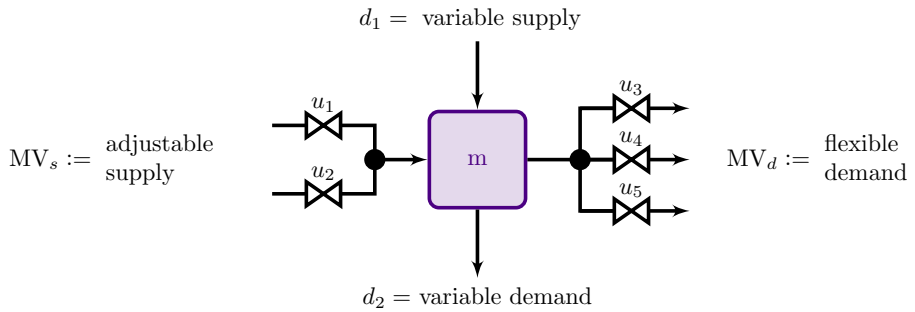

Figure 4.1: General solution for balancing a system with variable supply (d_1) and variable demand (d_2) using an adjustable supply (MV_s) and an adjustable demand (MV_d).

The mass balance Eq.4.1 shows that the inventory is a measure for the demand-supply equilibrium, and we do not need to measure directly the supply or demand.

$$\frac{dm}{dt} = \text{MV}_s + d_1 - \text{MV}_d - d_2 \tag{4.1}$$

The idea is that the adjustable supply MV_s should be used when the variable demand (d_2) is larger than the base load (cheap) supply (d_1), and the adjustable demand (MV_d) should be used when $d_1 > d_2$. One should

normally not use MV_s and MV_d simultaneously, though this may happen for economic reasons. For example, the general system in Figure 4.1 can be a district heating network (DHN) where cheap time-varying waste heat (d_1) is available, and a DH operator minimizes its heat generation (MV_s) cost, i.e., allocation of heat sources u_1 and u_2. The flexible demand MV_d is represented by any form of dissipating excess waste heat, for example using thermal storage (hot water tank or building thermal inertia), or to the environment. The operational objective here is to satisfy the given time-varying heat demand of a set of consumers (d_2).

4.2 Control structures design for active constraints switching

The scope of this work is to design decentralized feedback control structures that set the values of MV_s and MV_d to control the inventory m, thus keeping the balance between demand and supply. Moreover, we consider how to handle cases when the MV used to control the inventory, that is the active MV, saturates at its max limit and we loose control of the CV. For example, for the general system in Figure 4.1, when the adjustable supply MV_s saturates, we need to start using the adjustable demand MV_d for controlling the inventory. To do this, we need a MV-MV switching and possibly also a CV-CV switching (selector) if the MV is already used for another CV.

To implement MV-MV switching, we first need to identify if there are any unused MVs. With no additional MVs left (case 1), we have to give-up controlling a second and less important CV by using a selector for CV-CV switching, and use this second MV to control the inventory, which is the more important CV. Note that this is a case of CV-MV switching (Reyes-Lúa and Skogestad, 2020). As we will later see in Section 5, this CV-MV switching involves moving the throughput manipulator (TPM) to the new bottleneck and it may affect many units as we need to rearrange relevant

loops to be radiating around the new TPM (see Section 5). With additional (unused) MVs (case 2), multiple inflows or outflows may be used when the original MV reaches a max constraint. Compared to case 1, the advantage is it eliminates the need to reconfigure the direction of the inventory loop such that MV-MV switching has only local effect. We first decide if the MVs should become active in a predefined order, that is if MV_{i+1} activates when MV_i saturates (subcase 1), or, if all additional MVs should be used simultaneously (subcase 2). Usually this choice is made based on economic reasons, that is on the price of using each MV. An example for the first subcase is using the MVs in a predefined order by a district heating operator with different heat sources (MVs) such as waste heat, hot water storage tank (dynamic storage) and electric heating (given in order of increasing prices). The desired value for the expensive heat sources (MV) is fully closed, but we start using this MV when the inventory y (pressure) drops to $y^{\min} = p^{\text{low}}$ (see Section 6). An example for the second subcase is the power grid, where several power plants run in parallel and share the load for balancing the variable time-varying consumers demand (see Figure 2.15). Another example relevant to chemical processing plants is a steam distribution network where several boilers (steam generators) are operated in parallel to supply the steam requirement of the plant. To implement this using decentralized control, we may use one controller with I-action and the rest only with P-action, or simply all P-controllers (also known as droop control). In droop control, the proportional gain (K) is used to proportionally allocate the change in load to the MVs. Here we get some offset for y (and this is the reason for the word droop). This subcase is not further extended in this thesis, but simulations results for a balancing supply and demand in a steam distribution network are available in the master thesis of Vik (2021).

Particularly, the examples in this thesis compare simulations split range control (SRC) and controllers different setpoints together with min selectors. Thus these control structures are explained next.

4.2.1 MV-MV switching: split range control

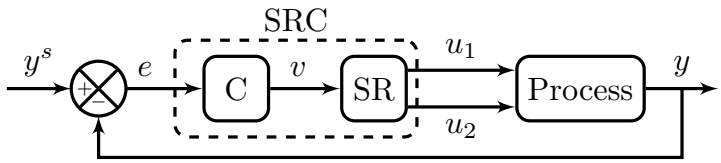

Figure 4.2: Split range control (SRC) with two MVs (u_1 and u_2) and one CV (y). Controller (C) sends an internal signal (v) to the split range block.

SRC is a multiple-input single-output (MISO) control structure that uses a new MV when the initial MV is at its limiting value to keep the CV at a constant setpoint. Thus it extends the steady-state operating range for the CV. SRC is a classical advanced control structure included in many process control textbooks (Bequette, 2002; Seborg et al., 2003) and in industrial applications (e.g., Forsman and Adlouni (2018)).

Figure 4.2 shows the block diagram for SRC that keeps one CV (y) at the setpoint by manipulating two MVs (u_1 and u_2). Note that more MVs can be handled. A feedback controller (C), sends an internal signal (v) to the split range block (SR). The split range block returns the values for the physical MVs (u) based on a predefined function, Eq. 4.2 and Figure 4.3.

$$u_i = u_i^0 + \alpha_i v \quad \forall i = (1 \dots N) \tag{4.2}$$

where u_0 is a bias, α is the slope in the split range block and N is the number of MVs.

There are different alternatives for the split range block, e.g., logic (if-else statements), lookup tables, or functions, which is the implementation we use in this work. Figure 4.3 shows a split range block for two MVs (u_1 and u_2) with two positive and not equal slopes (α) corresponding to the effect from the MVs to the CV, i.e. different gains with the opposite sign. For $v < v^*$, u_1 is active while u_2 is fully open. On the other side, for $v > v^*$, u_2 is active

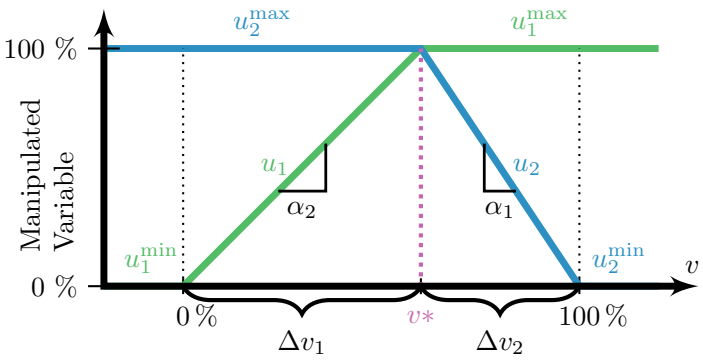

Figure 4.3: Split range block for Fig. 4.2. The slopes α are different because the two MVs have different effect on the CV.

and u_1 is fully open.

Although its broad use, a systematic tuning procedure has only recently been introduced by the work of Reyes-Lúa et al. (2019). This procedure considers the different effects from each MV on the CV to tune the slopes (α) in the split range block and get the desired controller gain for each MV. In SRC we can only have one integral time. However, the controller gain for the individual MV_i-CV pair is adjusted by selecting the slopes α_i in the split range block. (Reyes-Lúa et al., 2019) proposes to select α_i from $K_{C,i} = \alpha_i K_C$, where K_C is the common proportional controller gain, and $K_{C,i}$ is the proportional gain for each manipulated variable.

4.2.2 MV-MV switching: controllers with different setpoints

Controllers with different setpoints is an alternative to SRC. Figure 4.4 shows the block diagram for two independent PI-controllers with different setpoints y_1^s and y_2^s that control y by manipulating u_1 and u_2 respectively. Note that it is possible to use more than two controllers. The idea is to start using a new u_j once y has reached a new threshold given by $y_j = y_i^s + \Delta y_j^s$. During normal operation, one and only one of the controller gives an output

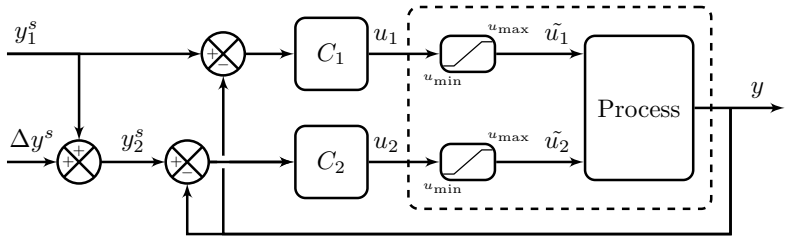

Figure 4.4: Controllers with different setpoints for controlling y using u_1 and u_2. During normal operation, u_1 is the active MV, and u_2 activates when y reaches a new threshold given by $y_1^s + \Delta y^s$.

$u_i^{\min} < u_i < u_i^{\max}$, i.e. within the physical limitations of the actuator. The remaining $N-1$ controllers are not active because their output u_j is beyond the physical limit of the actuator, and thus $\tilde{u_j}\ \forall j \in (1 \ldots N) \setminus i$ is either fully closed or fully open. Controller j becomes active, $(u_j^{\min} < u_j < u_j^{\max})$ when y deviates from the setpoint y_i^s and reaches the next setpoint $y_j = y_i^s + \Delta y_j^s$, usually when u_i saturates. Dynamically, y may reach y_j^s even though u_i is not saturated, for example because of a large disturbance, and it may happen that more than one controller are active simultaneously. It follows that the order in which the controller j activates is *a-priori* determined by the selected Δy_j^s. The value and sign of Δy_j^s is selected during the design phase based on physical understanding of the process, that is on the sign of the process gain from u to y and if the MV should be fully open or fully closed at nominal operation.

The advantages are that the controllers can easily be tuned independently, and the switching is directly handled by the CV value, and not the MV maximum or minimum limit as in the split range block, and therefore logic is not needed. In applications with the objective of tight setpoint control, this structure has the disadvantage that the setpoint is not constant and this will cause some delay during switching. However, the disadvantage of waiting for the controllers to activate becomes an advantage when we

want to maintain production because it allows the level to be uncontrolled between the two setpoints. This effect is used in the example in Section 5, where the control objective is to maintain production for tanks in series when temporary bottlenecks occur.

4.2.3 CV-CV switching: selectors

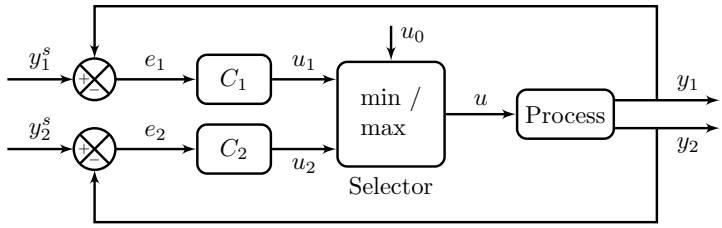

Figure 4.5: Selector (min or max or mid) to switch from controlling CV1= y_1 to CV2= y_2 when CV2 becomes an active constraint. All controllers have tracking antiwind-up (not shown).

Selector logic blocks, also called overrides, are used when only one MV is available for several CVs. There is an independent controller for each controlled variable and a min or max or combination thereof is used to select the plant input (u) from all controller outputs (u_i). When the controller output is not selected, the integral action in the controller will continue to increase and the controller winds-up, which will cause a delayed activation. To avoid this issue, all controllers must have antiwind-up implemented (Åström and Hägglund, 2006). Figure 4.5 shows the block diagram for two CVs and one MV, where we give up controlling the less important CV1 when the more important controlled variable CV2 reaches a constraint. The work by (Krishnamoorthy and Skogestad, 2020) presents a systematic design of selectors used for switching between controlling different CVs. The theory states that a max-selector is used for constraints that are satisfied with a large input, and a min-selector for constraints that are satisfied with a small input.

4. *General system for balancing supply and demand*

Examples. This generalization of balancing supply and demand using inventory control is a result of working on different applications for MV-MV and CV-CV switching. These are:

1. *No extra MV available:* Bidirectional inventory control with optimal use of intermediate storage (Chapter 5).

2. *Extra MVs available:* Balancing supply and demand in a district heating system with thermal energy storage (Chapter 6).

Chapter 5

Bidirectional inventory control with optimal use of intermediate storage

The scope of this chapter is to advocate the use of a decentralized control system that is able to maximize production when temporary or permanent bottlenecks occur for multiple units in series by employing the buffer inventories at intermediate storage. This bidirectional inventory control scheme has for each inventory two controllers, one for the inflow and one for the outflow, with high and low inventory setpoints, respectively. The inventory can typically be liquid (level) or gas (pressure). When production cannot be maintained without breaching physical constraints on the inventory, this control structure automatically reconfigures the loops for consistent inventory control, which means that it is radiating around the throughput manipulator to assure local consistency and feasible operation. The chapter is based on Zotică et al. (2022) with the addition of more simulation responses presented and analyzed.

5.1 Introduction to inventory control

Process down-time due to failures, extended operation at non-optimum points, long periods of switch-over from one mode of operation to another or prolonged operation with off-specification products are identified as causes for economic loss in a chemical plant (Stephanopoulos and Ng, 2000). The root cause for these problems is often that the normal control system is not able to handle certain disturbances or failures, which makes it necessary to switch some control loops to manual mode.

In general, the operation of a system has two main objectives. The first is to stabilize the process and avoid that it drifts into an undesired operating region. The second is to minimize the economic cost J (or equivalently maximize the profit) subject to satisfying the operational constraints. The focus in this paper is on the economic objective.

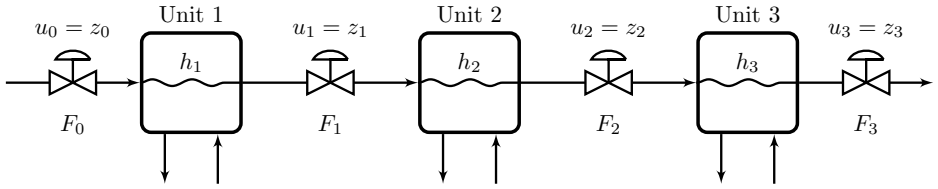

Figure 5.1: Flowsheet of the three units in series studied in this work. For simplicity the inventory is assumed to be liquid, but it could also be gas. We will not include the six flows without a valve in the later figures. These can be considered additional disturbances.

Figure 5.1 shows a simplified process consisting of three units ($N = 3$) in series which we consider. In Figure 5.1, there are four manipulated variables (MVs), which are the adjustable flows F_k (valves z_k) into and out of each unit. Three of these MVs must be used to control (stabilize) the inventory (level) in the units, whereas the remaining degree of freedom, which we denote the throughput manipulator (TPM), sets the flowrate through the system. Although most process plants have some units in series, this is certainly not

a general processing flowsheet, as for example, recycle flows are not included. Nevertheless, it is a fairly general structure for the case where we have N inventories that should be controlled using $N + 1$ MVs. The inventories need to be controlled with given minimum and maximum bounds but otherwise the inventory (buffer) setpoints are degrees of freedom for optimizing the economics (minimizing operational cost J). This decision is a key part of the present paper.

The location of the TPM has a significant effect on the structure of the inventory loops which have to be radiating around the bottleneck for steady-state consistency (Price et al., 1994) (see also Figure 5.3). The desired production rate is typically set by the production planning team, and this determines the desired value (setpoint) for the TPM (at least when averaged over time). In other cases, the production rate may be set by one critical unit, which should operate at a fixed or maximum production rate (for example, the paper machine in a pulp and paper mill). However, during operation one may encounter disturbances which restrict the processing capacity. One important disturbance, which is the main focus in this paper, is a temporary or permanent reduction of the flow through one of the units, that is, the appearance of a new bottleneck in the process.

Bottleneck definition. *A bottleneck is an active constraint that limits further increase in throughput (gives maximum network flow subject to feasible operation).*

There may be some flexibility in temporarily isolating or containing a temporary bottleneck by making use of the stored or available (empty) buffer volume by temporarily giving up inventory control. However, inventories are restricted by minimum and maximum values, hence eventually it will be necessary to either stop production or to move the TPM to the new bottleneck, thus to rearrange the inventory loops correspondingly.

From this, we identify two challenges when encountering a new bottleneck:

Challenge 1. *Use of intermediate storage for bottleneck isolation (con-*

tainment): How to optimally select the inventory (level) setpoints to maximize the time until a new bottleneck makes it is necessary to decrease the throughput?

Challenge 2. *Inventory control rearrangement to handle bottlenecks: How to implement a logic that automatically rearranges the inventory loops to maintain consistent inventory control when encountering a new bottleneck?*

In this work, we explore these challenges by considering temporary and permanent bottlenecks. For a *temporary bottleneck*, the duration of the new active constraint may be short enough to isolate locally its effect such that we can utilize the buffer capacity thus avoid reducing the TPM (challenge 1). For a *permanent* bottleneck, the new active constraint propagates to the adjacent units and, after some delay which we want to maximize (challenge 1), we will need to rearrange the loops and reduce the TPM (challenge 2).

Mathematically, let the MVs be the four valve positions in Figure 5.1: $u = [z_0\ z_1\ z_2\ z_3]$, and let $\bar{F}$ denote the average production over a given time T

$$\bar{F} = \frac{1}{T}\int_0^T F_k(t)dt, \qquad k \in [0 \dots N]. \tag{5.1}$$

The primary operational objective is to keep F_k at a given location k at a given value (setpoint) F_k^s, but if this cannot be achieved, the average production should be maximized (Eq. 5.2a). Thus, the operational objective is to maximize $\bar{F}$ subject to Eq. 5.2b. The buffer inventories (levels h_i) in each tank they must be kept within high and low bounds (Eq. 5.2c). The degrees of freedom u are the valve positions z. They are physically limited by upper and lower bounds (Eq. 5.2d), where typically $z^{\min} = 0$ (fully closed

valve) and $z^{\max} = 1$ (fully open valve).

$$J = \max_{u} \bar{F} \tag{5.2a}$$

$$\text{s.t.} \quad F_k(t) \leq F_k^s(t) \qquad \forall k \in [0, \ldots, N] \tag{5.2b}$$

$$h_i^{\min} \leq h_i(t) \leq h_i^{\max} \qquad \forall i \in [1, \ldots, N] \tag{5.2c}$$

$$z_k^{\min} \leq z_k(t) \leq z_k^{\max} \qquad \forall k \in [0, \ldots, N] \tag{5.2d}$$

The main disturbances will be assumed to be changes in the maximum flow through the units, which may be represented as a change in $z_j^{\max}$.

These operational objectives are also found in batch-plant scheduling and the operation research literature under the names intermediate storage (Lee and Reklaitis, 1989) or buffer management strategy (Chong and Swartz, 2016). For example, the work by (Dubé, 2000) presents a numerical optimization method with the objective of maximizing throughput by coordinating the inventories for planned and unplanned shutdowns and reducing down time. This means that previous work benefits from pre-shutdown preparation, that is, charging the inventory of the tank downstream in anticipation of *a-priori* known reduced production or shut-down upstream.

In this paper, we consider the use of standard advanced control, which includes the use of single-loop decentralized PID controllers combined with simple blocks such as selectors. The original goal of this work was to propose a simple control structure to automatically rearrange the inventory control loops (challenge 2). This corresponds to automatic MV-MV switching. The first obvious choice is to use split range control (SRC, also see Section 4.2.1) (Reyes-Lúa and Skogestad, 2020). However, SRC (for MV-MV switching) in combination with selectors (for CV-CV switching) is difficult to implement in a way that avoids delays during switching. An alternative to SRC is to use two controllers, one for each level setpoint (H and L) (also see Section 4.2.2). The resulting proposed control strategy is shown in Figure 5.2. A similar control structure is presented in Shinskey (1981), ch. 3.7. The main difference

is that we present a more detailed analysis of how it solves both challenges 1 and 2.

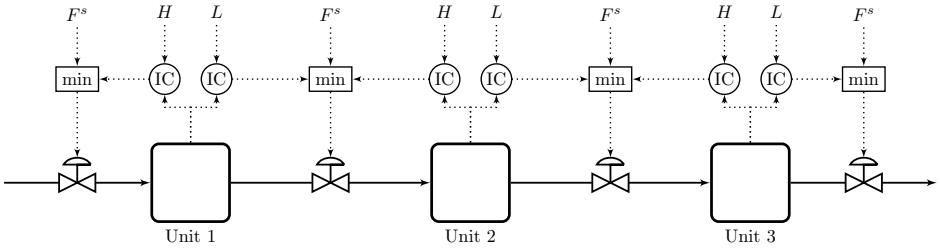

Figure 5.2: Bidirectional inventory control (IC) using selectors as proposed by (Shinskey, 1981). H and L are the high and low inventory setpoints. The operator can set the desired throughput F^s at any given location ($k \in [0 \dots N]$). F^s should be set to $F^s = \infty$ to maximize throughput at this location.

5.2 Inventory (level) control with fixed control structure

In this section, we consider inventory control with a fixed control structure (fixed pairings), and review existing results. Level control is common in process plants and it has been extensively studied in the literature (Buckley, 1964; Marlin, 2000; Seborg et al., 2003; Shinskey, 1988; Stephanopoulos, 1984).

We consider the use of single-loop controllers. There are then two decisions that we need to make:

1. Choice of input-output pairings for inventory controllers.

2. Controller tuning.

We will consider them in opposite order.

5.2.1 Tuning of inventory controllers

With a fixed level control pairing, there are two extreme cases which are frequently studied in the literature, *tight* and *averaging* level control (Marlin, 2000). The main difference between the two is in the selection of controllers tuning parameters.

Tight level control. The control objective is to keep the level (y) close to its setpoint (y^s), and MV variations are not important. In this case, we want to use *tight* tunings (largest possible controller gain subject to satisfying robustness requirements). For example, using the SIMC tuning rules (Skogestad, 2003), we select the closed loop time constant $\tau_C = \theta$, where θ is the effective time delay in the level loop.

Averaging level control. The objective is to average out the flow disturbances by allowing variations in the level. There is no fixed level setpoint except for keeping the level within bounds. Thus the control objective is to minimize the dynamic MV variations. This may be important if MV variations cause disturbances to other units. In this case, we want to use *smooth* tunings (smallest possible controller gain subject to satisfying level constraints). For example, Skogestad (2006) recommends for *smooth* tunings to choose the minimum proportional gain K_C, and the integral time τ_I as given in Eq. 5.3.

$$K_C = \frac{|\Delta F|}{|\Delta h|} \tag{5.3a}$$

$$\tau_I = 4\tau_r \tag{5.3b}$$

where $|\Delta F|$ is the maximum change in flow disturbance,$|\Delta h|$ is the maximum allowed change in the level h, and τ_r is the tank residence time.

In this paper, we allow for level variations, so one may at first think that this is a use of *averaging level control* where smooth tunings are desired. However, the objective is not to minimize the dynamic MV variations, but rather to maximize the flow through the system subject to satisfying the

level and flow constraints in Eq. 5.2c and Eq. 5.2d, respectively. The optimal is then to use tight level control tunings to be able to make full use of the buffer volume by operating close to the physical constraints $h^{\max}$ and $h^{\min}$. Note that the high (H) and low (L) inventory setpoints in Figure 5.2 are set fairly close to these physical constraints.

5.2.2 Input-output pairings for consistent inventory control

As we will see, for consistency the choice of input-output inventory pairings depends on the location of the throughput manipulator (TPM), so let us first define the TPM and consistency (Aske and Skogestad, 2009a).

Throughput manipulator (TPM). *A TPM is a degree of freedom that affects the network flow, and which is not directly or indirectly determined by the control of the individual units, including their inventory control.*

For systems operating at maximum production, we have reached a bottleneck (active constraint) such that there is not really any degree of freedom left for changing the network flow. In such cases, we will refer to this limiting bottleneck (active constraint) as the TPM. This is in agreement with the above definition, because the limiting value of the active constraint affects the network flow.

Consistency. *An inventory control system is said to be consistent if the steady-state mass balances are satisfied for any part of the process, including the individual units and the overall plant. Consistency is equivalent with internal stability of the system, and therefore this is a required property for steady-state operation. In addition, we usually want to have* local consistency*, which means that we want to control all inventories locally, that is, using the local inflow or outflow.*

For local consistent inventory control we need to follow the radiation rule, which says that the input-output pairings must be radiating around the location of a given flow (TPM) (Price et al., 1994).

Radiating rule for local consistency. *Inventory control must be in the*

direction of flow downstream the location of a given flow (TPM). Inventory control must be in the direction opposite to flow upstream the location of a given flow (TPM).

For the simple example process in Figure 5.1, the radiating rule leads to the four different pairing solutions in Figure 5.3 (Price et al., 1994). The aim of this paper is to follow the radiating rule. Figure 5.3a shows a control structure with the plant feed setting the throughput with the TPM at F_0. The inventories (levels) are controlled in direction of the flow, that is, all levels are controlled by the outflow. This is most common configuration in process plants (Stephanopoulos, 1984). Figures 5.3b and 5.3c show a control structure with the throughput set by some conditions inside the plant with the TPM at F_1 and F_2, respectively. The inventories (levels) are controlled radiating from the TPM, that is, the levels upstream are controlled using the inflow, and the levels downstream are controlled using the outflow. Finally, Figure 5.3d shows a control structure with the plant product setting the throughput with the TPM at F_3. The inventories (levels) are controlled in opposite direction of the flow, i.e. all levels are controlled by the inflow.

It is also possible to have consistent structures with use of non-local pairings ("long loops") that do not follow the radiating rule. One example is shown in Figure 5.4 for the case with the TPM located at the feed F_0. It is possible to device more complex rules for the consistency of such complex structures (see for example Kida (2004), in Japanese) and one important rule is that it is not allowed to have any inventory loops crossing the TPM location. However, such complex structures with "long loops" are undesirable for obvious reasons and will not be considered in this paper.

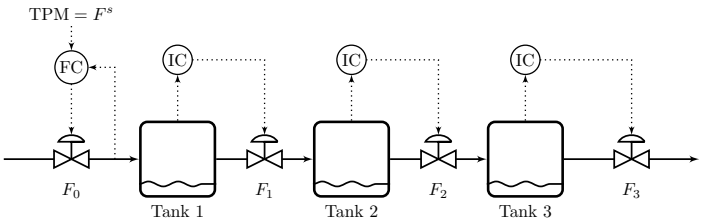

(a) The TPM location is at the plant feed at F_0. Inventory control in direction of flow.

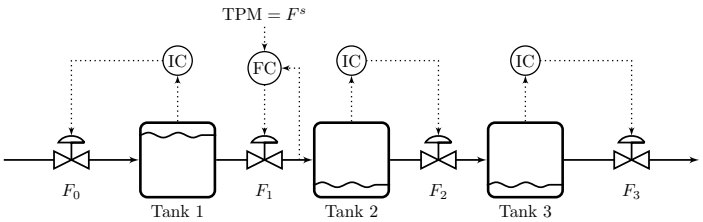

(b) The TPM location is inside the plant at F_1. Inventory control radiating around the TPM.

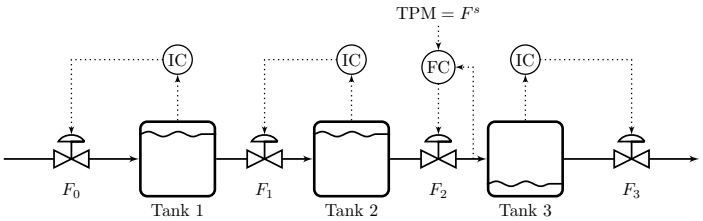

(c) The TPM location is inside the plant at F_2. Inventory control radiating around the TPM.

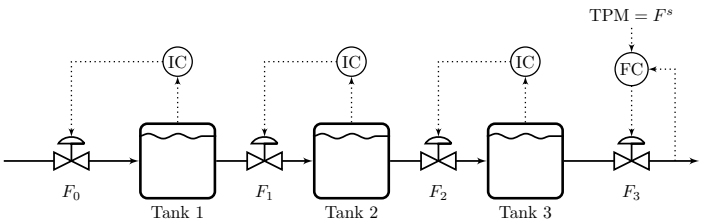

(d) The TPM location is at the plant product at F_3. Inventory control in direction opposite of flow.

Figure 5.3: Locally consistent inventory control system radiating around the throughput manipulator (TPM). The location of the TPM also determines the optimal inventory setpoints for temporarily isolating the effect of new bottlenecks on the TPM flowrate (see Section 5.3).

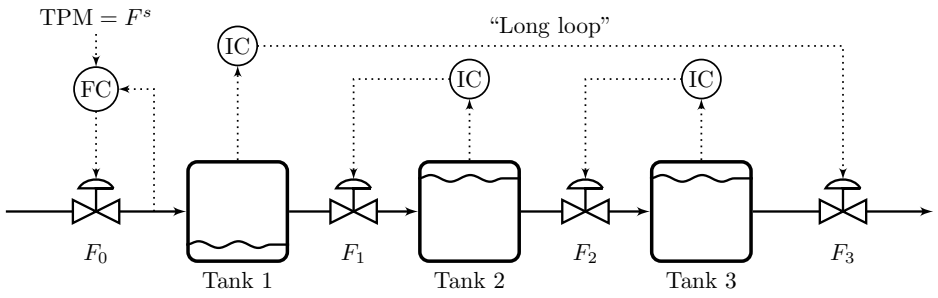

Figure 5.4: Consistent (but not locally consistent) inventory control structure with undesirable non-local pairing ("long loop"). Such structures are not studies in this paper.

5.3 Optimal inventory (buffer) setpoints (challenge 1)

In this section, we analyze how to isolate or contain the effect of bottlenecks for as long time as possible. We consider here the case of a temporary bottleneck. As an example, consider a temporary flow reduction (new bottleneck) in the feed F_0 for a case where F_0 is used for inventory control of a downstream unit (Figure 5.3b, Figure 5.3c and Figure 5.3d). If we do nothing, then the level (h_1) in unit 1 starts falling below its setpoint (h_1^s) and without input constraints, h_1 reaches its minimum value $h_1^{\min} = 0\,\%$ after the buffer time

$$t_{b1} = \frac{A_1(h_1^s - h_1^{\min})}{\Delta F_0} \tag{5.4}$$

Here ΔF_0 is the reduction in the flowrate F_0 and A_1 [m^2] is the unit (tank) cross-sectional area which we for simplicity have assumed is constant. We assume that $h_1^s = 0.9h_1^{\max} = 2.07\,\text{m}$ and $h_1^{\min} = 0\,\text{m}$. Setting $\Delta F_0 = 0.5F_0$ and substituting the model parameters given in 5.9.1 in Eq. 5.4 yields $t_{b1} = 4.14\,\text{min}$. This means that if the downtime for F_0 is less than t_{b1}, then the strategy of doing nothing will be acceptable, and give no loss in the

production rate (reduction of the TPM). This is confirmed by a simulation of a flow reduction from 100% to 50% of its original value for 3 min in Figure 5.5 (see 5.9.1 for model parameters and controllers tunings). We see that we by making use of the stored volume in tank 1 have been able to isolate the effect of the temporary reduction in the flow F_0 to tank 1. From this simple analysis we conclude that in order to maximize the time t_{b1}, we should maximize the value of h_1^s, that is, to have a high inventory setpoint if the inventory is controlled by the inflow.

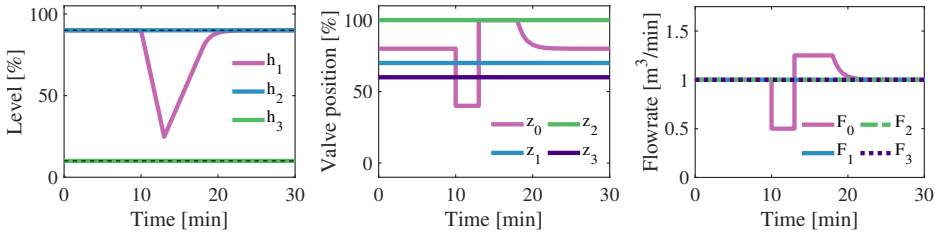

(a) Levels (CVs) **(b)** Valve positions (MVs) **(c)** Flows

Figure 5.5: Simulation of a 3 min temporary bottleneck in feed flow F_0 used for control of downstream level for the control structures in Figure 5.3b, Figure 5.3c and Figure 5.3d. Note that the downstream flowrates (F_1, F_2 and F_3 are not affected.)

For similar reasons, it will be optimal to have low inventory setpoints if the outflow is used for inventory control. A simulation is shown in Figure 5.6 for a 5 min temporary flow reduction (bottleneck) in F_2.

This leads to the following general rule for selection of inventory setpoints (which provides the solution to challenge 1).

Rule for bottleneck isolation (Figure 5.3). *To delay as long as possible the time before a new bottleneck will affect other units, the inventory setpoints should be set high for all inventories controlled by the inflow and the inventory setpoint should be set low for all inventories controlled by the outflow.*

A closer look at Figure 5.3 shows that all the inventories have been selected to follow this rule. Also note that Figure 5.4 follows this rule.

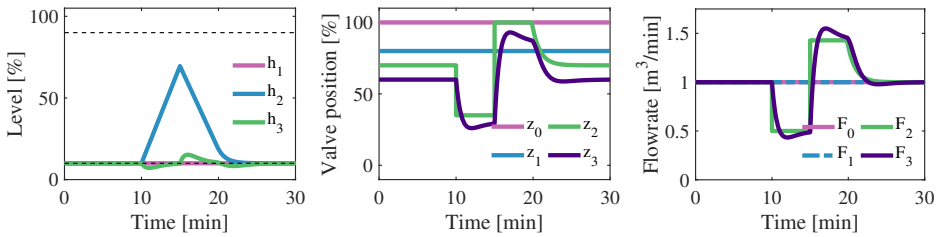

(a) Levels (CV) **(b)** Valve positions (MVs) **(c)** Flows

Figure 5.6: Simulation of a 5 min temporary bottleneck in flow F_2 used for control of upstream level h_2 for the control structures (Figure 5.3a and Figure 5.3b). Note that the upstream flowrates (F_0 and F_1 are not affected).

5.4 Inventory control rearrangement to handle bottlenecks (challenge 2)

Let us first note that the TPM sets the steady-state flow through the system. If we during a dynamic transition fix also another flow or encounter a new bottleneck, then there will temporarily be two TPMs and this inconsistency is resolved by temporarily giving up the control of one of the inventories. This was what we did in Section 5.3 (Figure 5.5 and Figure 5.6), but the bottleneck was temporary so it was not necessary to move the TPM and rearrange the inventory control loops. We now expand the analysis to a longer time or even permanent bottleneck. The goal is therefore to identify the new bottleneck, and select it as the new TPM and then rearrange the inventory loops between the new and old TPM such that we follow the radiation rule (Figure 5.3). For example, if originally the TPM is at the product F_3 (Figure 5.3d), but then the feed rate F_0 becomes the bottleneck, we would need to rearrange all the three level loops to get the structure in Figure 5.3a. It may seem that this requires a centralized supervisor which identifies the new bottleneck and then uses logic to rearrange the control loops accordingly. However, as shown in this section, it can be achieved also with decentralized single-loop PID controllers (Figure 5.2).

The root cause for rearranging loops is that we have encountered a new bottleneck. That is, a MV used for level control is saturated and no longer available. However, we want to maintain level control and therefore need to find a *new* MV to use. This is the issue of MV-MV switching. However, since all MVs are already used to control other CVs, we need in addition a CV-CV switching, that is, a min or max selector (Reyes-Lúa and Skogestad, 2020).

5.4.1 Bidirectional inventory control using split range control and $\min -$ selectors

Figure 5.7 shows the bidirectional inventory control structure using SRC for MV-MV switching and min-selectors for CV-CV switching. In Figure 5.7, z_k^1 sets the desired flow at location k (it is set at ∞ if the goal is to maximize at this location), and the remaining signals z_k^i are the SRC outputs from the inventory controllers.

However, SRC is not recommended in combination with CV-CV switching because of delays in switching as it is also apparent from the simulation in Figure 5.8 and also discussed in Section 5.9.5. The responses in Figure 5.8 are for a permanent reduction of 50 % at the plant feed (F_0) which implies reconfiguring the inventory loops to move the TPM from the product (F_3) to the feed (F_0). The SRC scheme is able to handle the reconfiguration of loops, but as it can be seen from Figure 5.8, the level control is not very good and there are large overshoots in the MVs (flows). The reason is that SRC in combination with CV-CV switching results in delays in the MV-MV switching. The reason for the delay is that the min and max limits in the split range block are not the same as the actual values encountered during switching (see Section 5.9.5). There are possible ways to avoid this, but it becomes complicated to implement (see 5.9.5.1). Fortunately, there is a simpler alternative solution, namely to use controllers with different setpoints (Figure 5.9).

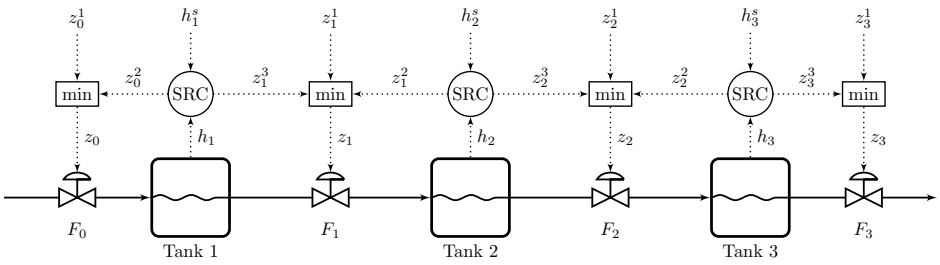

Figure 5.7: Bidirectional inventory control with SRC for MV-MV switching and min-selectors for CV-CV switching. The scheme rearranges the inventory control loops (challenge 2) but it does not solve challenge 1 of optimizing the inventory setpoints because h_i^s is fixed.

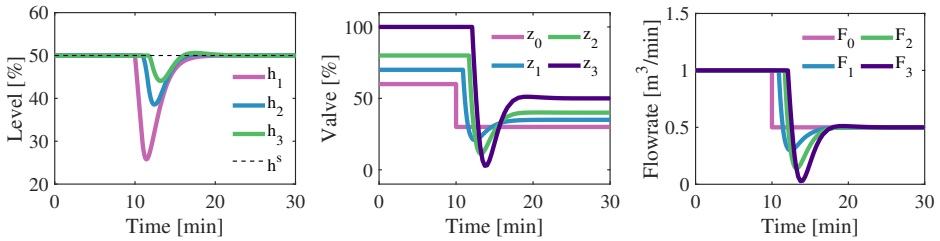

(a) Levels (CVs) **(b)** Valve positions (MVs) **(c)** Flows

Figure 5.8: Simulation of the SRC structure (Figure 5.7) for reconfiguring the inventory loops to move the TPM from F_3 to F_0. The plant feed F_0 decreases by 50 % at time $t = 10$min.

5.4.2 Bidirectional inventory control using controllers with different setpoints and min selectors

Figure 5.9 shows the bidirectional inventory control structure using two controllers, with different setpoints (H and L), and min-selectors. In Figure 5.9, z_k^1 sets the desired flow at location k, z_k^2 is the output of the controller with a high (H) inventory setpoint located downstream of valve k for $k = [0, 1, 2]$, and z_k^3 is the output of the controller with a low (L) inventory setpoint located upstream of valve k for $k = [1, 2, 3]$.

Since the root cause is that we have encountered a new bottleneck, it means that we must reduce the flow. Thus, a min selector is needed. From this the proposed structure in Figure 5.2 (and in Figure 5.9) follows directly. The main difference between Figure 5.2 and Figure 5.9 is that we in Figure 5.2 have implicitly assumed to have implemented flow controllers (although not shown), whereas we in Figure 5.9, directly manipulate the valve positions z_k. Otherwise, they behave in the same way, and they will always maximize the network flow and keep the levels within bounds. We can set the flow at any location k by setting F^s in Figure 5.2 or z_k^1 in Figure 5.9, but it will only be selected if it is sufficiently low such that it becomes a bottleneck for the network.

Figure 5.10 shows the simulation responses for a permanent reduction of 50 % at the plant feed (F_0) which implies reconfiguring the inventory loops to move the TPM from the product (F_3) to the feed (F_0). To reduce the switching time and make the results more comparable to the SRC structure in Figure 5.8, we use a small difference between the high (H) and the low (L) setpoints (see Eq. 5.4); the high setpoint is $h_i^H = 55\,\%$ and the low setpoint is $h_i^L = 45\,\%$.

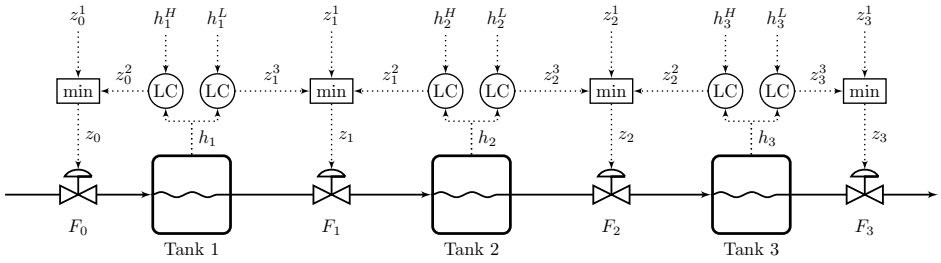

Figure 5.9: Proposed bidirectional inventory control structure, which lets the levels optimally vary between high (H) and low L limits. This is the same structure as in Figure 5.2, except that that we have introduced the valve position z_i as the MV_i. This also allows for using valve saturation to represent new bottlenecks in the simulation.

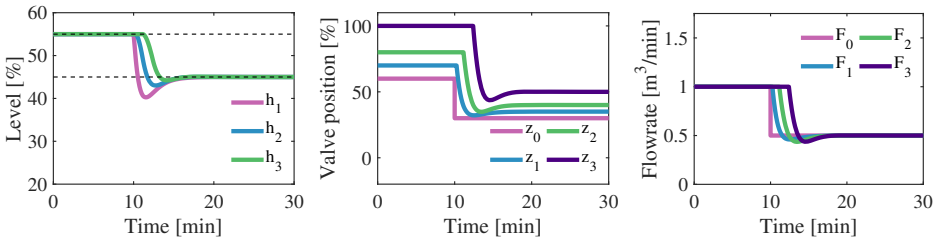

(a) Levels (CVs) **(b)** Valves positions (MVs) **(c)** Flows

Figure 5.10: Simulation of the proposed structure with different setpoints (Figure 5.9) for reconfiguring the inventory loops to move the TPM from F_3 to F_0. Note that the difference between the level setpoints ($h_i^H = 55\%$ and $h_i^L = 45\%$) is quite small in this case to give a short switching time.

5.4.3 Comparison of the two bidirectional control structures

The details of the tuning for the two bidirectional control (Figure 5.7 and Figure 5.9) structures are given in 5.9.3 and 5.9.4, respectively. All controllers are PI-controllers tuned with the SIMC-rules (Skogestad, 2003) with the closed loop time constant $\tau_C = 0.5$ min, which gives an integral time $\tau_I = 4\tau_C = 2$ min.

The simulations show that the control structure with different setpoints (Figure 5.9) is much better than with SRC (Figure 5.7). As mentioned, the reason for the poor performance is the switching delays encountered within SRC. The structure with different setpoints in Figure 5.9 avoids these delays because the switching is done based on the CV measurement and not on the saturation limits of the MV as in SRC, and because of the use of antiwindup which tracks the plant input (we use a back-calculation implementation (Åström and Hägglund, 2006)). There will be some delay because of the difference in setpoints (H and L), but as shown next this can be an advantage.

In summary, we find that the scheme with two controllers (Figure 5.9) is better for rearranging the inventory loops than standard SRC (Figure 5.7). It is thus best for addressing challenge 2. Since it has two inventory setpoints it may also address challenge 1. This is discussed in the next section.

5.5 Optimal use of intermediate storage (challenges 1 and 2)

We have shown that the scheme in Figure 5.2 and Figure 5.9 with two controllers addresses challenge 2, and by making use of the two inventory setpoints (H and L) it can also optimally solve challenge 1. The reason is that the ordering of the level setpoints needed to address challenge 2 is consistent with the optimal setpoints given by the rule for bottleneck isolation given in section 5.3. That is, to make use of the maximum flexibility we

select the setpoint h^H close to $h^{\max}$ and the setpoint h^L close to $h^{\min}$.

To better demonstrate the usefulness of this scheme, we show several simulation cases. We consider the case where the TPM is originally located at the product F_3, but the scheme works equally well with the TPM at other locations (see the additional simulations in Section 5.6). Thus, originally, the controllers in Figure 5.9 are active in the direction opposite of flow as shown in Figure 5.3d, and with all levels at their high setpoints. The system is then ideally suited to delay the effect of bottlenecks appearing in the upstream process (F_0, F_1, F_2).

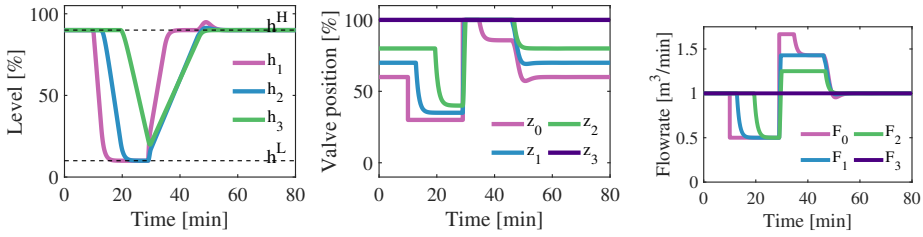

(a) Levels **(b)** Valve positions **(c)** Flows

Figure 5.11: Simulation of a temporary (19 min) 50 % decrease in feed F_0 for the proposed control structure in Figure 5.9 at $t = 10$ min. The TPM is initially at the product (F_3). During the recovery period after $t = 29$ min, the flows are at their maximum value due to physical valve constraints.

In Figure 5.11, we consider a temporary (19 min) 50 % decrease in feed F_0, by changing $z_0^{\max}$ from 1 to 0.3. Because F_0 is located further away from F_3, we can make use of all the inventories h_1, h_2 and h_3 to isolate the effect of the new bottleneck in F_0 on F_3. This is the same case as in Figure 5.10, but we have chosen the level setpoints far away ($h^H = 90$ % and $h^L = 10$ %) in order to delay as much as possible the effect of the reduction in the feed F_0 on the product F_3. Initially, the system responds with the level h_1 dropping (Figure 5.5a). When the level h_1 starts approaching its minimum value (h_1^L), the level controller with a low setpoint for h_1 becomes active and starts reducing F_1. This makes level h_2 drop and eventually this gives a reduction

also in F_2. This effect propagates and h_3 starts decreasing. However, in this case the bottleneck in F_0 disappears at $t = 29\,\text{min}$, before h_3 reaches its minimum value (h_3^L), and thus there is no effect on F_3. During the recovery period, when we want to increase F_0 again (and also F_1 and F_2), the flows F_0, F_1 and F_2 need to overshoot to regain the lost production, while F_3 is kept at its original desired throughput. Because the selector blocks have been set up to maximize the flow (we can show this more clearly by noting that we could have set $F_k^s = \infty$ or $z_k^1 = \infty$), we initially reach the maximum constraints on F_0, F_1 and F_2 (or more exactly on their valve positions). During the recovery period, we lose control of all inventories until they are close to their maximum bounds when the level controllers with high inventory setpoints (h_i^H) becomes active. Then, for $t > 60\,\text{min}$ (approximately), the inventory loops are again in the direction shown in Figure 5.3d, and the system is prepared for future bottlenecks. Detailed response of the controller outputs are shown in 5.9.2.

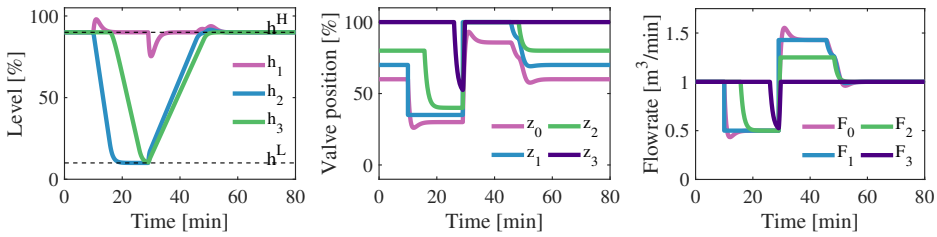

(a) Levels **(b)** Valve positions **(c)** Flows

Figure 5.12: Simulation of a temporary (19 min) bottleneck in flow F_1 for the proposed control structure in Figure 5.9. The TPM is initially at the product (F_3).

In Figure 5.12, we consider a temporary (19 min) bottleneck (disturbance) for F_1. Here the upstream level h_1 initially has a small increase above its high setpoint h_1^H, but it is restored to h_1^H by the activation of the level controller which reduces F_0. In this case, the new bottleneck is closer to the TPM, so we have less isolation and we get a short-term reduction in the TPM F_3 at about $t = 28\,\text{min}$.

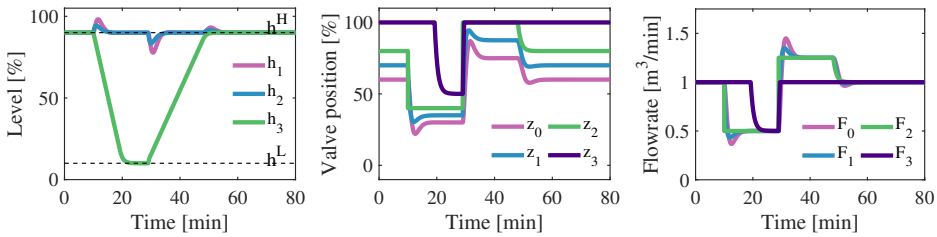

(a) Levels **(b)** Valve positions **(c)** Flows

Figure 5.13: Simulation of a (19 min) temporary bottleneck in flow F_2 for the proposed control structure in Figure 5.9. The TPM is initially at the product F_3.

Finally, in Figure 5.13, we consider a temporary (19 min) bottleneck for F_2. In this case, the new bottleneck is even closer to the TPM, and we get a reduction in the desired product (TPM) F_3 from $t = 20$ min. Note that we initially have some small increase on the levels h_1 and h_2. This makes the disturbance in F_2 propagate quickly to reduce F_1 and F_0.

5.6 Additional simulations for challenge 1 and 2

This section completes Section 5.5 and presents additional simulations for all other TPM locations at the feed F_0, and inside the plant at F_1 and F_2.

5.6.1 The throughput manipulator is originally at the feed F_0

We consider first the case where the TPM is originally located at the feed F_0. Thus, originally, the controllers in Figure 5.9 are active in the direction of flow as shown in Figure 5.3a, and with all levels at their low setpoints. The system is then ideally suited to delay the effect of bottlenecks appearing in the downstream processes (in F_1, F_2 and F_3).

In Figure 5.14, we consider a temporary (19 min) 50 % decrease in flow F_1, by changing $z_1^{\max}$ from 1 to 0.4. This new bottleneck is close to the

original TPM at F_0, thus we can only make use of the inventory h_1 to delay the effect of the reduction in the internal flow F_1 on the feed F_0. Initially, the system responds with the level h_1 increasing (Figure 5.14a). When the level h_1 starts approaching its maximum value (h_1^H), the level controller with a high setpoint for h_1 becomes active and starts reducing F_0. From time $t = 19\,\text{min}$ to $t = 29\,\text{min}$) (approximately), the location of the TPM has changed from z_0 to z_1, that is the controllers are active in the direction shown in Figure 5.3b.

During the recovery period (from time $t = 29\,\text{min}$ to $t = 35\,\text{min}$ approximately), when we want to increase F_1 again (and also F_1 and F_2), the flows F_1, F_2 and F_3 need to overshoot to regain the lost production, while F_0 is kept at its original desired throughput. Because the selector blocks have been set up to maximize the flow (we can show this more clearly by noting that we could have set $F_k^s = \infty$ or $z_k^1 = \infty$), we initially reach the maximum constraints on F_1(or more exactly on the valve position). During the recovery period, we lose control of h_1 until it becomes close to it's minimum bound when the level controller with low inventory setpoint (h_1^L) becomes active. Then, from $t > 45\,\text{min}$ (approximately), the inventory loops are again in the direction shown in Figure 5.3a, and the system is prepared for future bottlenecks.

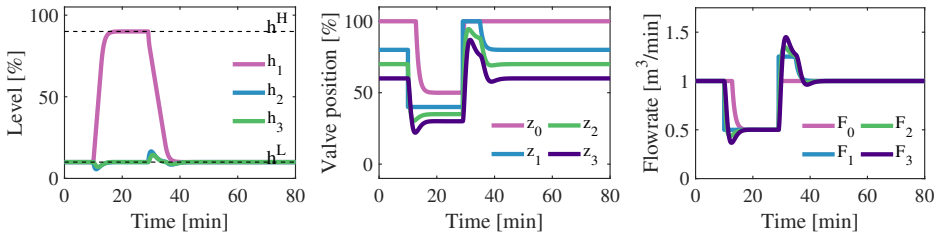

(a) Levels **(b)** Valve positions **(c)** Flows

Figure 5.14: Simulation of a (19 min) temporary bottleneck in flow F_1 for the proposed control structure in Figure 5.9. The TPM is initially at the feed F_0.

In Figure 5.15, we consider a temporary (19 min) 50 % decrease in flow

F_2, by changing $z_1^{\max}$ from 1 to 0.35. In this case, we can make use of both inventories h_1 and h_2 to delay the effect of the reduction in the internal flow F_1 on the feed F_0. Thus the bottleneck is isolated for a longer period compared to a reduction in flow F_1 in Figure 5.14. Initially, the system responds with the level h_2 increasing (Figure 5.15a). When the level h_2 starts approaching its maximum value (h_2^H), the level controller with a high setpoint for h_2 becomes active and starts reducing F_1, which increases the level h_1. When the level h_1 starts approaching it's maximum bound (h_1^H), we give-up maximizing the flow F_0 and use this flow to control h_1. This changes the TPM location to z_2, and the controllers are active in the direction shown in Figure 5.3b. Finally, when the bottleneck on F_2 disappears at $t = 29\,\text{min}$, the lost production is recovered by maximizing F_0, F_1 (until $t = 35\,\text{min}$) and F_2 (until $t = 40\,\text{min}$) during which time we loose control of h_1 and h_2. Note that the reduction in flow F_2, level h_3 is controlled by F_3, and the temporary deviations from setpoint are caused by the disturbances in F_2.

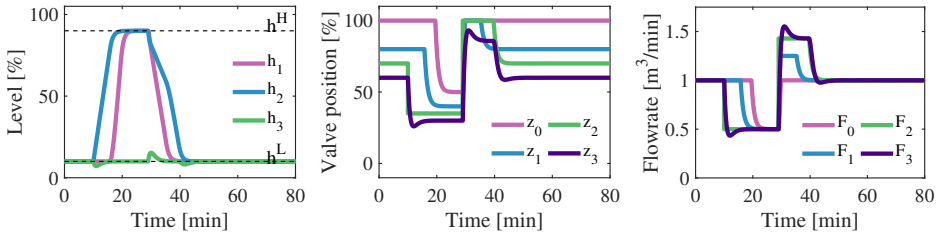

(a) Levels **(b)** Valve positions **(c)** Flows

Figure 5.15: Simulation of a (19 min) temporary bottleneck in flow F_2 for the proposed control structure in Figure 5.9. The TPM is initially at the feed F_0.

Finally, in Figure 5.16 we consider a temporary (19 min) 50 % decrease in flow F_3, by changing $z_1^{\max}$ from 1 to 0.5. Here, the original TPM is furthest away from the new bottleneck we can use all three inventories to isolate the effect of reduction in product F_3 on the feed F_0.

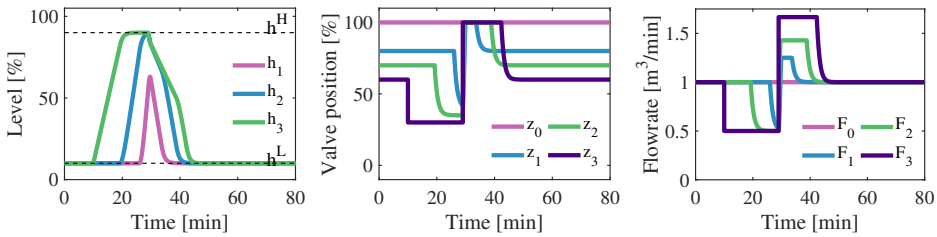

(a) Levels **(b)** Valve positions **(c)** Flows

Figure 5.16: Simulation of a (19 min) temporary bottleneck in flow F_3 for the proposed control structure in Figure 5.9. The TPM is initially at the feed F_0.

5.6.2 The throughput manipulator is originally inside the plant at F_1

We consider next the case where the TPM is originally located inside the plant at F_1. Thus, originally, the controllers in Figure 5.9 are active in the direction shown in Figure 5.3b, and with the upstream level at it's high setpoint and with the downstream levels at their low setpoints. The system is then ideally suited to delay the effect of bottlenecks appearing in the upstream process (F_0) and the downstream processes (F_2 and F_3).

In Figure 5.17, we consider a temporary (19 min) 50 % decrease in the feed F_0, by changing $z_1^{\max}$ from 1 to 0.4. In this case, the reduction in flow is close to the original TPM, and we can only use the inventory h_1 to maintain production and delay the effect of the reduction in the feed F_0 on the internal flow F_1. Initially the level h_1 decreases, and when it approaches it's minimum bound (h_1^L), the output of the controller with a low setatpoint becomes selected by the min selector, and we give-up maximizing the flow F_1 and use it to control the level h_2. The TPM is now at the feed F_0 and the controllers are active in the direction of the flow shown in Figure 5.3a. After the disappearance of the bottleneck and the production recovery period, the TPM returns inside the plant at F_1.

In Figure 5.18, we consider a temporary (19 min) 50 % decrease in flow

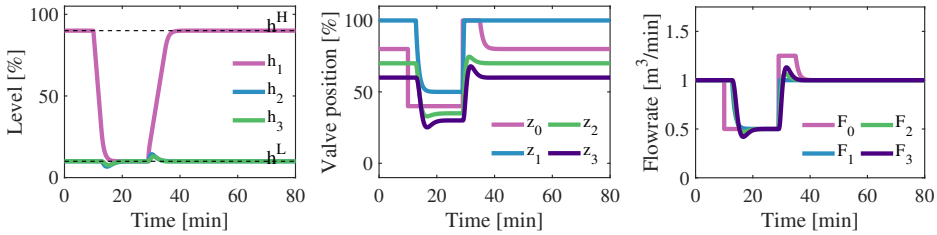

(a) Levels **(b)** Valve positions **(c)** Flows

Figure 5.17: Simulation of a (19 min) temporary bottleneck in flow F_0 for the proposed control structure in Figure 5.9. The TPM is initially is inside the plant at F_1.

F_2, by changing $z_2^{\max}$ from 1 to 0.35. In this case, the reduction in flow is close to the original TPM, and we can only use the inventory h_2 to delay the effect of the reduction in F_2 on the internal flow F_1. Initially, the level h_2 increases, and when it approached the maximum bound the controller with a high setpoint (h_2^H) becomes selected and F_1 is no longer maximized, but used to control h_2. Thus temporarily, the TPM changes to F_2 and the controllers are active as shown in Figure 5.3c. Note that the overshoots for h_3 is caused by the disturbance in F_2, while for h_1 is caused by the decrease in F_1 given by change in TPM from F_1 to F_2.

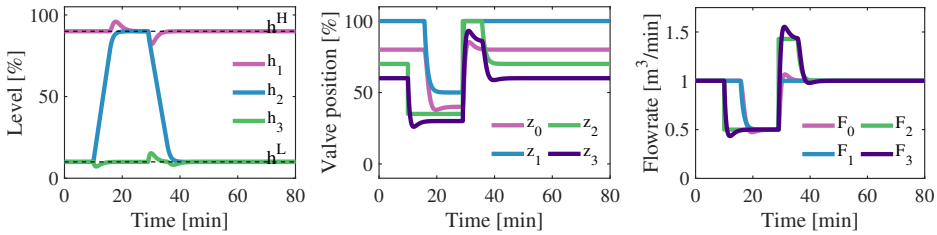

(a) Levels **(b)** Valve positions **(c)** Flows

Figure 5.18: Simulation of a (19 min) temporary bottleneck in flow F_2 for the proposed control structure in Figure 5.9. The TPM is initially is inside the plant at F_1.

Finally, in Figure 5.19, we consider a temporary (15 min) 50 % decrease

in flow F_3, by changing $z_3^{\max}$ from 1 to 0.3. Here we can make use of both inventories h_1 and h_2 to completely isolate the effect of the new bottleneck in product F_3 on the flow F_1 (and the upstream feed F_2). The disturbance in F_3 does not propagate to the feed at F_0 and the level h_1 does not change.

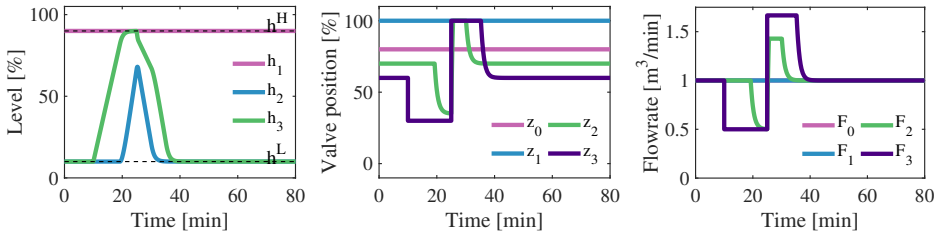

(a) Levels **(b)** Valve positions **(c)** Flows

Figure 5.19: Simulation of a (15 min) temporary bottleneck in flow F_3 for the proposed control structure in Figure 5.9. The TPM is initially is inside the plant at F_1.

5.6.3 The throughput manipulator is originally at inside the plant at F_2

Similarly, we consider next the case where the TPM is originally located inside the plant at F_2. Thus, originally, the controllers in Figure 5.9 are active in the direction shown in Figure 5.3c, and with the upstream levels at their high setpoints and with the downstream levels at it's low setpoints. The system is then ideally suited to delay the effect of bottlenecks appearing in the upstream processes (F_0 and F_1) and the downstream process (F_3).

In Figure 5.20 we consider a temporary (9 min) 50 % decrease in the feed F_0, by changing $z_0^{\max}$ from 1 to 0.5. As the new bottleneck is located furthest away from the original TPM, we are able to use the intermediate inventories h_1 and h_2 to completely isolate the effect of a reduction in the feed F_0 on the internal flow F_2 and the product F_3. Thus the level h_3 it kept at its minimum bound h_3^L.

Initially the level h_1 decreases. When h_1 approaches it's minimum bound, the controller with a low setpoint is selected and F_1 starts decreasing to control h_1. This propagates the disturbance in F_0 to the second tank, and the level h_2 starts decreasing. However, the bottleneck in F_0 disappears at $t = 19\,\text{min}$ which explains the small overshoot for h_1 at $t = 20\,\text{min}$ (approximately). The level h_1 is still controlled at the low setpoint using F_1, so to keep the level constant when F_0 increases, F_1 must also increases, which subsequently increases the level h_2. When h_2 approaches it's maximum bound h_2^H, the controller with a high setpoint is selected, and F_1 is reduced to control h_2. Eventually, the decrease in flow propagates to the feed F_0, and the controller become active in the original direction in Figure 5.3c.

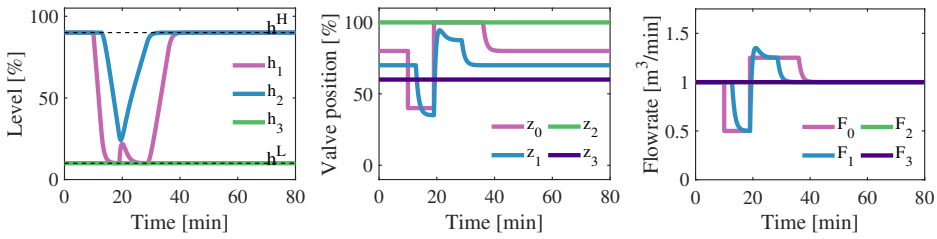

(a) Levels **(b)** Valve positions **(c)** Flows

Figure 5.20: Simulation of a (9 min) temporary bottleneck in flow F_0 for the proposed control structure in Figure 5.9. The TPM is initially is inside the plant at F_2.

In Figure 5.21 we consider a temporary (9 min) 50 % decrease in the internal flow F_1, by changing $z_1^{\max}$ from 1 to 0.35. In this case, the new bottleneck is close to the original TPM, and it is not possible to isolate complete the effect of reducing F_1 on the flow F_2. Thus, when h_2 approaches it's minimum bound, the controller with a low setpoint h_2^L is selected and we give-up maximizing F_2 for a short time. Thus F_2 is reduced it to keep h_2 at the low setpoint. The reduction in F_2 is a disturbance for $h3$, and F_3 must also be reduced accordingly to keep h_3 at the low setpoint h_3^L. After the disappearance of the bottleneck, F_1 increases, which decreases h_1 and

increases h_2. After a period of recovery, once h_2 approaches it's maximum bound, the controller with a high setpoint, h_2^H is selected and F_1 is decreased to maintain control of h_3. This effect propagates to h_1 which increases, and eventually, F_0 is also reduced to keep control of h_1 at the high setpoint, thus restoring the control loops in the direction shown in Figure 5.3c.

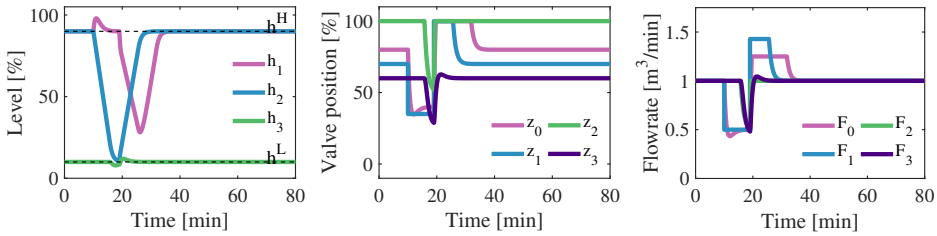

(a) Levels **(b)** Valve positions **(c)** Flows

Figure 5.21: Simulation of a (9 min) temporary bottleneck in flow F_1 for the proposed control structure in Figure 5.9. The TPM is initially is inside the plant at F_2.

Finally, in Figure 5.22 we consider temporary (9 min) 50 % decrease in the product F_2, by changing $z_3^{\max}$ from 1 to 0.3. In this case, the duration of the new bottleneck is short enough that we isolate the effect of reducing F_3 on the flow F_2 only by using the inventory h_3.

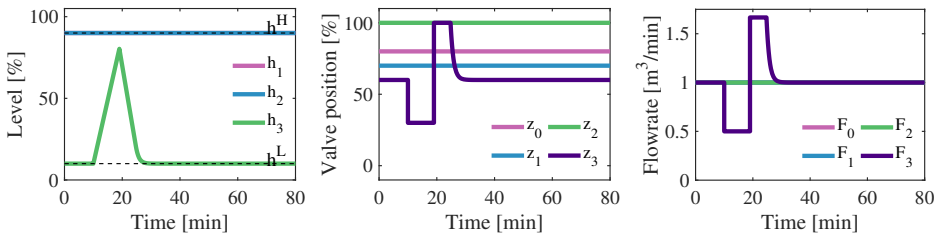

(a) Levels **(b)** Valve positions **(c)** Flows

Figure 5.22: Simulation of a (9 min) temporary bottleneck in flow F_3 for the proposed control structure in Figure 5.9. The TPM is initially is inside the plant at F_2.

5.7 Discussion

5.7.1 Choice of throughput manipulator location

The proposed control system in Figure 5.2 (and the more detailed Figure 5.9) automatically moves the TPM to the new (permanent) bottleneck and reconfigures the inventory loops to give the arrangement in Figure 5.3 (challenge 2). However, there may also be cases where the production rate is not determined by a bottleneck, but rather has a given setpoint, for example, determined by market conditions. Where should the TPM be located in this case? There may be many considerations. If we do not expect bottlenecks, then it is often recommended to locate the TPM at a place where we want small dynamic variations, for example, at the feed of a critical unit. For a process with a long recycle loop, it is often recommended to locate the TPM inside the recycle loop (Luyben, 1993). For cases where bottlenecks are expected, it is recommended in the literature that the TPM should be located at the expected future bottleneck (Aske and Skogestad, 2009b). The reason is to be able to achieve tight control at the bottleneck when it occurs. This avoids "long loops" (Figure 5.4) and reduces the back-off. However, this recommendation is under the assumption that we are not allowed to rearrange the inventory control loops, hence it does not apply for the proposal in Figure 5.2 (and Figure 5.9) with bidirectional inventory control. Interestingly, for the proposed control system in Figure 5.2 (and Figure 5.9), which have *automatic* reconfiguration of the loops, the recommendation is opposite: *The set flow F^s (and thus the TPM) should be located as far away as possible from the expected next bottleneck.* We can then use all the inventories between the new bottleneck and TPM to isolate the new bottleneck, that is, we can delay as long as possible the time before we must reduce the throughput (challenge 1). Of course, if the bottleneck is permanent, the TPM will move to the new bottleneck, which is consistent with the recommendation by (Aske et al., 2007; Aske and Skogestad, 2009b).

5.7.2 Alternative implementation: model predictive control (MPC)

MPC handles constraints changes by design, and it therefore seems to be a good alternative for our case. However, while it may be suited for fast MV-MV switching and tight level control (challenge 2), we do not see an easy implementation of changing the inventory setpoints in an optimal manner (challenge 1). A possible approach would be to set the objective function as to maximize the flows subject to constraints on the valves. However the implementation effort may not be worth because the same result can be achieved with decentralized control (controllers with different setpoints)

Moreover, the decentralized solutions that we propose in this work have six advantages over more advanced multivariable control such as MPC:

1. they are easier to implement
2. they do not require a full dynamic plant model
3. they require only local information (i.e. level measurement in our case)
4. they do not require solving a dynamic optimization problems
5. they do not require disturbance measurement or forecast
6. it is easier to embed information about what to do in case of future disturbances.

5.8 Conclusion

In this work we propose to use the bidirectional inventory control structure in Figure 5.2 with a high and a low setpoints for each inventory. This scheme maximizes throughput when there are changes in the operation that give new temporary or permanent bottlenecks in other units. In order to isolate the effect of a new bottleneck, the inventories will be floating between the

minimum and maximum values at certain times. This structure automatically identifies the new bottleneck without the need for centralized logic, and thus it automatically reconfigures the inventory loops to be radiating around the TPM to get local consistency of the inventory control system (challenge 2). That is, it automatically gives the four desired structures in Figure 5.3 as special cases. Moreover, it automatically adjusts the inventory setpoints for optimal disturbance isolation (challenge 1), by setting large inventory setpoint upstream TPM and small inventory setpoint downstream. Finally, it automatically recovers the lost production for a temporary bottleneck.

5.9 Appendix

5.9.1 Process model and parameters

Assuming constant density (ρ) and constant cross-sectional tank area, the mass balance for each tank is

$$\frac{dh_i}{dt} = \frac{1}{A_i}(F_{i-1} - F_i) \quad \forall i \in (1,2,3) \tag{5.5}$$

where $h\,[\mathrm{m}]$ is the level, $A\,[\mathrm{m}^2]$ is the cross-sectional tank area (Table 5.1) and $F\,[\mathrm{m}^3/\mathrm{min}]$ is the volumetric flowrate in and out of the tank respectively calculated from Eq. 5.6.

$$F_i = \underbrace{C_{v,i}\sqrt{\frac{\Delta P_i}{\rho}}}_{k_{v,i}} f_i(z) \quad \forall i \in [0,1,2,3] \tag{5.6}$$

where C_v is the valve coefficient, $\Delta P\,[\mathrm{Pa}]$ is the pressure drop over the valve assumed constant, $\rho\,[\mathrm{kg}/\mathrm{m}^3]$ is the water density assumed constant and $f(z)$ is the valve characteristic, which we assume linear, i.e. $f(z) = z$,.

Table 5.1 shows the tank design parameters, V_{Tank} is the design volume, A is the tank cross-sectional area and h_{Tank} is the tank design height.

Table 5.1: Design parameters for the three tanks

i	$V_{\text{Tank}}\,[\text{m}^3]$	$A\,[\text{m}^2]$	$h_{\text{Tank}}\,[\text{m}]$
1	2.3	1	2.3
2	4.2	1.5	2.8
3	6.4	2	3.2

Table 5.2 shows parameter k_v (Eq. 5.6) for the four valves together with the nominal valve openings (z^*) corresponding to a flow value of $F = 1$ m^3/min. Note that for the different cases we locate the smallest k_v value at the original TPM at $z^{\max} = 1$, and this is the reason for the different initial valve openings between Figure 5.6, Figure 5.5 and Figure 5.11.

Table 5.2: Design parameters for the four valves.

z^*	$k_v\,[\text{m}^3/\text{min}]$
1	1
0.8	1.25
0.7	1.428
0.6	1.667

5.9.2 Controllers outputs for the structure in Figure 5.9

Figure 5.23 complements the simulation results in Figure 5.11 and it shows the inputs to (interrupted lines), and the outputs from (continuous lines) the four min selectors blocks of the structures with controllers with different setpoints (Figure 5.9).

5.9.3 Tuning of controllers with different setpoint

We can tune the two PI-controllers independently, meaning that we can consider the different effects from the MVs (valves) on the CV (level) given by the different valve characteristics C_v and and pressure drops (ΔP) over

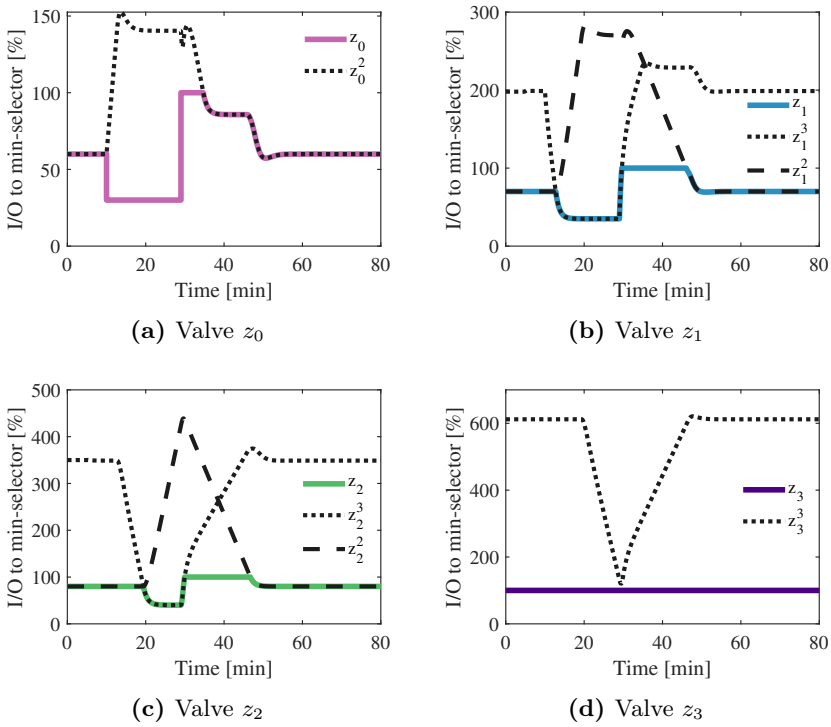

(a) Valve z_0 **(b)** Valve z_1

(c) Valve z_2 **(d)** Valve z_3

Figure 5.23: Inputs and outputs for all min −selectors in Figure 5.9 corresponding with the simulation responses in Figure 5.11. The continuous line is the selected physical valve position. To maximize throughput we set $z_0^1 = z_1^1 = z_2^1 = z_3^1 = \infty$.

Table 5.3: Tuning parameters for controllers with different setpoints.

Tank	LC	h^s	K_C TPM=F_0	K_C TPM=F_2	K_C TPM=F_3	τ_I	τ_T	τ_C
1	high	90 %	2	1.6	1.2	2	1	0.5
	low	10 %	-1.6	-1.4	-1.4	2	1	0.5
2	high	90 %	2.4	2.1	2.1	2	1	0.5
	low	10 %	-2.1	-3	-2.4	2	1	0.5
3	high	90 %	2.8	4	3.2	2	1	0.5
	low	10 %	2.4	-2.4	-4	2	1	0.5

the valve. For example, we may apply the SIMC tuning rules (Skogestad, 2003) to the model given in 5.9.1, which is an integrating process with a large open loop time constant $\tau \to \infty$. Table 5.3 shows the tuning parameters. These are the high and low level setpoints (h^s), the controller proportional gain K_C, the integral time τ_I, and the tracking time constant τ_T. Here, τ_C is the desired closed loop time constant.

5.9.4 Tuning of SRC

We follow the procedure proposed by Reyes-Lúa et al. (2019) to tune the SRC parameters. These are the common controller gain K_C, the common integral time τ_I and the individual slopes α_i. The slopes α_i allow for different controller gains for each MV considering the different valve size (Eq. 5.7a). We define the normal range for the internal signal v to be from 0 % to 100 %, and we scale the MVs also from 0 % to 100 %. Then, for each tank, we solve the system formed by the Eq. 5.7.

$$K_{C,i} = \alpha_i K_C, \quad \forall i \in (1,2) \tag{5.7a}$$

$$\Delta v_1 + \Delta v_2 = 100 \tag{5.7b}$$

$$\Delta v_i = \frac{u^{\max} - u^{\min}}{|\alpha_i|} = \frac{100}{|\alpha_i|}, \quad \forall i \in (1,2) \tag{5.7c}$$

Table 5.4: Modified K_C and τ_I for the three SRC in Figure 5.7.

Tank	h^s	K_C	τ_I	τ_C min	α_1	α_2	v^*	$u_{0,1}$	$u_{0,2}$
1	50 %	65	2	0.5	1.8571	-2.1667	53.85	0	216.167
2	50 %	112	2	0.5	1.875	-2.1429	53.33	0	214.286
3	50 %	178	2	0.5	1.8	-2.25	55.55	0	225

where the significances of Δv and α are shown in Figure 5.24a.

However, we can only have one integral time (τ_I) and we need to compromise on its value. Because the slowest process is critical we select the largest τ_I of the two options (for inlet and outlet valves in Table 5.3). However, with no delay and same τ_C, all τ_I are equal. However, the common controller gains K_C were found to be too small in simulations, and the min selector output would alternate between the two controllers. To improve the dynamic performance, we increased them and the new values are given in Table 5.4. The slopes α remain the same.

Figure 5.24a shows the split range block for tank 1. Figure 5.24b shows the split range block for tank 2. Figure 5.24c shows the split range block for tank 3.

5.9.5 Performance of bidirectional inventory control using split range control

SRC gives poor level control, especially of h_1 (Figure 5.8a). The reason is that there are two delays in the MV-MV switching. Initially, the TPM is a the product F_3 (Figure 5.3d), and the valve openings are $z_0 = z_0^2 = 0.6$ and $z_1 = z_1^2 = 0.7$ (Figure 5.7). Then at $t = 10$ min, the feed flow F_0 drops to 50 % of its original value. In the simulation, we do this by changing the value of z_0^1 from 1 to 0.3, but physically it could be caused by a bottleneck inside process which the controller does not know about. This causes the level h_1 in tank 1 to drop, and the SRC responds by trying to open the valve z_0.

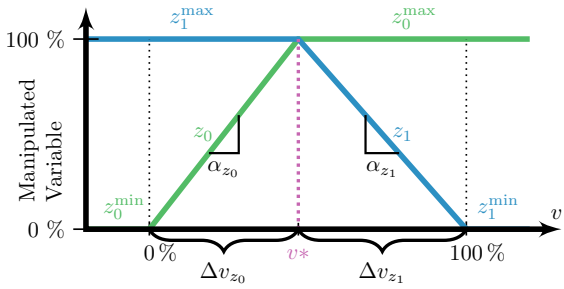

(a) Tank 1

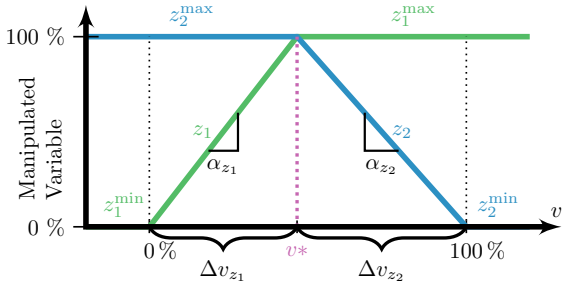

(b) Tank 2

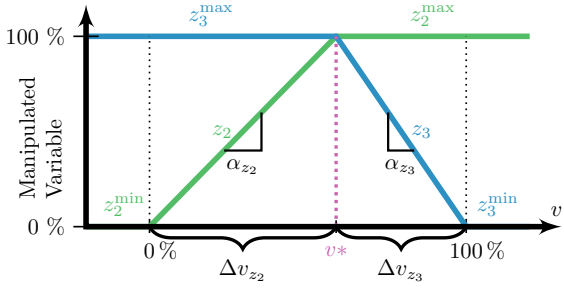

(c) Tank 3

Figure 5.24: Split range blocks for Figure 5.7.

This has no initial effect because z_0 is fixed at $z_0 = 0.3$ due to the bottleneck in the unit. This causes the first delay. Eventually, when z_0 reaches 1 (the max-value in the SR-bock), the SRC switches the MV to z_1, which starts at its max value, $z_1^3 = 1$, which is larger then the nominal $z_1^2 = 0.7$. Thus, the action of SRC now has to decrease the value down to $z_1 = 0.7$ before the min-selector changes the level control direction. This causes the second delay, before finally the action of SRC has some effect on the level h_1. To improve the level control performance for SRC, we may do some more complex fixes such as updating the bias for the internal controller.

5.9.5.1 Bias update for SRC

We propose here a method to avoid the two delays in switching within SRC and achieve tight level control by updating the bias for the internal controller. In Figure 5.25, we make a "jump" in Δv such that the switching happens immediately, without having to wait for the signal v to travel the pattern area. The figure refers to tank 2 in particular, but it is also valid for the other two tanks.

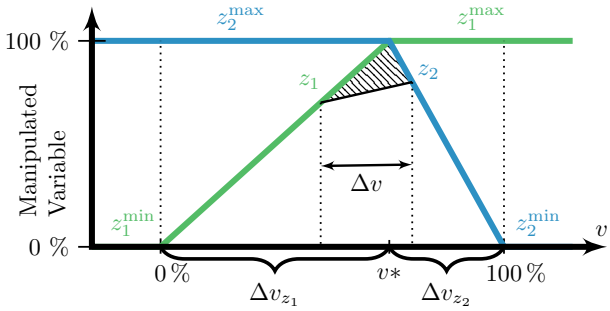

Figure 5.25: Possible bias update for SRC for tank 2 to achieve tight level control. Without the update, the controller would have to integrate over the pattern area which is the cause of the delay in switching.

To compute what the actual value of z_2 should be, we set $F_1 = F_2$, and invert the valve equation (Eq. 5.6) to solve for z_2 with known flowrate F_2

(Eq. 5.8). This is similar to a type of nonlinear feedforward (ratio) control.

$$z_2 = \frac{k_{v1}}{k_{v2}} z_1 \tag{5.8}$$

where k_{v1} and k_{v2} are given in Table 5.2.

Then, we can update the internal PI-controller bias (v_0) by adding to it the value

$$\Delta v = v(z_2) - v(z_1) \tag{5.9}$$

where $v(z_1)$ and $v(z_2)$ are the values of the output (v) of the internal PI-controller in SRC for the two valve positions (z_1 and z_2), for example, determined from Figure 5.25 (or the corresponding equations).

Chapter 6

Supervisory control design for balancing supply and demand in a district heating system with thermal energy storage

This chapter is based on Zotică et al. (2021) and presents a systematic comparison between three alternatives to design the supervisory control layer of a district heating network composed of a waste heat boiler, an electric boiler, a dump, a hot water storage tank, and a set of consumers. The three alternatives are split range control (SRC), controllers with different setpoints, and model predictive control (MPC). We evaluate the closed-loop performance in the face of time-varying supply and demand, and constant electricity prices. All alternatives were found to give similar performance. Controllers with different setpoints is the easiest to implement, while model predictive control is the most difficult.

6.1 Introduction

The storage of thermal energy is an effective solution to the problem of integrating intermittent heat sources such as solar thermal and industrial waste heat into district heating systems (Lund et al., 2014; Miró et al., 2016; Guelpa and Verda, 2019). The most common form of storage currently used in district heating is the accumulation of hot water in tanks due to its low installation cost and high reliability (Hennessy et al., 2019).

The optimal use of energy storage has been studied extensively in the operations research literature (van de Ven et al., 2013; Harsha and Dahleh, 2014; Zhou et al., 2016, 2019). Despite a few problems with special structure, most energy storage problems relevant in applications do not have a closed-form solution and a numerical solution by dynamic programming is impractical. Therefore, we resort instead to suboptimal, yet effective, policies. Economic model predictive control (EMPC) is an example of such policy (Ma et al., 2009; Kumar et al., 2020). An alternative approach is to design a hierarchy of optimization and control layers that work independently on different time scales (Skogestad and Postlethwaite, 2005). This is known as hierarchical control and is the approach we adopt in this paper.

Within the hierarchical control paradigm, MPC has become the technique of choice for designing the supervisory control layer in most of the thermal energy storage systems reported in the literature due to its ability to handle constrained multivariable systems by design (Cole et al., 2012). On the other hand, classical advanced PID-based control structures are widely used in practice (Powell and Edgar, 2012; Oliveira et al., 2016). However, the systematic design and benchmarking of these control structures for thermal energy storage systems have received little attention in the literature.

We consider a district heating system with thermal energy storage. The system is assumed to be already designed and we only consider its operation. We also assume constant electricity prices.

This chapter proposes an alternative decentralized control solution based on PI controllers with different setpoints. The advantage of SRC and controllers with different setpoints is that they handle active manipulated variable (MV) constraint switching without explicitly solving an optimization problem.

The main contribution of this work is a systematic comparison of two decentralized control solutions (SRC and PI controllers with different setpoints) and MPC for designing the supervisory control layer for a district heating system with thermal energy storage.

6.2 Supervisory control layer: Model predictive control as alternative to decentralized switching

MPC is an alternative to MV-MV switching using SRC (see Section 4.2.1) and controllers with different setpoints (see Section 4.2.2).

MPC is a unified systematic procedure for controlling constrained multivariable systems commonly used in industrial applications (Qin and Badgwell, 2003; Mayne, 2014). At each sampling time, it uses the current plant measurement as the initial state to solve a finite-horizon open-loop optimal control problem to determine the optimal control sequence. Then, the first control is applied to the plant and the process is repeated at the next time step (Mayne et al., 2000). It handles constraints and interactive processes by design. However, it requires a detailed process model, which may not be available at the plant start-up.

The closed-loop performance of MPC depends firstly on the accuracy of the dynamic model and secondly on the choice of tuning parameters, e.g., weights in the objective function, prediction and control horizon, input rate constraints or constraints back-off (Lu et al., 2020).

Finding the MPC tuning parameters is done by trial and error, heuristics, or optimization of indicators of the closed-loop performance, e.g., overshoot, integral square error, robustness, etc. The work by Garriga and Soroush

(2010) presents an overview of theoretical and practical guidelines for tuning the controller parameters in an MPC. The work by Santamaría and Gómez (2016) presents a gradient-based tuning algorithm with application to chemical processes. The work by Lu et al. (2020) presents derivative-free tuning algorithms based on Bayesian optimization techniques. In this work, we use trial and error.

6.3 District heating control problem

Figure 6.1 shows the thermal energy storage system analyzed in this work, where the working fluid is hot water. For example, this can be a district heating network supplying hot water to residential households. This system has a direct physical connection between supply and demand, such that hot water can be directly sent to the consumers bypassing the storage tank (flowrate q_{SP}). There are also other distribution networks, for example, in industrial clusters, that exchange energy only through the storage tank (Scholten et al., 2017; Knudsen et al., 2019; Thombre and Krishnamoorthy, 2019).

The operational objective of the network in Figure 6.1 is to manipulate the inputs u to minimize the electric boiler usage ($u_2 = q_{EP}$) (Eq. 6.1a), while balancing the supply and demand (Eq. 6.1b). Furthermore, the storage capacity constraints (Eq. 6.1c) and the model equations (see Section 6.4 for details) must be satisfied.

$$\min_{u} \quad J = \int_0^\infty q_{EP}(t)\, dt \tag{6.1a}$$

$$\text{s.t.} \quad \text{supply} = \text{demand} \tag{6.1b}$$

$$V^{\min} \leq V_h(t) \leq V^{\max} \tag{6.1c}$$

The four inputs (degrees of freedom) in Figure 6.1 are $u = [q_D\, q_{EP}\, q_{ST}\, q_{TP}]$.

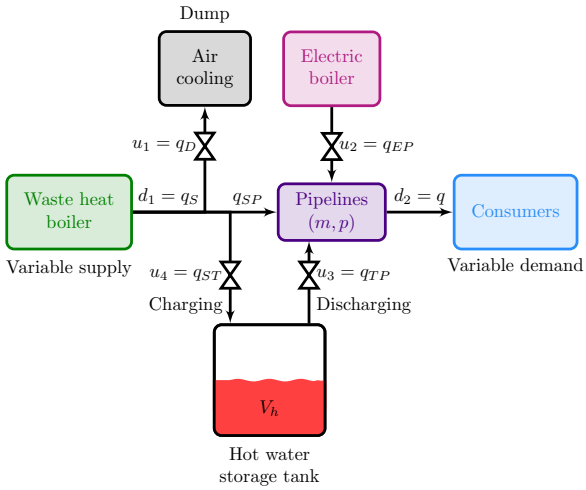

Figure 6.1: Flowsheet of distribution network studied in this work with one waste heat boiler, one electric boiler, one air cooling (dump), and one hot water storage tank supplying hot water through pipelines to consumers.

In the system, heat is mainly supplied by the waste incineration boiler (q_S), which extracts heat by burning waste. This may be viewed as a disturbance to the system along with the consumer demand (q), i.e. $d = [q_S\, q]$. Note that the inputs u correspond to physical valves in Figure 6.1. Later, we will make use of some transformed inputs (MVs) for the purpose of balancing supply and demand. Based on process insight, the four degrees of freedom can be used to balance supply and demand as follows:

1. Excess supply: charge hot water to storage (q_{ST}).
2. Excess supply (when storage is full): dump hot water to air (q_D).
3. Excess demand: discharge hot water from storage (q_{TP}).
4. Excess demand (when storage is empty): use electric boiler (q_{EP}).

The switching between these four operating regions must be taken care

of by the supervisory control layer. Given that electricity prices are assumed constant, this corresponds with the optimal storage policy. That is, this is the optimal solution to Eq. 6.1. If electricity prices were time-varying, it would be optimal to store energy at low prices to be used later when prices are high, but this is beyond the scope of this work.

The main objective of the supervisory control system is to meet the energy demand of the consumers by switching between the four operating regions. To simplify the design of the supervisory control system, we will consider three MVs in this layer, rather than the four physical valves (degrees of freedom) shown in Figure 6.1:

MV1: hot water from waste heat boiler (q_{SP})

MV2: hot water from storage tank (q_{TP})

MV3: hot water from electric boiler (q_{EP}).

The motivation of selecting the three MVs is that they are the three suppliers of hot water to the consumers in an actual district heating system. Here, MV1 is the flow in the direct physical connection from the variable supply to the consumers. Note that MV1 does not correspond to a physical valve, but it is indirectly given by the material balance in Eq. 6.2.

$$\text{MV1} := q_{SP} = q_S - q_{ST} - q_D \tag{6.2}$$

Here, the supply q_S is a disturbance, whereas the charge q_{ST} and dump q_D are physical valves. For cases where we want q_{SP} to be smaller than q_S (that is, we have excess supply), we first charge the tank (q_{ST}) and then, when it is full, we start dumping (q_D). We will assume that this logic is taken care of by a separate block "charging policy logic", which will be part of the regulatory control system (see Section 6.5.1). As mentioned, the reason for doing this is to simplify the design of the supervisory control system.

In summary, the three MVs are related as follows to the physical inputs (u):

$$\text{MV1} := d_1 - u_1 - u_4 \tag{6.3a}$$

$$\text{MV2} := u_3 \tag{6.3b}$$

$$\text{MV3} := u_2 \tag{6.3c}$$

Note that the maximum values for MV1 = q_{SP} and MV2 = q_{TP} are time-varying. That is, q_{SP} is limited by the hot water from the waste-heat boiler ($q_{SP} \leq q_S$), and $q_{TP} = 0$ when the storage tank is empty.

The temperature of the hot water produced in the waste heat and electric boiler is kept constant by water injection, not shown in Figure 6.1. This is a common practice in district heating networks. There are also other flows not shown in Figure 6.1, for example, the water supply to the electric boiler and the water return from the air cooling. Actually, in Figure 6.1, it may be better to view the varying water flows $q\,[\text{m}^3/\text{h}]$ as being energy flows $Q\,[\text{J}/\text{h}]$. Because of the assumption of constant temperature, q and Q are directly proportional: $Q = kq$.

In practice, measurement of the heat demand is not available. Therefore, and we choose to control the network pressure (p), which is proportional to the mass m (see Figure 6.1) in the pipeline. This is a dynamic variable that couples the supply and demand. Therefore, it is an indirect and reliable measurement of the supply-demand balance in a water distribution network.

In summary, Table 6.1 shows the three MVs, one CV and the two main disturbances (DVs) for the supervisory control considered in this work.

Table 6.1: MVs, CVs, and DVs for supervisory control.

Manipulated variables	Controlled variables	Disturbances
MV1: Hot water from waste heat boiler (q_{SP})	CV1: Network pressure (p)	DV1: Hot water from waste heat boiler (q_S)
MV2: Hot water from storage tank (q_{TP})		DV2: Hot water demand (q)
MV3: Hot water from electric boiler (q_{EP})		

6.4 Process model

The change of mass (m) in the pipelines system is given by the mass balance in the network, Eq. 6.4.

$$\frac{dm}{dt} = \rho(q_{SP} + q_{TP} + q_{EP} - q) \tag{6.4}$$

where, ρ [kg/m^3] is the water density, assumed constant.

To model the changes in the network (pipeline) pressure (p), we consider that it is proportional to the change of network mass (m), Eq 6.5.

$$p = p_0 \left(1 + \frac{m - m_0}{\epsilon m_0}\right) \tag{6.5}$$

where, m [kg] is the network water mass, m_0 [kg] is the water mass at the reference flow, ϵ is the constant compressibility coefficient and p_0 [bar] is the pressure at the reference flow. Hence $m = \rho V$, the compressibility factor ϵ takes into account the increase in liquid density and more importantly the increase in pipelines volume by increasing the pressure.

Substituting Eq. 6.5 into Eq. 6.4 yields the mass balance expressed in

terms of the network pressure, Eq. 6.6.

$$\frac{dp}{dt} = \frac{p_0 \rho}{m_0 \epsilon}(q_{SP} + q_{TP} + q_{EP} - q) \tag{6.6}$$

To model the storage tank inventory, we neglect changes in density (ρ) and assume no heat losses. The dynamic mass balance for the storage tank is given by Eq. 6.7

$$\frac{dV_h}{dt} = q_{ST} - q_{TP} \tag{6.7}$$

where, V_h [m^3] is the volume of the hot water, which must be within the limits $V^{\min} = 0$ and $V^{\max}$.

With constant inlet temperature (T_S), constant heat capacity (c_P) and perfect mixing, the tank temperature (T_h) is constant and equal to the inlet temperature ($T_S = T_h$).

6.4.1 Model parameters

Table 6.2 shows the model parameters.

Table 6.2: Model parameters

Definition	Variable	Value	Unit
Hot water storage tank volume	$V^{\max}$	5000	m^3
Maximum flowrate	$q^{\max}$	1000	m^3/h
Network reference mass	m_0	15000	kg
Network reference pressure	p_0	5	bar
Compressibility coefficient	ϵ	0.1	-
Water density	ρ	1000	kg/m^3

6.4.2 Dynamic behaviour

The dynamic behaviour of the model is analyzed from step responses in the disturbances and inputs. MV3 = q_{EP} has the same effect on p as MV1 and

MV2 and is not shown. Figure 6.2 shows the response for a step increase in MV1 = $\Delta q_{SP} = 250\,\mathrm{m}^3/\mathrm{h}$ given by an increase in the available hot water supply (DV1 = $\Delta q_S = 250\,\mathrm{m}^3/\mathrm{h}$). Figure 6.2c shows the network pressure response which is an integrating process as given in Eq. 6.5 with slope $k' = 3.33\,\mathrm{bar}/\mathrm{m}^3$. The hot water volume (Figure 6.2b) is constant. Note that the time scale is in seconds because the pressure dynamics are fast.

Figure 6.3 shows the response to an increase in the discharge MV2 = $\Delta q_{TP} = 250\mathrm{m}^3/\mathrm{h}$. The hot water volume (Figure 6.5b) is an integrating process with initial slope $k' = -1$.

Figure 6.4 shows the response for a step increase in the available hot water supply (DV1 = $\Delta q_S = 250\,\mathrm{m}^3/\mathrm{h}$) with MV1 = q_{SP} constant. The "charging policy logic" first sends the excess hot water to the storage tank, and once the tank is full, it is dumped (Figure 6.4a). The time scale is in hours because the storage tank dynamics are slow. Figure 6.4b shows the hot water volume. The network pressure (Figure 6.4c) is constant because MV1 =q_{SP} is constant.

Finally, Figure 6.5 shows the response to an increase in the demand DV2 = $\Delta q = 250\,\mathrm{m}^3/\mathrm{h}$ with the MVs constant.

6.5 Control system design

We want to implement a control system that optimally switches the operation between the four options described in Section 6.3.

6.5.1 Regulatory control: charging policy logic

As mentioned before, to simplify the design of the control system we include the charging policy logic in the regulatory control system. The logic is:

1. The storage tank is charged with excess hot water (q_{ST}) when the hot

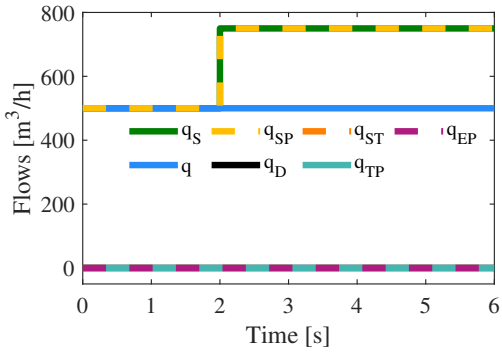

(a) Hot water flowrates

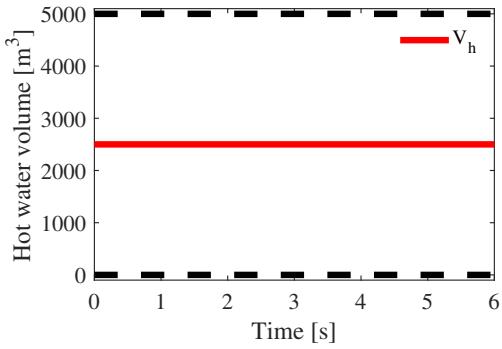

(b) Tank storage

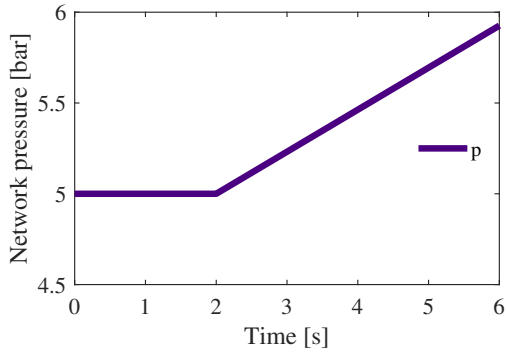

(c) Network pressure

Figure 6.2: Open-loop step responses for an increase in MV1 = $\Delta q_{SP} = 250\,\mathrm{m}^3/\mathrm{h}$. The excess heat is sent to the consumers.

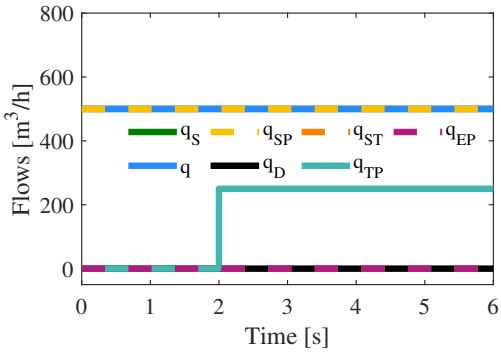

(a) Hot water flowrates

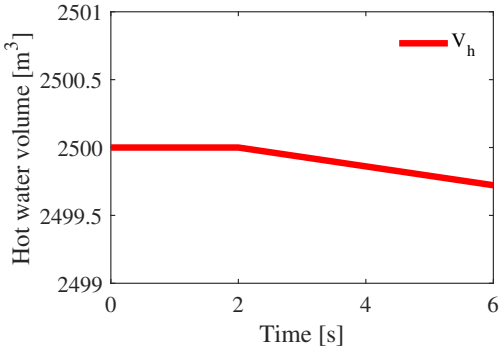

(b) Tank storage

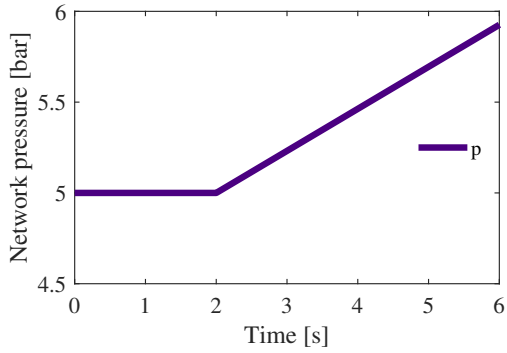

(c) Network pressure

Figure 6.3: Open-loop step responses for an increase in $MV2 = \Delta q_{TP} = 250\,\mathrm{m}^3/\mathrm{h}$.

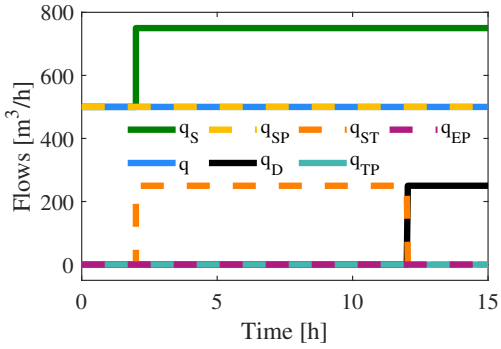

(a) Hot water flowrates

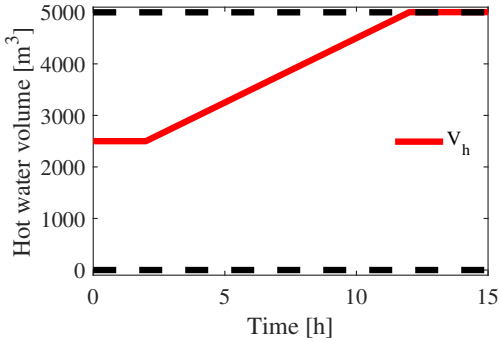

(b) Tank storage

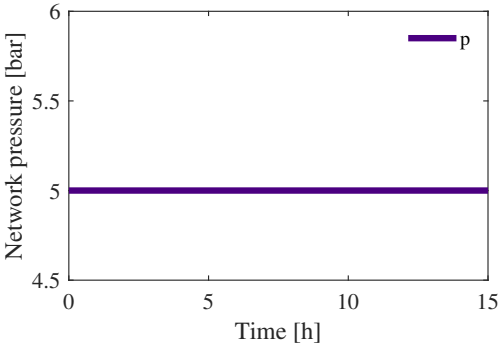

(c) Network pressure

Figure 6.4: Open-loop step responses for an increase in waste heat supply DV1 $= \Delta q_S = 250\,\mathrm{m}^3/\mathrm{h}$ with MV1 $= q_{SP}$ constant and with charging logic. First the excess hot water supply is charged to the tank (q_{ST}) and then at $t = 12\,\mathrm{h}$ it is sent to air dump (q_D).

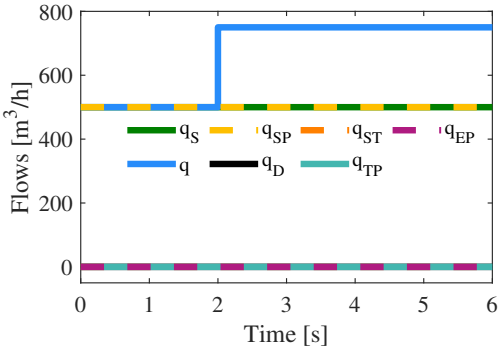

(a) Hot water flowrates

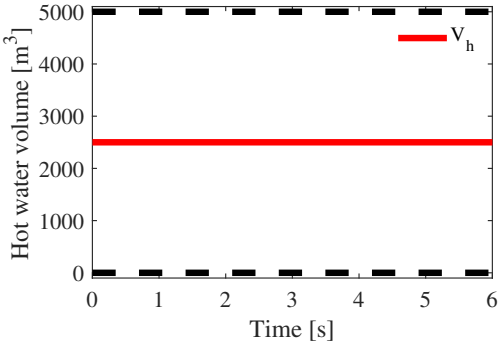

(b) Tank storage

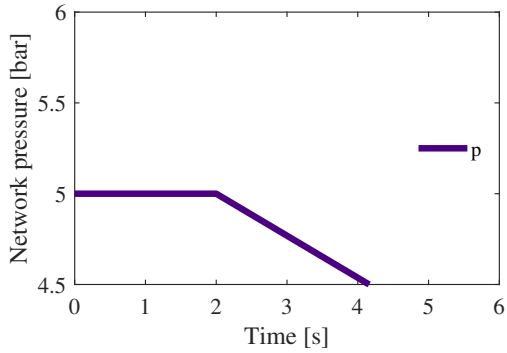

(c) Network pressure

Figure 6.5: Open-loop step responses for an increase in $DV2 = \Delta q = 250\,\mathrm{m}^3/\mathrm{h}$.

water storage is below maximum capacity, Eq. 6.8.

$$q_{ST}\,(\%) = \begin{cases} 100\,\% - q_{SP}\,(\%) & \text{if } V_h < V^{\max} \\ 0 & \text{if } V_h = V^{\max} \end{cases} \tag{6.8}$$

2. On the other hand, when the storage tank is full, excess heat is dumped, Eq. 6.9.

$$q_{D}\,(\%) = \begin{cases} 0 & \text{if } V_h < V^{\max} \\ 100\,\% - q_{SP}\,(\%) & \text{if } V_h = V^{\max} \end{cases} \tag{6.9}$$

6.5.2 Alternative 1 for supervisory control: split range control

We first consider SRC (see Section 4.2.1 for definition) to keep the network pressure at the setpoint by using one MV at a time, starting with the cheapest, and switching to the more expensive as demand increases or the availability of the cheap MV decreases. In our case, we first want to use the available hot water from the waste heat boiler (MV1 = q_{SP}), followed by the hot water stored in the tank (MV2 = q_{TP}), and lastly the electric boiler (MV3 = q_{EP}). Figure 6.6 shows the SRC implementation.

6.5.2.1 Tuning parameters for SRC

We follow the procedure of Reyes-Lúa et al. (2019). We define the normal range for the internal signal v to be from 0 % to 100 %, and we scale the MVs from 0 % to 100 %, see Figure 6.7. The tuning parameters for SRC are the PI-tunings for the common controller C and the slopes α_i in the split range block in Figure 6.7. The slopes α_i are used to allows for different controller gains for each MV, however, from the network mass balance (Eq. 6.4), all MVs have the same effect on the CV. Therefore, the three slopes in the split range block are equal, and we get $\alpha_{SP} = \alpha_{TP} = \alpha_{EP} = 3$. Figure 6.7 shows

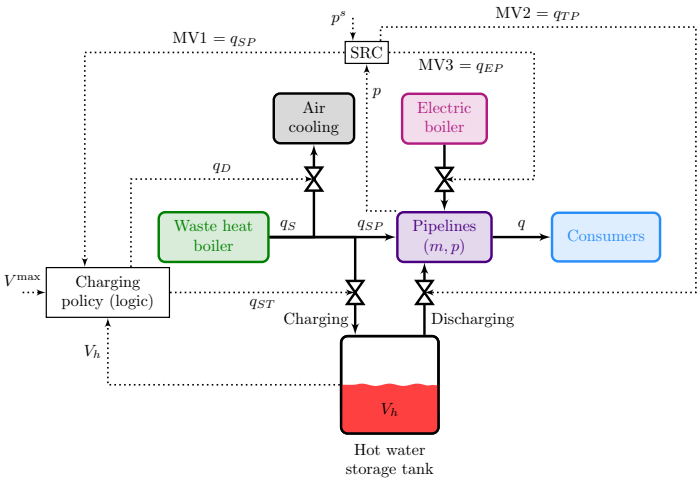

Figure 6.6: SRC structure for balancing supply and demand by controlling the network pressure.

the split range block. The controller parameters are obtained by applying the SIMC tuning rules (Skogestad, 2003) for an integrating process (i.e. the network pressure balance Eq. 6.6). We select the closed-loop time constant $\tau_C = 10\,\text{s}$, resulting in the proportional gain for each MV is $K_{C,i} = 54$ and the integral time $\tau_I = 8\,\text{s}$ (see Section 6.7.4). We find the common controller gain $K_C = K_{C,i} = 54/\alpha_i = 18$. To handle the time-variable availability of MV1 and MV2 we update the PI-controller bias (u_0), such that when one MV is no longer available, the new MV starts from the value of the former. Alternatively, this could have been handled by using a "discharging policy logic" block and only four MVs for the SRC (see Section 6.7.1).

Note that we have assumed that we directly manipulate the flows q_i, that is, we have assumed that all valves have flow controllers. Without flow controllers, we would have had to use different slopes α_i in the split range block (Figure 6.7).

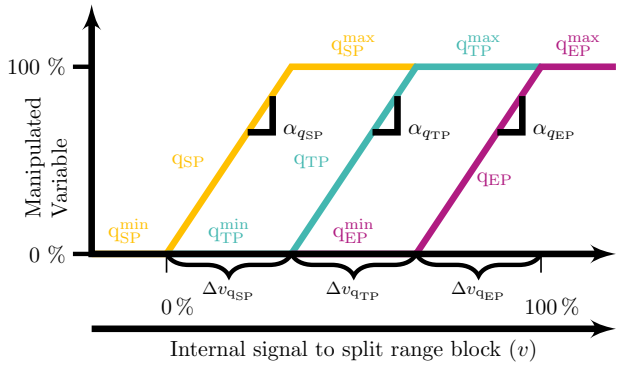

Figure 6.7: Split range block for Figure 6.6.

6.5.3 Alternative 2 for supervisory control: controllers with different setpoints

Figure 6.8 shows the control structure with three different PI-controllers with different setpoints for controlling the network pressure (p) that uses as degrees of freedom MV1 (q_{SP}), MV2 (q_{TP}) and MV3 (q_{EP}). Similar to SRC, we order the use of MVs based on economics, and we use the cheapest MV first. Therefore, we order the three setpoints $SP1 > SP2 > SP3$ ($p^s_{SP} > p^s_{TP} > p^s_{EB}$) such that only one MV is actively used at any given time. See Section 4.2.2

6.5.3.1 Setpoint selection

We select the setpoints order based on physical insight. The process gain from the MVs to the CV is positive (Figure 6.2). Therefore the controller gain is positive, and a negative controller error ($p^s - p$) gives a negative controller output (see Eq. 6.12). Setting the controller bias $u = 0$, and considering that the minimum physical limit for the MV is 0, the MV only starts to open when the controller error becomes positive. Specifically, when $p \geq p^s_{TP}$, MV1 is active, and MV2 and MV3 are fully closed. Once MV1 reaches its maximum

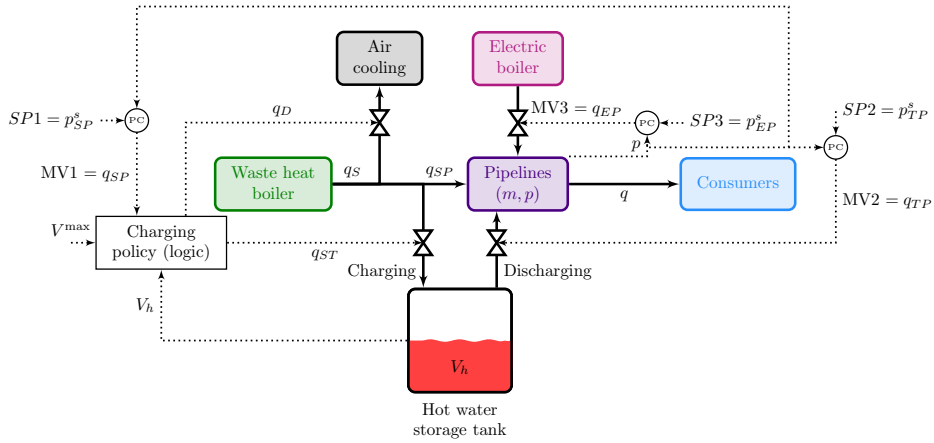

Figure 6.8: Three controllers with different setpoints for balancing supply and demand by controlling the network pressure. The order of the setpoints is: $SP1 > SP2 > SP3$ ($p^s_{SP} > p^s_{TP} > p^s_{EB}$).

limit, supply is smaller than demand, and the network pressure drops. Once the pressure reaches a lower threshold, $p^s_{EP} < p < p^s_{TP}$, MV2 becomes the active MV, while MV3 is fully closed. Finally, when the supply is smaller than demand, MV2 becomes saturated at its maximum and the pressure drops. Once it reaches an even lower threshold $p < p^s_{EP}$, MV3 becomes the active MV. This control structure handles the intermittent availability of MV1 and MV2 by design as long as antiwindup with tracking of the plant input is implemented.

6.5.3.2 Tuning parameters for controllers with different setpoints

As mentioned, all MVs have the same effect on the CV and we use equal controller tuning parameters: $K_C = 54$, $\tau_I = 8\,\text{s}$. The setpoints are: $SP1 = p^s_{SP} = 5\,\text{bar}$, $SP2 = p^s_{TP} = p^s_{SP} - \Delta p^s_{TP} = 4.5\,\text{bar}$, $SP3 = p^s_{EP} = p^s_{TP} - \Delta p^s_{EP} = 4\,\text{bar}$. We implement antiwind-up with the back-calculation method (Åström and Hägglund, 2006) with the tracking time constant set to half of

the integral time.

6.5.4 Alternative 3 for supervisory control: model predictive control

We design the MPC to handle also the charging of the storage tank. Therefore it has the role of the supervisory and regulatory layer previously described. We include q_D as the fourth MV, while q_{ST} is calculated from the mass balance (Eq. 6.2).

The system we are analyzing is somewhat atypical because it has more MVs than CVs. Therefore, the tuning of MPC is not straightforward, and we must give careful consideration in setting up the objective function to prioritize the use of MVs. We achieve this by selecting the weights (ω) in the objective function (Reyes-Lúa et al., 2018). We formulate the optimal control problem with the objective function given in Eq. 6.10a. We want to maximize discharging the tank (q_{ST}), minimizing dump (q_D), minimize using the electric boiler and keep the network pressure (p) at its setpoint (p^s). As mentioned before, the MPC controls the network pressure as an indirect measure of the hot water demand. However, the MPC uses the full model (Section 6.4), and it requires information about the demand hot water. We solve the optimization problem subject to model Eqs. 6.10b, 6.10d and 6.10c, and operation constraints (Eqs. 6.10e, 6.10f, 6.10g and 6.10h).

$$\min \sum_{k=1}^{N} \omega_{TP}\, q_{TP,k}^2 + \omega_D\, q_{D,k}^2 + \omega_{EP}\, q_{EP,k}^2 + \omega_p\, (p_k - p^s)^2 \tag{6.10a}$$

$$\text{s.t.} \quad p_k = g(q_{SP,k}, q_{TP,k}, q_{EP,k}, q_k) \tag{6.10b}$$

$$V_{h,k} = h(q_{ST,k}, q_{TP,k}) \tag{6.10c}$$

$$q_{ST,k} = q_{S,k} - q_{D,k} - q_{SP,k} \tag{6.10d}$$

$$0 \leq V_{h,k} \leq V^{\max} \tag{6.10e}$$

$$p^{\min} \leq p_k \leq p^{\max} \tag{6.10f}$$

$$q_{SP,k} \leq q_{S,k} \tag{6.10g}$$

$$0 \leq q_{i,k} \leq q_i^{\max} \quad \forall i \in \{\mathrm{D}, \mathrm{TP}, \mathrm{EP}\} \tag{6.10h}$$

Here, k is the current iteration, N is the number of control intervals, ω_i are the weights in the optimization problem, and Eqs. 6.10b and 6.10c are discretized versions of the mass balances Eqs. 6.6 and 6.7, respectively.

We formulate the MPC problem using CasADi (Andersson, 2013), and we use IPOPT to solve the NLP (Wächter and Biegler, 2006). The tuning parameters were found by trial and error. We use 10 control intervals, 10 min prediction horizon and 1 min sampling time. In practice, the sampling time will need to be smaller because of the fast pressure dynamics. The weights in the optimization function were also found by trial and error and are $\omega_{TP} = 10^{-6}$, $\omega_D = 10^{-5}$, $\omega_{EP} = 10^{-3}$ and $\omega_p = 10^4$.

6.6 Simulation case study

We compare the performance of the three control system alternatives to switch between the four operating options (see Section 6.3) using the model described in Section 6.4.

At the initial state of the system, the tank is half full ($V_h = 2500\,\mathrm{m}^3$),

and the hot water supply from the waste heat boiler is equal to the demand, i.e. $q_S = q = 500\,\mathrm{m^3h}$.

6.6.1 Simulations step changes

We perform the following series of step changes (see also Figure 6.9):

Step 1 at time $t = 1\,\mathrm{h}$: The hot water supply from the waste heat boiler (DV1) increases from $q_S = 500\,\mathrm{m^3/h}$ to $q_S = 1000\,\mathrm{m^3/h}$.

Step 2 at time $t = 12\,\mathrm{h}$: The hot water demand (DV2) increases from $q = 500\,\mathrm{m^3/h}$ to $q = 1000\,\mathrm{m^3/h}$.

Step 3 at time $t = 15\,\mathrm{h}$: The hot water supply from the waste heat boiler (DV1) decreases from $q_S = 1000\,\mathrm{m^3/h}$ to $q_S = 500\,\mathrm{m^3/h}$.

Step 4 at time $t = 30\,\mathrm{h}$: The hot water demand (DV2) decrease from $q = 1000\,\mathrm{m^3/h}$ to $q = 750\,\mathrm{m^3/h}$.

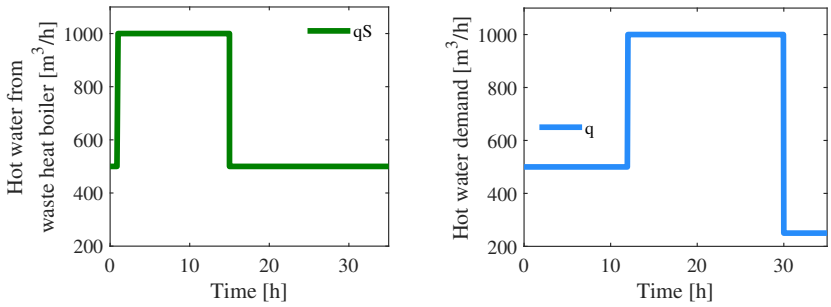

(a) Supply (q_S) **(b)** Demand (q)

Figure 6.9: Disturbances in supply and demand profiles.

Figure 6.10 compares the closed-loop responses for split range control (SRC-left), three PI-controllers with different setpoints (3C-middle) and model predictive control (MPC-right). Figures 6.10a, 6.10b and 6.10c show the response for the MVs, Figures 6.10d, 6.10e and 6.10f show the response

for the tank storage, Figures 6.10g, 6.10h and 6.10i show the response for the network pressure.

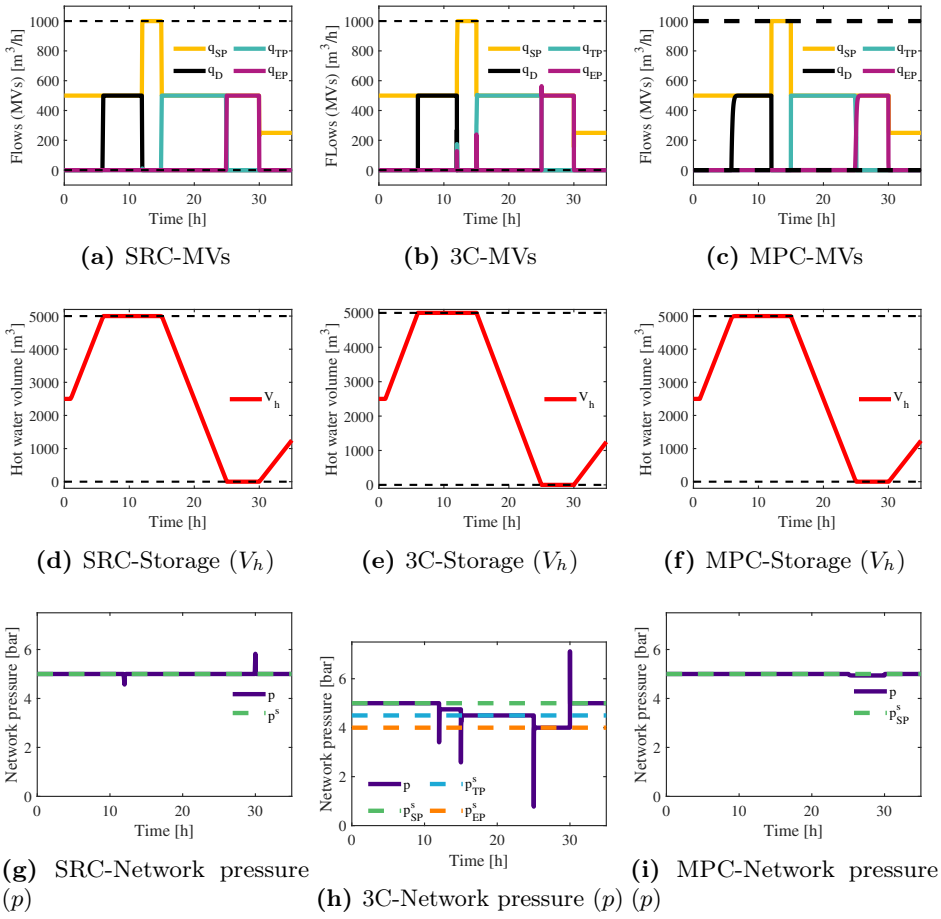

(a) SRC-MVs **(b)** 3C-MVs **(c)** MPC-MVs

(d) SRC-Storage (V_h) **(e)** 3C-Storage (V_h) **(f)** MPC-Storage (V_h)

(g) SRC-Network pressure (p) **(h)** 3C-Network pressure (p) **(i)** MPC-Network pressure (p)

Figure 6.10: Closed-loop simulation results for SRC (left), three PI-controllers with different setpoints (middle), and MPC (right).

6.6.2 Results analysis

The closed-loop simulation results in Figure 6.10 demonstrate that all three alternative control structures can successfully implement optimal operation

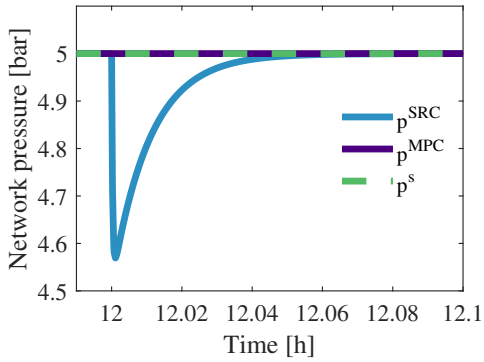

Figure 6.11: Comparison of network pressure for SRC and MPC (short time scale).

for this system. Because the simulation time scale is in hours, it is not easy to see some of the differences between the three alternatives for MV3 = q_{EP} and for the network pressure (p). SRC and MPC perform similarly. In the MPC formulation, the step changes in disturbances happen at the sampling time and there is feedforward action from disturbances q_S and q at each sampling time. Therefore, there is less variation in the network pressure p in Figure 6.10i compared to Figure 6.10g. This is shown more clearly at time $t = 12$ h in Figure 6.11.

The pressure response for controllers with different setpoints (Figure 6.10h) is as expected different from SRC (Figure 6.10g) and MPC (Figure 6.10i). However, the response for the tank storage (Figure 6.10e) and MVs (Figure 6.10b) is not significantly different because 1) the pressure only has a dynamic effect on the flows, that is, the flow values are independent of the pressure setpoint and 2) pressure dynamics are fast compared to the storage dynamics.

In Figure 6.10a, SRC changes q_{TP} instantaneously because we update the controller bias. However, for controllers with different setpoints (3C), there is a small delay until the new MV takes over, because the pressure (p) has to drop below the setpoint (p_i^s) given to the controller that regulates

the respective MV. The MV overshoots, leading to two MVs being active simultaneously for a short period (Figure 6.10b and Table 6.3).

In terms of dynamic input usage, table 6.3 compares the total input variation (i.e. $TV = \sum_1^\infty |u|$) for SRC, controllers with different setpoints (3C) and MPC. Among the three, the alternative of controllers with different setpoints shows the highest input usage. The total variation for q_{EP} is equal for SRC and MPC, meaning that the electricity cost is equal. Compared to SRC, MPC uses slightly less q_{SP} compensated by using slightly more q_{TP} and marginally dumping more heat q_D. This means that in the MPC implementation, the tank is simultaneously charged and discharged. However, the short-term peaks in q_{EP} for controllers with different setpoint (3C) which do not matter much for the integrated cost, see Eq.6.1.

Table 6.3: Comparison of input usage: total input variation

MV	SRC	3C	MPC
q_{SP}	1290	1444	1281
q_D	1000	1539	1000.1
q_{TP}	1022	1359	1027
q_{EP}	1000	1897	1000

6.7 Discussion

6.7.1 General control structure for balancing supply and demand in a district heating network with thermal energy storage

We explore how does this example fit in the framework of the general system for balancing supply and demand presented in Section 4.

The system in Figure 6.1 has four available MVs, though only three MVs were selected because these are the ones used in a practical application. At

the time of implementation, the simplest options seemed to be choosing these three MVs to be the controller outputs in the three compared control structures, SRC (Figure 4.2), controllers with different setpoint (Figure 4.2) and MPC.

Upon further consideration of this example, a much simpler alternative was found to be using only two MVs, one variable supply (MV_s) and one variable demand (MV_d), as shown in Figure 4.1. Thus for inventory control, we may use SRC or controllers with different setpoints.

Figure 6.12 shows the split range block At the split value ($v*$), $d_1 = d_2$ and the variable demand balances the variable supply.

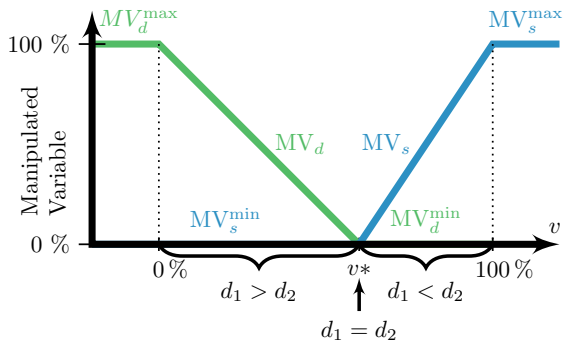

Figure 6.12: Split range block for general control structure for balancing supply and demand. At $v*$, the variable supply (d_1) balances the variable demand (d_2) and $\text{MV}_s = \text{MV}_d = 0$.

Alternatively, we may use two controllers for MV_s and MV_d with two different setpoints for the inventory m.

Next, we need to decide on how to implement MV_s and MV_d using the

physical inputs (u_1, u_2, u_3 and u_4, in our case). From Figure 4.1 we have

$$\begin{aligned} \mathrm{MV}_s &= q_{\text{from storage}} + q_{\text{electric boiler}} && \text{(6.11a)} \\ &= u_2 + u_3 \\ \mathrm{MV}_d &= q_{\text{to storage}} + q_{\text{dump}} && \text{(6.11b)} \\ &= u_1 + u_4 \end{aligned}$$

Since the objective is to minimize the use of electric boiler (and minimize dump to store when possible), it becomes clear what we should do. If MV_s is active, we first use hot water from storage (u_3) until the storage tank is empty, and then use the more expensive electric boiler (u_2). If MV_d is active, we first send excess hot water to storage (u_4) and when the storage tank is full, send it to dump (u_1). This corresponds to the four operation regions in Section 6.3. In practice, this may be implemented using a "charging policy" logic for MV_s and a "discharging policy" for MV_d.

6.7.2 Ease of implementation

In terms of ease of implementation, the use of three controllers is the simplest. It allows for using three independently tuned controllers and it avoids the logic needed in SRC. The logic can be avoided because the switching is done based on the output ($\mathrm{CV} = p$) and not the limit on the MV-value. However, it has two disadvantages: 1) somewhat worse dynamic performance (see Table 6.3) and 2) varying setpoint. Because each controller can be tuned independently, we do not need to compromise on the integral time as in SRC. This was not relevant for the process studied because the MVs have the same effect on the CV (see the model in Section 6.4), but it can become important for other systems with different dynamics, for example with different valve sizes.

The MPC controller is by far the most difficult to implement. In addition

to requiring a dynamic model, it was also difficult to adjust the tuning parameters (e.g. weights in the objective function, prediction horizon and sampling time) to obtain the desired performance. We selected a short prediction horizon because with larger values, hot water was dumped before the tank was at maximum storage capacity. Formulating the objective function (Eq. 6.10a) was also done by trial and error. In the end, the weights on q_{TP} and q_D were added to give information to the MPC about which flowrates to prioritize. Without these, the MPC would use two MVs simultaneously. For example, with no excess heat, it would discharge the storage tank instead of using hot water from the waste heat boiler, and dump the remaining hot water. This was because the MPC does not have information about future demand in its prediction, and it is not aware that it should charge the storage tank. One could also add a penalty for not charging the storage tank in the objective function. However, as with any multi-objective problem, there will be a compromise and the tank will not be charged to maximum capacity.

6.7.3 Setpoint difference for three controllers

We select the setpoints for the three controllers in Section 6.5.3.2 by trial and error. This choice is a trade-off. A smaller setpoint difference may result in having more than one MV active at a given time, while a larger setpoint difference results in a larger delay until the next MV activates.

6.7.4 PI controller tuning

The PI-controller is given in Eq. 6.12.

$$u = u_0 + K_C(y^s - y) + \frac{K_C}{\tau_I}\int_0^t (y^s - y)dt \tag{6.12}$$

where K_C is the proportional gain, τ_I is the integral time constant, derived from applying the SIMC tuning rules (Eq. 6.13) (Skogestad, 2003).

$$K_C = \frac{1}{k'} \frac{1}{\tau_C + \theta} \tag{6.13a}$$

$$\tau_I = \min(\tau, 4(\tau_C + \theta)) \tag{6.13b}$$

where k' is the initial slope of the step response, θ is the time delay, τ is the time constant, and τ_C is the desired closed-loop time constant. The PI-controllers in this paper are for integrating process, when $\tau \to \infty$.

6.8 Conclusion

The use of inventory (pressure) control is an effective way of balancing supply and demand for the district heating system. For the case of constant electricity prices, optimal operation for the system studied is easy to identify based on physical insight (see Section 6.3). In this work, we compare three alternative control implementations (split range control, controllers with different setpoints, and model predictive control) to handle MV-MV switches. The closed-loop simulation results in Figure 6.10 show that all control structure successfully switch between the four operating options to balance supply and demand. However, MPC requires careful tuning to obtain the desired performance, making it more difficult to implement than the decentralized solutions.

Part IV

Conclusions and future work

Chapter 7

Conclusions and future work

This chapter summarizes the content of this thesis and presents the key findings and suggestions for future work. Part I presents a plantwide control perspective on optimal operation and control of heat-to-power cycles. It consists of a steady-state and a dynamic analysis for a steam cycle with one pressure level, a drum boiler and producing power only. The steady-state analysis concerns systematically identifying the operational objective, available degrees of freedom, process and environmental constraints, main disturbances and the location of the throughput manipulator. A heat-to-power cycle has two main operational objectives: 1. to produce energy as electric power, steam or both, and 2. to process a given amount of by-product, e.g., waste gases from an upstream gas turbine or biomass incineration. After stabilizing the process and controlling the active constraints, there are two degrees of freedom left, the fuel (MV1) and the steam turbine valve (MV2). The second has a small steady state effect on the power output corresponding to throttling losses. The dynamic analysis concerns implementing the operating strategies resulting from the steady-state analysis. The control objectives are separated on a time scale. On a short-time scale, the control system is responsible for grid frequency regulation, stabilizing the plant

and rejecting local disturbances. On a long time scale, it achieves optimal operation. The dynamic analysis starts with understanding current control strategies used in industrial settings, namely turbine driven (Figure 2.7), boiler driven (Figure 2.6) and floating pressure (Figure 2.5). Further, it proposes two parallel control structures that use both the fuel (MV1) and steam valve (MV2) to control the power while the steam pressure is floating, i.e., it follows the heat input. The two control structures are valve position control (VPC, Figure 2.10) and using one P and one PI controllers with the same power setpoint (Figure 2.11). Note that in this case, both P and PI controllers are active simultaneously, unlike to using two PI controllers with different setpoints when only one PI-controllers is active. This setup makes use of the fast dynamic response from the steam valve to the power output, in addition to minimizing the steady-state throttling losses by keeping the steam valve close to maximum opening (e.g., 90 %).

In summary, the results in Figure 2.12 show that turbine drive is fastest to respond to a power setpoint change, while floating pressure is the slowest at the expense of higher throttling losses. These results are in agreement with the pair-close rule.

The analysis done in this work can be extended to other types of heat-to-power cycles. These included steam cycles with more than one pressure level, once-through boilers, cycles producing both electric power and heat, cycles recovering heat from an upstream process, or using other working fluids such as supercritical CO_2.

Part II presents a systematic theory for deriving and implementing transformed inputs that give linearization, decoupling and feedforward disturbance rejection. Control structures using model-based calculation blocks are often found in industrial settings. Typical examples for the chemical industry are ratio, decoupling or feedforward elements, while a supporting example related to steam cycles is introduced in Section 3.1. However, their development is case-specific and an unifying theory is missing in the control literature. In

this work, the transformed input is formally defined as $v = g(u, w, y, d)$, and can be derived from either a static model ($y = f_0(u, d)$) or a dynamic model ($\frac{dy}{dt} = f(u, y, w, d)$). For the static case, the ideal transformed input is the right-hand side of the model, $v_0 = f_0$, which substituted in the model gives $y = v_0$ which is linear, decoupled and independent of the disturbances. For the dynamic case, we also use the right-hand side of the model equation, and we introduce two tuning parameters A and B to define the transformed input v_A in Eq. 3.20 (see Sections 3.4.2.2-3.4.2.1 for how to select A and B). The idea is to obtain a first-order transformed system of the form $\frac{dy}{dt} = Ay + Bv_A$, which is also linear, decoupled and with no effect from disturbances.

There are two options for systems with relative order greater than 1. First, we may use measurements of additional internal states w to replace their respective dynamic model equations (see Section 3.4.3). Second, we may introduce a chain of transformations (see Section 3.4.5). The first option is easier to implement, and is recommended. However, there is a potential problem due to internal instability of these "hidden internal dynamics". First, using the measurement of w in the transformation may slow-down or speed-up the dynamics of the original system. Second, it may result in internal instability if the indirect (dynamic) effect of u on v through w is large compared to the direct (static) effect of u on v (see example in Section 3.6).

To implement transformed inputs, we need to generate the physical input u from a given value of $v = g(u, w, y, d)$. We may use the model-based inverse in Figure 3.4a, or the feedback-based inverse with an inner controller for v or w shown in Figure 3.4b, or a combination of the two shown in Figure 3.4c. The cascade implementation is recommended when we make use of the w measurement, or when there is no analytical solution to $u = g^{-1}(v, w, y, d)$. In some cases, the implementation of transformed input may be simplified by introducing transformed outputs $z = h(y, w, d)$ because the model is easier to express in terms of z than y. This was used in the heat exchanger example in Section 3.9.

The outer controller C is needed to correct for model and measurements errors and to reject unmeasured or unmodelled disturbances thus to achieve offset-free control at steady state. For multivariable systems, single-loop PID-controllers are usually sufficient because the response from v to y is linear and decoupled, at least in the ideal case.

Several simulation examples are presented throughout Sections 3.7-3.10. The simple mixing example in Section 3.7 illustrates how to combine the transformed inputs derived from static and dynamic model equations. The benefit of using the dynamic transformed input v_A rather than the static transformed input v_0 is mainly that we get a linear transformed system for designing the outer controller C. This benefit is not seen in the simulations in Figure 3.11 because we have set the outer control to $C = 0$. The same example is used to illustrate the effect of input saturations (Section 3.11.1) and unmeasured disturbances (Section 3.11.2). The feedback-based implementation is more robust to input saturations because we can keep track of the plant input, and we only loose control of some of the controlled variables (CVs), at least for multivariable systems. We select the pairing $u - v$ according to the input saturation rule (Reyes-Lúa and Skogestad, 2020), i.e. pair the input that is most likely to saturate with the CV that we can give-up controlling. Both Section 3.8 and Section 3.9 present heat exchangers examples. The former is a simple process with no phase change. The latter is a complex once-through boiler with phase change from water to superheated steam. The control objective for both is to control the process side outlet temperature. The examples show that processes with complex dynamics may benefit from simple input transformations derived from simple static models to improve the disturbance rejection response. Finally, the steam network example in Section 3.10 illustrates using w as measured variables to substitute part of the model dynamics for higher order systems. In this particular case and similarly to the heat exchanger example in Section 3.8, the response was slowed down by introducing the w variable measurement.

For general cases, including cases with more complex dynamics or constraints, there are other control approaches that may be more suitable. One approach is nonlinear model predictive control which allows for more general dynamic models and control objectives, including constraints and the trade-off between input usage and output performance. The main advantage in using transformed inputs is simplicity, ease of understanding and that they can be implemented into the basic control layer.

In Part III, the focus is on designing decentralized supervisory control systems for handling constraints on manipulated variables (MVs) used for inventory control to balance supply and demand (Figure 4.1). Two systems are analyzed. In the first case, i.e, maintaining production for units in series in Chapter 5, there are no additional MVs left and we have to give-up controlling a second and less important CV by using a selector for CV-CV switching in addition to MV-MV switching. In the second case, i.e., district heating network with thermal energy storage, in Chapter 6, there are additional MVs which we can activate in a predefined order, from cheap to expensive, when the previous MV reaches a constraint.

For both cases, MV-MV switching is implemented using split range control (SRC) and controllers with different setpoints. SRC keeps track of the MVs (see the split range block in Figure 4.3) and it switches to a new MV as soon as the original MV saturates. On the other hand, controllers with different setpoints only uses the CV measurement, and it switches to a new MV once its corresponding controller setpoint has been reached. This implies a delay in switching. The duration of delay is related to the chosen setpoint difference between the controllers. This means that SRC has the advantage of tighter CV control, which may be preferred for the district heating network with thermal energy storage in Chapter 6. However, the delay in switching maximizes throughput for the system in Chapter 5 when changes in operation give new temporary or permanent bottlenecks in other units. Further, controllers with different setpoints structure is easier to

implement and the controllers can be tuned to account for different MV-CV dynamics.

The work for maintaining production for units in series in Chapter when bottleneck occurs may be extended to include min flow constrains, that is to avoid the the flow in or out of a unit reaches a min bound. The work for district heating systems with thermal energy storage can be extended to include systems with variable energy prices, or with demand side management measures in which the consumers actively participate in supply-demand balance.

Bibliography

ABB (2022). Drum level control systems in the process industries. Application guide. library.e.abb.com/public/b18bcd185bebfee1c125695800554ad6/DLC_1GG.pdf.

Åberg, M., Windahl, J., Runvik, H., and Magnuson, F. (2017). Optimization-friendly thermodynamic properties of water and steam. In *Proceedings of the 12th International Modelica Conference, Prague, Czech Republic*.

Alobaid, F., Mertens, N., Starkloff, R., Lanz, T., Heinze, C., and Epple, B. (2017). Progress in dynamic simulation of thermal power plants. *Progress in Energy and Combustion Science*, 59:79–162.

Andersson, J. (2013). *A general purpose software framework for dynamic optimization*. PhD thesis, KU Leuven.

Aske, E. M. and Skogestad, S. (2009a). Consistent inventory control. *Ind. Eng. Chem. Res*, 48:10892–10902.

Aske, E. M. B. and Skogestad, S. (2009b). Dynamic degrees of freedom for tighter bottleneck control. In *10th International Symposium on Process Systems Engineering - PSE2009*, volume 27, pages 1275–1280. Elsevier Inc.

Aske, E. M. B., Skogestad, S., and Strand, S. (2007). Throughput maximization by improved bottleneck control. In *8th International IFAC*

Symposium on Dynamics and Control of Process Systems, volume 1, pages 63–68. IFAC.

Balchen, J. G. and Mummé, K. (1988). *Process control.* Van Nostrand Reinhold Company.

Bartusiak, D., Georgakis, C., and Reilly, M. (1989). Nonlinear feedforward/feedback control structures designed by reference system synthesis. *Chemical Engineering Scince*, 44:1837.

Bastin, G. and Dochain, D. (1990). *On-line estimation and adaptive control of bioreactors.* Elsevier Science Publishers B.V.

Bequette, W. (1991). Nonlinear control of chemical processes: A review. *Ind. Eng. Chem. Res.*, 30:1391–1413.

Bequette, W. (2002). *Process control: modeling, design, and simulation.* Prentice-Hall.

Bertrand, C. R. and McAvoy, T. J. (1986). Short-cut analysis of pressure control in steam headers. In *1986 American Control Conference*, pages 1757–1763.

Buckley, P. S. (1964). *Techniques of process control.* John Wiley and Sons, 1st edition.

Chen, C., Zhou, Z., and Bollas, G. M. (2017). Dynamic modeling , simulation and optimization of a subcritical steam power plant. Part I: Plant model and regulatory control. *Energy Conversion and Management*, 145:324–334.

Chong, Z. and Swartz, C. L. E. (2016). Optimal response under partial plant shutdown with discontinuous dynamic models. *Computers & Chemical Engineering*, 86:120–135.

Cohn, N. (1984). Recollections of the evolution of realtime control applications to power systems. *Automatica*, 20:145–162.

Cole, W. J., Cole, W. J., Powell, K. M., and Edgar, T. F. (2012). Optimization and advanced control of thermal energy storage systems. *Reviews in Chemical Engineering*, 28:81–99.

Cooke, D. H. (1985). On prediction of off-design multistage turbine pressures by Stodola's ellipse. *Transactions of the ASME*, 107:596–606.

Cordes, G. (1963). *Strömungstechnik der gasbeaufschlagten Axialtrubine*. Springer-Verlag Berlin Heidelberg GmbH.

der Autumation, F. A. (2003). VDI-Standard: VDI/VDE 3508, Unit control of thermal power stations. Technical report.

Downs, J. J. and Skogestad, S. (2011). Annual reviews in control: An industrial and academic perspective on plantwide control. *Annual Reviews in Control*, 35:99–110.

Dubé, J.-F. H. (2000). Pulp mill scheduling: optimal use of storage volumes to maximize production. Master's thesis, McMaster University.

Farmer, E. J. and Lipták, B. G. (2006). Steam turbine controls. In Lipták, B. G., editor, *Instrument Engineer's Handbook*, pages 2137–2151. CRC Press, fourth edition.

Forsman, K. and Adlouni, M. (2018). Control structures for optimization: examples from chemical industry. In *10th IFAC International Symposium on Advanced Control of Chemical Processes*. IFAC Papers Online.

Garriga, J. L. and Soroush, M. (2010). Model predictive control tuning methods: A review. *Ind. Eng. Chem. Res.*, 49:3505–3515.

Govatsmark, M. S. (2003). *Integrated control and optimization*. PhD thesis, Norwegian University of Science and Technology.

Guelpa, E. and Verda, V. (2019). Thermal energy storage in district heating and cooling systems: A review. *Applied Energy*, 252:113474.

Harsha, P. and Dahleh, M. (2014). Optimal management and sizing of energy storage under dynamic pricing for the efficient integration of renewable energy. *IEEE Transactions on Power Systems*, 30:1164–1181.

Hennessy, J., Li, H., Wallin, F., and Thorin, E. (2019). Flexibility in thermal grids: a review of short-term storage in district heating distribution networks. *Energy Procedia*, 158:2430–2434.

Henson, M. and Seborg, D. (1997). *Nonlinear process control*. Prentice-Hall.

HighEFF, F. (2022). Centre for an Energy Efficient and Competitive Industry for the Future. sintef.no/projectweb/higheff. Accessed: 2022-10-30.

Isidori, A. (1995). *Nonlinear control systems*. Springer London, 3rd ed. edition.

Isidori, A. and Ruberti, A. (1984). On the synthesis of linear input-output responses for nonlinear systems. *Systems & Control Letters*, 4:17–22.

Jonshagen, K. and Genrup, M. (2010). Improved load control for a steam cycle combined heat and power plant. *Energy*, 35:1694–1700.

Khalil, H. K. (2015). *Nonlinear control*. Pearson, second edition.

Kida, F. (2004). -. *Chem. Eng (Tokyo) (in Japanese)*, 49:144–151.

Kingstree, C. R. (2021). Application of transformed manipulated variables to cascade control cystems for linearization and disturbance rejection. Master's thesis, University of Edinburgh and Norwegian University of Science and Technology.

Klefenz, G. (1986). *Automatic control of steam power plants*. Bibliographisches Institut.

Knudsen, B. R., Kauko, H., and Andresen, T. (2019). An optimal-control scheme for coordinated surplus-heat exchange in industry clusters. *Energies*, 12:1877.

Krishnamoorthy, D. and Skogestad, S. (2020). Systematic design of active constraint switching using selectors. *Computers & Chemical Engineering*, 143:107106.

Kristoffersen, T. T., Snarheim, D., Imsland, L., and Govatsmark, M. S. (2014). Optimal and robust production of high pressure steam. In *2014 European Control Conference*, pages 491–497, Strasbourg. IEEE.

Kumar, R., Wenzel, M. J., ElBsat, M. N., Risbeck, M. J., Drees, K. H., and Zavala, V. M. (2020). Stochastic model predictive control for central HVAC plants. *Journal of Process Control*, 90:1–17.

Kurth, M. and Welfonder, E. (2006). Importance of the selfregulating effect within power systems. In *5th IFAC Symposium on Power Plants and Power Systems Control*, volume 39, pages 345–352. IFAC.

Lee, E. S. and Reklaitis, G. V. (1989). Intermediate storage and operation of periodic processes under equipment failure. *Computers & Chemical Engineering*, 13:1235–1243.

Lee, J., Mukherjee, R., and Khalil, H. K. (2016). Output feedback performance recovery in the presence of uncertainties. *Systems and Control Letters*, 90:31–37.

Lindsley, D. (2000). *Power-plant control and instrumentation: the control of boilers and HRSG systems*, volume 58. Institution of Electrical Engineers.

Lu, Q., Kumar, R., and Zavala, V. M. (2020). MPC controller tuning using bayesian optimization techniques.

Lund, H., Werner, S., Wiltshire, R., Svendsen, S., Thorsen, J. E., Hvelplund, F., and Mathiesen, B. V. (2014). 4th Generation district heating (4GDH): Integrating smart thermal grids into future sustainable energy systems. *Energy*, 68:1–11.

Luyben, W. L. (1993). Dynamics and control of recycle systems. 2. Comparison of alternative process designs. *Ind. Eng. Chem. Res.*, 32(3):476–486.

Ma, Y., Borrelli, F., Hencey, B., Packard, A., and Bortoff, S. (2009). Model predictive control of thermal energy storage in building cooling systems. In *Joint 48th IEEE Conference on Decision and Control and 28th Chinese Control Conference*, pages 392–397. IEEE.

Maffezzoni, C., Magnani, G., and Marcocci, L. (1983). Computer aided modelling of large power plants. In *IFAC Workshop on Modelling and Control of Electrical Power Plants*, pages 1–9.

Majanne, Y. (2005). Model predictive pressure control of steam networks. *Control Engineering Practice*, 13:1499–1505.

Marlin, T. E. (2000). *Process control. Designing processes and control systems for dynamic performance.* McGraw Hill.

Mathisen, K. W. (1994). *Integrated design and control of heat exchanger networks.* PhD thesis, University of Trondheim - The Norwegian Institute of Technology.

Mayne, D. Q. (2014). Model predictive control: Recent developments and future promise. *Automatica*, 50:2967–2986.

Mayne, D. Q., Rawlings, J. B., Rao, C. V., and Scokaert, P. O. M. (2000). Constrained model predictive control: Stability and optimality. *Automatica*, 36:789–814.

Miró, L., Gasia, J., and Cabeza, L. F. (2016). Thermal energy storage (TES) for industrial waste heat (IWH) recovery: A review. *Applied energy*, 179:284–301.

Montañés, R. M., Skaugen, G., Hagen, B., and Rohde, D. (2021). Compact steam bottoming cycles: minimum weight design optimization and transient response of once-through steam generators. *Frontiers in Energy Research*.

Nijmeijer, H. and Schaft, A. V. D. (2016). *Nonlinear dynamical control systems*. Springer.

Niva, L., Hultgren, M., Ikonen, E., and Jenö, K. (2017). Control structure design for oxy-fired circulating fluidized bed boilers using self-optimizing control and partial relative gain analyses. *IFAC-PapersOnLine*, 50:2023–2030.

Oliveira, V. D., Jäschke, J., and Skogestad, S. (2016). Optimal operation of energy storage in buildings: Use of the hot water system. *Journal of Energy Storage*, 5:102–112.

Ordys, A. W., Pike, A. W., Johnson, M. A., Katebi, R. M., and Grimble, M. J. (1994). *Modelling and simulation of power generation plants*. Springer-Verlag Berlin Heidelberg GmbH.

Polsky, M. P. (1982). Sliding pressure operation in combined cycles. *American Society of Mechanical Engineers*.

Powell, K. M. and Edgar, T. F. (2012). Modeling and control of a solar thermal power plant with thermal energy storage. *Chemical Engineering Science*, 71:138–145.

Prasad, G., Irwin, G. W., Swidenbank, E., and Hogg, B. W. (2000). Plant-wide predictive control for a thermal power plant based on a physical model. *IEE Proceedings - Control Theory and Applications*, 147:523–537.

Preisig, H. A. (2020). The ABC of modelling. folk.ntnu.no/preisig/HAP_Specials/Manuscripts/script.pdf.

Price, R. M., Lyman, P. R., and Georgakis, C. (1994). Throughput manipulation in plantwide control structures. *Ind. Eng. Chem. Res.*, 33:1197–1207.

Qin, S. J. and Badgwell, T. A. (2003). A survey of industrial model predictive control technology. *Control*, 11:733–764.

Quoilin, S., Aumann, R., Grill, A., Schuster, A., and Lemort, V. (2011). Dynamic modeling and optimal control strategy of waste heat recovery Organic Rankine Cycles. *Applied Energy*, 88:2183–2190.

Reid, R. C., Prausnitz, J. M., and Poling, B. E. (1987). *The properties of gases & liquids*. McGraw-Hill, 4th edition.

Reyes-Lúa, A. and Skogestad, S. (2020). Systematic design of active constraint switching using classical advanced control structures. *Ind. Eng. Chem. Res.*, 59:2229–2241.

Reyes-Lúa, A., Zotică, C., Das, T., Krishnamoorthy, D., and Skogestad, S. (2018). Changing between active constraint regions for optimal operation: classical advanced control versus model predictive control. *Computer-aided chemical engineering*, 43:1015–1020.

Reyes-Lúa, A., Zotică, C., Forsman, K., and Skogestad, S. (2019). Systematic design of split range controllers. *IFAC-PapersOnLineIFAC-PapersOnLine*.

Santamaría, F. L. and Gómez, J. M. (2016). An algorithm for tuning NMPC controllers with application to chemical processes. *Ind. Eng. Chem. Res.*, 55:9215–9228.

Scholten, T., Persis, C. D., and Tesi, P. (2017). Modeling and control of heat networks with storage: The single-producer multiple-consumer case. *IEEE Transactions on Control Systems Technology*, 25:414–428.

Seborg, D. E., Edgar, T. F., and Mellichamp, D. A. (2003). *Process dynamics and control*. John Wiley and Sons, 2nd edition.

Shinskey, F. G. (1978). *Energy conservation through control*. Academic Press.

Shinskey, F. G. (1981). *Controlling multivariable processes*. Instrument Society of America.

Shinskey, F. G. (1988). *Process control systems*. McGraw-Hill, 3rd edition.

Shinskey, F. G. and Louis, J. R. (1968). Once-through boiler control system.

Silvestri, G. J., Aanstad, O. J., and Ballantyne, J. T. (1972). A review of sliding throttle pressure for fossil-fueled steam turbine-generators. In *Proceedings of the American Power Conference*, pages 438–453.

Skogestad, S. (2003). Simple analytic rules for model reduction and pid controller tuning. *Journal of Process Control*, 13:291–309.

Skogestad, S. (2004). Control structure design for complete chemical plants. *Computers & Chemical Engineering*, 28:219–234.

Skogestad, S. (2006). Tuning for smooth PID control with acceptable disturbance rejection. *Ind. Eng. Chem. Res.*, 45:7817–7822.

Skogestad, S. (2008). *Chemical and energy process engineering*. CRC Press.

Skogestad, S. and Postlethwaite, I. (2005). *Multivariable feedback control: Analysis and design*. Wiley, second edition.

Skogestad, S., Zotică, C., and Alsop, N. (2023). Transformed inputs for linearization, decoupling and feedforward control. *Journal of Process Control*, 122:113–133.

Soave, N. and Barolo, M. (2021). On the effectiveness of heat-exchanger bypass control. *Processes*, 9(2).

Stephanopoulos, G. (1984). *Chemical process control: An introduction to theory and practice*. Prentice-Hall.

Stephanopoulos, G. and Ng, C. (2000). Perspectives on the synthesis of plant-wide control structures. *Journal of Process Control*, 10:97–111.

Åström, K. J. and Bell, R. (1987). Dynamic models for boiler-turbine alternator units: Data logs and parameter estimation for a 160 MW Unit. (Research Reports TFRT-3192). Technical report, Department of Automatic Control, Lund Institute of Technology (LTH).

Åström, K. J. and Bell, R. D. (2000). Drum-boiler dynamics. *Automatica*, 36:363–378.

Åström, K. J. and Hägglund, T. (2006). *Advanced PID-control*. ISA – Instrumentation, Systems, and Automation Society.

Sun, L. and Smith, R. (2015). Performance modeling of new and existing steam turbines. *Ind. Eng. Chem. Res.*, 54:1908–1915.

Thombre, M. and Krishnamoorthy, D. (2019). Data-driven online adaptation of the scenario-tree in multistage model predictive control. *IFAC-PapersOnLine*, 1:461–467.

van de Ven, P. M., Hegde, N., Massoulié, L., and Salonidis, T. (2013). Optimal control of end-user energy storage. *IEEE Transactions on Smart Grid*, 4:789–797.

Vik, E. A. K. (2021). Advanced control structures for balancing supply and demand in steam distribution networks. Master's thesis, Norwegian University of Science and Technology.

Wächter, A. and Biegler, L. T. (2006). On the implementation of an interior-point filter line-search algorithm for large-scale nonlinear programming. *Mathematical Programming*, 106:25–57.

Weissbach, T., Kurth, M., Welfonder, E., Haake, D., and Gudat, R. (2006). Control performance of large scale steam power plants and improvments. In Westwick, D., editor, *IFAC Symposium on Power Plants and Power Systems Control*, volume 39, pages 183–188. IFAC.

Welfonder, E. (1999). Dynamic interactions between power plants and power systems. *Control Engineering Practice*, 7:27–40.

Wood, A. J., Wollenberg, B. F., and B., S. G. (2014). *Power generation, operation, and control*. John Wiley & Sons, 3rd edition.

Zhou, Y., Scheller-Wolf, A., Secomandi, N., and Smith, S. (2016). Electricity trading and negative prices: Storage vs. disposal. *Management Science*, 62:880–898.

Zhou, Y., Scheller-Wolf, A., Secomandi, N., and Smith, S. (2019). Managing wind-based electricity generation in the presence of storage and transmission capacity. *Production and Operations Management*, 28:970–989.

Zotică, C., Alsop, N., and Skogestad, S. (2020a). Transformed manipulated variables for linearization, decoupling and perfect disturbance rejection. *IFAC-PapersOnLine*.

Zotică, C., Forsman, K., and Skogestad, S. (2022). Bidirectional inventory control with optimal use of intermediate storage. *Computers & Chemical Engineering*, 159:107677.

Zotică, C., Montañés, R. M., Reyes-Lúa, A., and Skogestad, S. (2022). Control of steam bottoming cycles using nonlinear input and output transformations for feedforward disturbance rejection. *IFAC-PapersOnLine*, 55:969–974.

13th IFAC Symposium on Dynamics and Control of Process Systems, including Biosystems (DYCOPS) 2022.

Zotică, C., Nord, L. O., Kovács, J., and Skogestad, S. (2020b). Optimal operation and control of heat to power cycles: A new perspective from a systematic plantwide control approach. *Computers & Chemical Engineering*, 141:106995.

Zotică, C., Pérez-Piñeiro, D., and Skogestad, S. (2021). Supervisory control design for balancing supply and demand in a district heating system with thermal energy storage. *Computers & Chemical Engineering*, 149:107306.

Zotică, C. and Skogestad, S. (2021). Input transformation for linearization, decoupling and disturbance rejection with application to steam networks. In Türkay, M. and Gani, R., editors, *31st European Symposium on Computer Aided Process Engineering*, volume 50, pages 1021–1027. Elsevier.